IS THE WEIS-FOGH PRINCIPLE EXPLOITABLE IN TURBOMACHINES ?

by S. B. Furber.

Emmanuel College,
University of Cambridge.

A dissertation
submitted for the degree of
Doctor of Philosophy,
October 1979.

Stephen Byram FURBER

PREFACE

The research described in this dissertation was carried out at the Engineering Department of the University of Cambridge during the period from October 1975 to September 1979. It is the original work of the author except where a reference to other work is given, and includes nothing which is the outcome of work done in collaboration.

The author is grateful to his research supervisor Professor J. E. Ffowcs Williams for his guidance and encouragement during the course of this work, and also to the other members of staff and fellow research students who have given advice and assistance. He would like to thank the technical staff of both the Aeronautical Laboratory and the Whittle Laboratory for their help with the experiments, and the design office and workshop for their respective parts in the construction of the isolated interaction apparatus.

Sections 2.1,2.2,2.3,3.1 and parts of sections 3.2 and 3.3 have been accepted by the Journal of Fluid Mechanics for publication with Professor J. E. Ffowcs Williams as co-author, and will appear shortly.

The author gratefully acknowledges the support of a Science Research Council research studentship at St. John's College, Cambridge, during the first three years of this work, and the opportunities afforded subsequently by the Rolls-Royce Research Fellowship at Emmanuel College, Cambridge.

SUMMARY.

In this dissertation we ask whether the Weis-Fogh effect, by which a hovering insect flies with an aerodynamic performance superior to anything previously known, can be exploited in turbomachinery. We think the answer is yes.

Normal turbomachinery design is based on the analysis of isolated cascades of blades with steady entry and exit flows. The interactions between adjacent cascades, and non-uniformities of the flow, are regarded as serious problems which have to be minimised. Unsteadiness gives rise to noise and causes damaging vibration. Despite these known disadvantages we take here the view that some benefits might accrue from controlled blade interactions, and that these advantages should be quantified. They might possibly outweigh the disadvantages that normally drive the designer to minimise blade interference. We therefore take the positive view of proposing a novel type of turbomachinery stage which depends on the interaction between the rotor and the stator for its normal operation. The stage exploits the Weis-Fogh principle, and has the unusual property that when started from rest it generates a pressure rise without shedding any vorticity into the fluid. We conclude from both our analysis and our experiments that there are definite performance advantages for stages of this new type, and that the noise and vibration problems they are likely to cause are not significantly greater than those found in existing high performance aero-engines.

Our experiments were performed to check the validity of a theoretical model, and these are described in detail. The results seem to show that strong blade interactions can cause aerofoils to work usefully at higher mean loadings than those in conventional designs, and that the increased loading is also associated with an improved aerodynamic efficiency. Our analysis seems to predict the

experimental performance very satisfactorily, and we see no fundamental reason why the beneficial effects should not carry over to the higher speed larger machinery of engineering importance, but we realise that the difficulties of engineering our device will be far from trivial! We would look to our principle for a measurable increase in the efficiency of such machines together with an improved surge margin. In our experiment these amounted to 3 percent and 10 percent respectively, and we are encouraged to expect these figures to be relevant to real machines from our interpretation of some test data on large scale machines with low blade clearances.

CONTENTS:

1. INTRODUCTION

1.1 The Weis-Fogh effect

An aerofoil accelerating from rest initially generates no lift. The lift will arise only as a circulation develops around the aerofoil, and since vorticity is conserved the circulation will grow only as the opposite vorticity is shed from the trailing edge. The shed vorticity affects the flow at the trailing edge in such a way as to delay further shedding, and so the development of full lift takes time. A hovering animal uses an oscillating wing on which circulation of opposite sign must be developed for succeeding beats. Its performance will be hindered by this delay, in that the lift impulse generated by each wing beat will be reduced. In his studies of animal hovering motions, Weis-Fogh (1973) observed that one small insect, the chalcid wasp Encarsia formosa, overcomes this problem by a remarkable interaction of the two wings; each wing acts as the starting vortex for the other.

The process operates as shown in figure 1.1. The previous wing beat ends in a 'clap', leaving the two wings parallel and in contact along their chordline, position (a). The 'fling' then proceeds as follows: The wings rotate about their trailing edges, which remain in contact (b). This rotation sucks air round the leading edge into the opening space between the wings, generating a circulation on each wing (c). At the required angle the wings break apart, retaining the circulation which arose during the rotation (d). No vorticity has been shed into the fluid, and both wings start their beat with full circulation.

The main reason that we are seeking an application of the Weis-Fogh effect in turbomachinery is that we expect a performance advantage

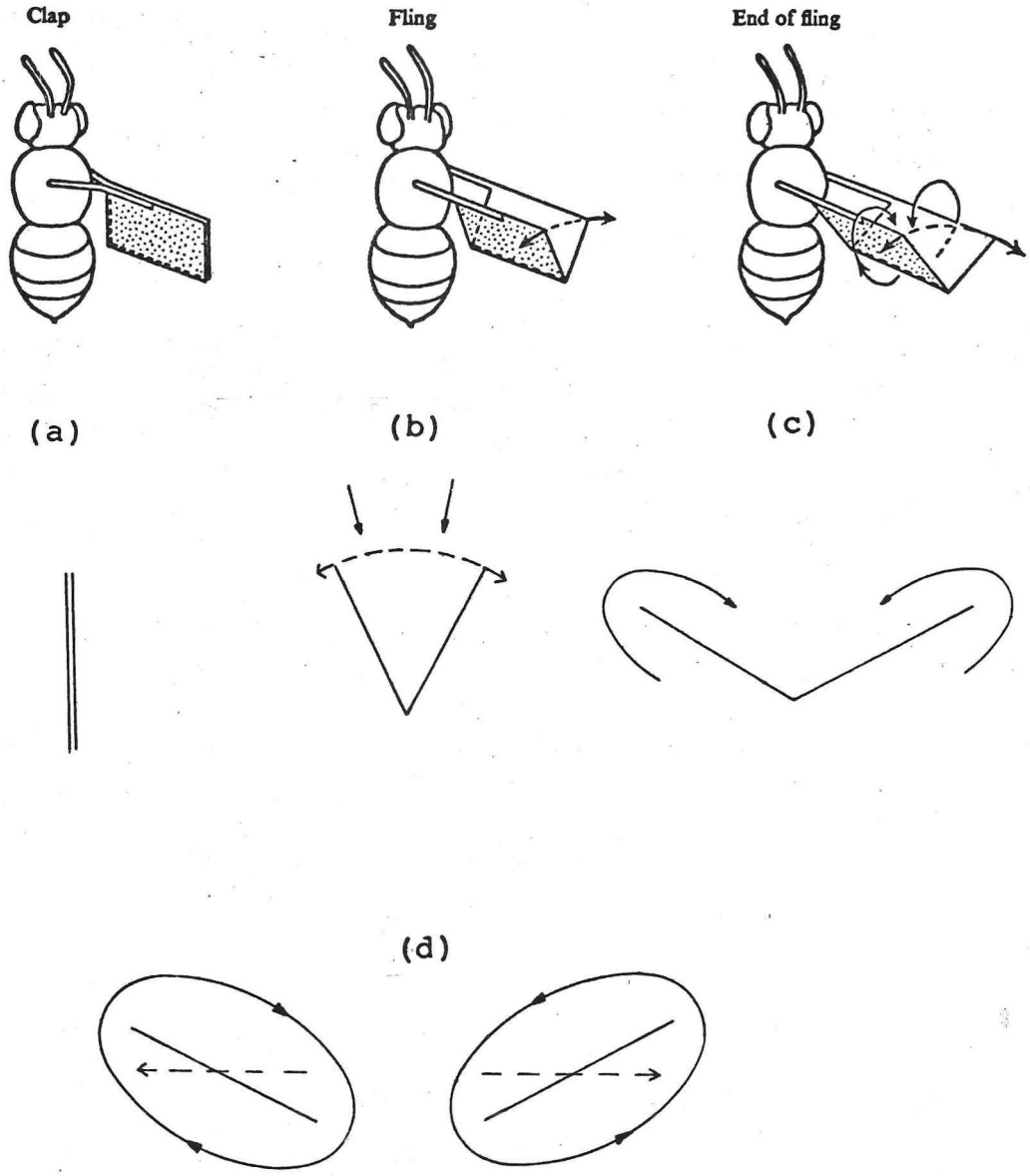

Figure 1.1 Weis-Fogh's interpretation of the 'clap and fling' mechanism used by Encarsia formosa.

over conventional systems. We base our expectation solely on the performance of insects which exploit the principle. The fact that the technique required to use the principle has been developed and preserved in nature demonstrates that advantages exist.

The insect has a wing span of about 3 mm. and operates at a Reynolds number around 15. Under these conditions a conventional hovering motion would work poorly. Encarsia formosa achieves a lift coefficient of about 3 based on wing dimensions and beat frequency, compared to 1.5 typical of other insects using normal (vortex shedding) lift generation. The 'clap and fling' interaction gives this insect great performance advantages.

Other insects have been observed to use similar wing interactions, and the number of known applications increases as knowledge grows. It has been suggested that the familiar clapping noise made by pigeons when taking off and landing may result from them using the same principle. In this dissertation we are concerned with the possibility of harnessing the effect in a machine. We shall see that not only is the lift increased, but the efficiency can be greater as well.

Lighthill (1973) has given a mathematical analysis of the Weis-Fogh effect and shown how the performance of the wing system is governed by parameters quite different from those determining the forces on conventional isolated aerofoils. It follows that we may find applications in precisely those areas that are out of reach of conventional machines. We shall give examples of possible ways of applying the principle for use in machines, and show how they may give a superior performance over a range of working conditions as well as at the extremes where the conventional flow starts to break down.

We know that the principle is used by many different species in

over conventional systems. We base our expectation solely on the performance of insects which exploit the principle. The fact that the technique required to use the principle has been developed and preserved in nature demonstrates that advantages exist.

The insect has a wing span of about 3 mm. and operates at a Reynolds number around 15. Under these conditions a conventional hovering motion would work poorly. Encarsia formosa achieves a lift coefficient of about 3 based on wing dimensions and beat frequency, compared to 1.5 typical of other insects using normal (vortex shedding) lift generation. The 'clap and fling' interaction gives this insect great performance advantages.

Other insects have been observed to use similar wing interactions, and the number of known applications increases as knowledge grows. It has been suggested that the familiar clapping noise made by pigeons when taking off and landing may result from them using the same principle. In this dissertation we are concerned with the possibility of harnessing the effect in a machine. We shall see that not only is the lift increased, but the efficiency can be greater as well.

Lighthill (1973) has given a mathematical analysis of the Weis-Fogh effect and shown how the performance of the wing system is governed by parameters quite different from those determining the forces on conventional isolated aerofoils. It follows that we may find applications in precisely those areas that are out of reach of conventional machines. We shall give examples of possible ways of applying the principle for use in machines, and show how they may give a superior performance over a range of working conditions as well as at the extremes where the conventional flow starts to break down.

We know that the principle is used by many different species in

nature, and it must therefore offer advantages under a range of conditions. The work presented here demonstrates that this range can be extended to include engineering applications where the effect is exploitable to similar advantage.

The number of possible ways of using the Weis-Fogh principle is limited only by the imagination, and we can present just a few here. We have guessed at examples which we thought would lend themselves readily to inclusion in machine designs. Our results encourage us not only to persue the further investigation of the geometries that we have analysed and tested here, but also to expect that other applications of the same principle will display as great, if not greater, exploitable potential.

1.2 General approach

The interaction used by Encarsia formosa is particularly suited to the rapid generation of large changes in circulation, which is of course the insect's requirement. Turbomachinery is not usually designed to require frequent changes in circulation, though cross-flow fans are an important exception which we shall discuss in detail later. The designer is constantly looking for ways of increasing steady circulations, and of controlling the machine's undesirable characteristics such as stall and flutter. We hope to help in this task in adapting the Weis-Fogh principle to different geometries. To keep to the title of this dissertation we must decide exactly what we understand the Weis-Fogh principle to be. A reasonable extension of the original process would include any motion where the flow around one rigid body is crucially modified by the transient presence of a second body, and particularly when the interaction amounts principally to a redistribution of circulation.

The model of the interaction process analysed by Lighthill (1973) is based on aerofoils rotating about a spanwise axis. That other members of this class exist may readily be seen by considering the motion of a plate sliding along with its trailng edge in contact with an infinite plane, as shown in figure 1.2(c). The boundary for this motion is a special case of that used by Lighthill, with the wing normal to the plane. Though the boundary conditions are different, the same transformation may be used to find the flow over all the half-plane and the effective circulation on the moving plate.

Lighthill used the Schwar z-Christoffel transformation

$$\frac{dz}{d\zeta} = K\left(\frac{\zeta-1}{\zeta+1}\right)^{\frac{\alpha}{\pi}}\left(\frac{\zeta-a}{\zeta-1}\right) \qquad (1.1)$$

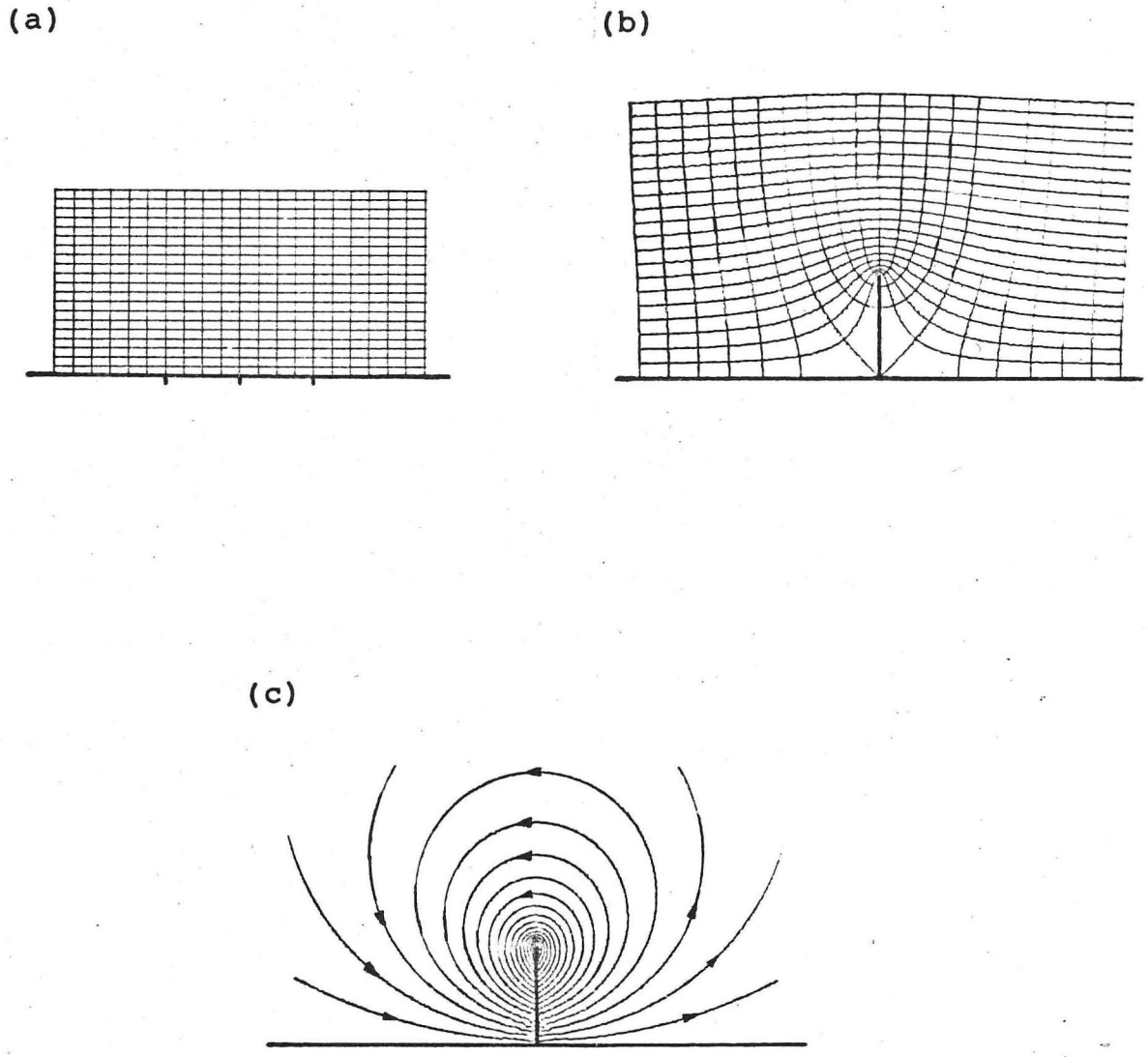

Figure 1.2. The flow generated by a plate moving along an infinite plane. (a) The mesh used for calculations shown in the ζ-plane, with one line in five drawn. (b) The same mesh in the z-plane. (c) The streamlines in the z-plane.

which, when $\alpha = \pi/2$, reduces to

$$\frac{dz}{d\zeta} = K\zeta(\zeta^2-1)^{-\frac{1}{2}} \tag{1.2}$$

This is integrable, and choosing K so that $z \sim \zeta$ as $\zeta \to \infty$ we obtain

$$z = (\zeta^2-1)^{\frac{1}{2}} \tag{1.3}$$

giving the length of the moving plate as 1. Figure 1.2(a) shows a rectangular mesh in the ζ-plane, and figure 1.2(b) shows how this mesh is transformed by equation (1.3) into the z-plane. The complex potential for the flow generated by the moving plate may be found by representing the motion with a source distribution on the surface of the blade, but a more simple approach is possible. If a uniform external flow parallel to the plane were added, with velocity equal to the plate velocity, then the plate would just move with the fluid and have no effect. The flow created by the plate motion is therefore a uniform flow in the absence of the plate less the same flow in the presence of a stationary plate at the same position, and if the plate velocity is normalised to unity this gives a complex potential

$$w = z - \zeta \tag{1.4}$$

The contours of Im(w) = constant are plotted in figure 1.2(c) to give the streamlines. The flow is the same as half of the flowfield generated by a plate moving normal to its surface with no other boundaries, the plane in our model being the plane of symmetry in the other, and can also be found by means such as transformation into a circle. The circulation on the moving plate is the change in Re(w) across the edge of the moving plate which is in contact with the plane,

and is 2 in our normalised model. The general result is therefore that the circulation on the plate is 2vc, where v is the velocity and c the chord.

If the infinite plane is replaced by a semi-infinite one, the flow will be similar to figure 1.2 as long as the moving plate is far from the edge of the plane. As the edge is approached, however, it will influence the flow increasingly. When the moving plate reaches the end of the plane (figure 1.3(c)) it will still have an effective circulation, which may be calculated by conformal transformation using a Schwarz-Christoffel transformation similar to that used by Lighthill.

$$\frac{dz}{d\zeta} = K(\zeta-a)\left(\frac{\zeta-1}{\zeta+1}\right)^{\frac{1}{2}} \tag{1.5}$$

This is also integrable, and yields

$$z = -(\zeta-1)(\zeta^2-1)^{\frac{1}{2}} \tag{1.6}$$

giving the length of the moving plate as $\frac{3\sqrt{3}}{4}$. The mesh shown in figure 1.3(a) is now transformed to that shown in figure 1.3(b). The complex potential describing the flow caused by the plate moving with unit velocity is

$$w = z + (\zeta-\tfrac{1}{2})^2 \tag{1.7}$$

found by a similar procedure to that used for the previous flow. The offset of 1/2 in the zeta plane is necessary to cancel a net flow round from above the half-plane to below it, and the value of the offset may be found from consideration of the behaviour of equation

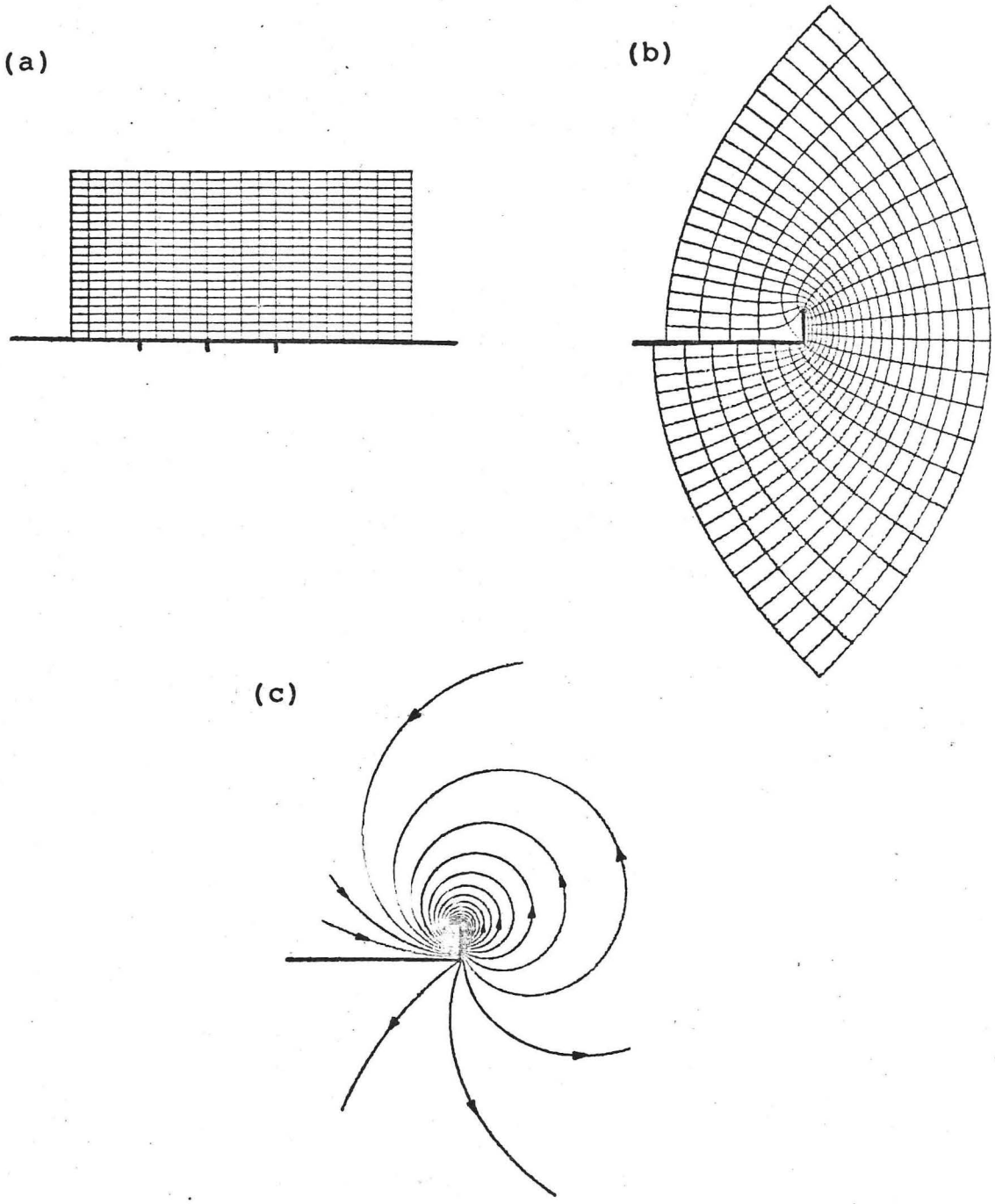

Figure 1.3. The flow generated by the moving plate at the edge of a semi-infinite plane. (a) The mesh used for calculations shown in the ζ-plane, with one line in five drawn. (b) The same mesh in the z-plane. (c) The streamlines in the z-plane.

(1.6) for large ζ.

As $\zeta \to \infty$,

$$z \to -\zeta(\zeta-1)(1+O(\zeta^{-2})) \tag{1.8}$$

which may be rewritten as

$$z \to -(\zeta-\tfrac{1}{2})^2 + O(1) \tag{1.9}$$

Now any term like ζ in the complex potential represents uniform flow parallel to the plane boundary in the ζ-plane, which is equivalent to flow around the half-plane in z-space. This is analogous to a total circulation on a finite body, and cannot be caused by the motion of the plate. We therefore insist that the coefficient of ζ in the expansion of w for large ζ be zero, which leads to the expression for w in equation (1.7).

The circulation on the plate is 2 , which gives the general result $\frac{8vc}{3\sqrt{3}}$, approximately 25 percent lower than when the blade is far from the edge.

The resulting flow is shown in figure 1.3(c). If the moving plate continues its motion past the end of the half-plane then, subject to continuity of the flows at separation, it will have a circulation that has been generated without any shedding of vorticity into the fluid. This is an example of how the Weis-Fogh effect may be brought to bear on flows involving aerofoils that pass close to a fixed surface.

If we go one step further and make the half-plane large but finite the above description should still be adequate for the motion around the time of separation. The moving blade may have approached the

stationary one with no circulation, but as we have seen it will leave with circulation. Since no vorticity has been shed it follows that the circulation gained by the moving blade must be balanced by an opposite circulation left on the stationary blade.

Something similar must happen even if the fixed blade is not much larger than the moving one, and then we see that the geometry is not very different from a conventional axial compressor stage. We can envisage a succession of inclined blades moving past a similar succession of fixed blades, each pair interacting as described above, and each blade being left with a circulation. It can be seen that these circulations are of the same sign as those generated by vortex shedding in a conventional machine where axial flow is represented by a velocity at a large distance parallel to the y-axis. The only additional geometric constraint that we must impose is that the rotor-stator clearance be maintained at exactly zero.

Since the geometry is so similar to a conventional axial-flow compressor it is possible to conceive of a machine which uses both principles; indeed it would appear inevitable that a real machine would shed vorticity between interactions unless the circulations generated were exactly those that satisfy the Kutta condition at all times. Here one might hope for benefit in that the interaction might be used to maintain higher average circulation levels. We note that since the circulations are generated by a completely different mechanism from that involved in maintaining the Kutta condition, it might be possible to set the blades at an incidence that would normally result in stall, but prevent this from happening by the interaction repeatedly regenerating the full circulation. That would be an extremely useful aspect worthy of the most serious attention.

This then is the approach of this dissertation. We start by analysing more thoroughly the isolated interaction between a pair

of aerofoils. This furnishes the same canonical problem for our interacting stage as does the isolated aerofoil for conventional cascades. We shall see that the circulations generated are of the same order as those generated by conventional vortex shedding. We shall then look at the results of some wind tunnel tests on an isolated interaction between two blades, in order to establish that the Weis-Fogh effect can still be made to work at high Reynolds number. We shall also see how the inclusion of vortex shedding affects the interchange of circulation, and deduce an estimate of the usefulness of the analysis that ignores this effect. Finally we shall see how the interaction performs in cascade, though at that stage we find it necessary to introduce some approximations. Some distinctly encouraging results of tests on axial stages are presented, which support the conclusion that the interaction is significant and useful. We conclude that the principle will find useful applications in turbomachinery and that the advantages will outweigh the problems created by the constraint on the rotor-stator axial spacing. Indeed the benefits accrue in areas where conventional ideas are stretched to the limit, the single most promising aspect being the possibility of delaying surge and permitting higher stage loadings at low speeds than could conceivably be obtained with isolated cascades of aerofoils.

Any machine based on strong unsteady effects will generate noise, and we shall estimate the sound levels our machine is likely to produce. The blades in a conventional machine experience significant unsteady lifts, due to inlet maldistributions and the wakes of upstream blades, and we shall compare the noise levels of the two types of machine on the basis of these unsteady forces. We will deduce that though noise may be a significant problem, the principle cannot be ruled out at this stage on noise grounds.

This is how the subject stands at present. We have shown how the

principle used in nature and first observed by Weis-Fogh may be applied in turbomachinery, and we have predicted the characteristics of such machines. These predictions have been shown to be reasonable in practice, and the application of the principle has resulted in performance improvements. The next step should be a thorough search of the performance characteristics of past machines to see if any would have been subjected to this effect, particularly those with narrow interstage gaps. We know already that there is circumstantial evidence in favour of our thesis from some experimental axial compressors. If we can induce enough confidence in prospects of useful advantage then a demonstration of a larger scale compressor stage should be based on the results of this work. Perhaps then we may look forward to full-scale tests and the principle finding its way to applications in more effective production power-plant.

2 THE ISOLATED INTERACTION

2.1 Mathematical Model.

For an initial investigation of how the Weis-Fogh principle might be applied we seek a model that illustrates the effect in a geometry more easily used in turbomachinery than that used in the original insect motion, which involved simultaneous translation and rotation of both wings. To this end we choose the model shown in figure 2.1, which imposes only one further constraint on a conventional axial compressor stage, namely that the axial gap between the rotor and stator be closely controlled.

The rotor AB and the stator EF are represented by flat plates. The stator is aligned parallel to the direction of motion of the rotor, and the trailing edge of the rotor maintains contact with the upper surface of the stator while the blades pass. Thus the two blades form one deforming body for a finite part of the motion. This will be relaxed later, and we shall insist only on instantaneous contact. For the time being, however, it is convenient to be able to consider the initial contact and final separation as distinct events.

This geometry allows us to calculate analytically full details of the flow field using potential flow theory, at least for that part of the motion when the blades are in contact. Later we shall develop an approximate model to describe our experiment which will give the flow at all times, but in this section we restrict our attention to finding exact results.

The problem is unusual in that the boundary is deforming, and eventually splitting into two disconnected bodies. A potential flow, however, does not depend on the history of the boundaries, but only on the instantaneous boundary velocities. Thus rather than analysing

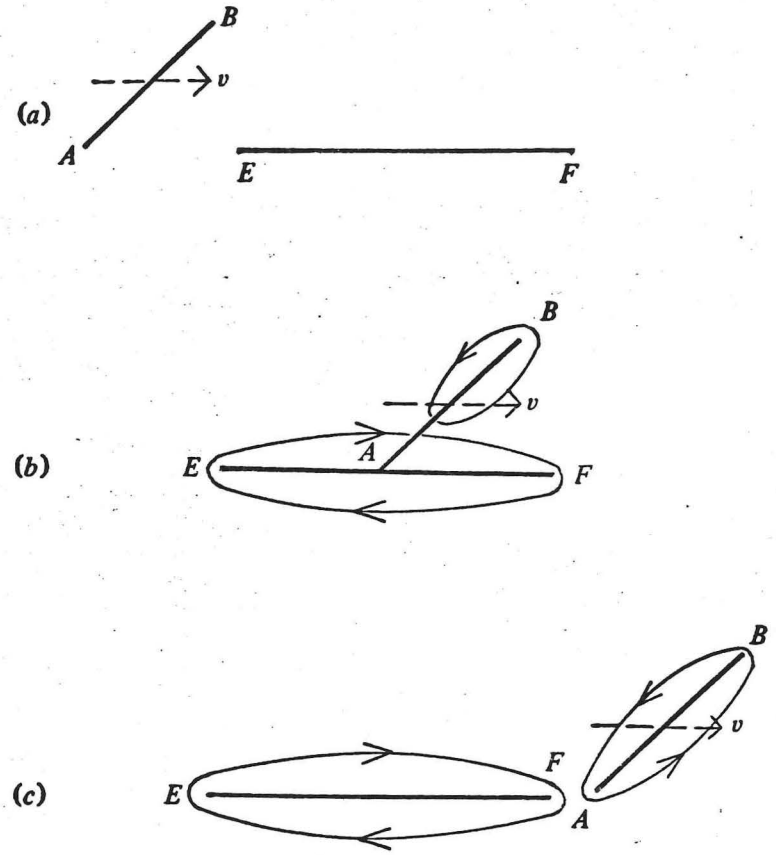

Figure 2.1. The physical plane. The rotor AB moves with a velocity v parallel to the fixed stator EF. The blades are in an external flow with velocity components (U,V) at infinity, and the total circulation on the system is C.

the problem with a moving physical rotor, we may consider the equivalent problem where AB in figure 2.1 is a fixed boundary on which a normal velocity is prescribed. We may then transform the boundary by conformal mapping into something more easily handled. The flow region in figure 2.1(b) may be considered to be the exterior of a polygon, and this may be transformed into the exterior of the unit circle (Jeffreys & Jeffreys 1956, section 13-094) via the conformal mapping

$$\frac{dz}{d\zeta} = K\zeta^{-2}\left(\frac{\zeta-\zeta_{a2}}{\zeta-\zeta_{a1}}\right)^{\alpha/\pi}\left(\frac{\zeta-\zeta_b}{\zeta-\zeta_{a2}}\right)(\zeta-\zeta_e)(\zeta-\zeta_f), \tag{2.1}$$

where α is the angle of incidence of the rotor, K is a scaling constant, and ζ_b is the mapping of B into the ζ-plane, etc. Note that, since the polygon in the z-plane is degenerate, the trailing edge of the rotor (A) corresponds to two vertices, which transform distinctly into ζ_{a1} on EAB and ζ_{a2} on BAF (figure 2.2).

This transformation enables us to find a complex potential, and hence full details of the flow field, but first it is relevant to consider the geometrical details of the transformation.

We want $z(\zeta)$ to be single valued, and this requires that the coefficient of ζ^{-1} in the expansion of equation (2.1) in negative powers of ζ be zero. This gives the following interrelation between the values of ζ at the transformed vertices:

$$(\alpha/\pi)(\zeta_{a2}-\zeta_{a1})+\zeta_f+\zeta_b+\zeta_e-\zeta_{a2} = 0 \tag{2.2}$$

We are free to prescribe any value on the unit circle for one of

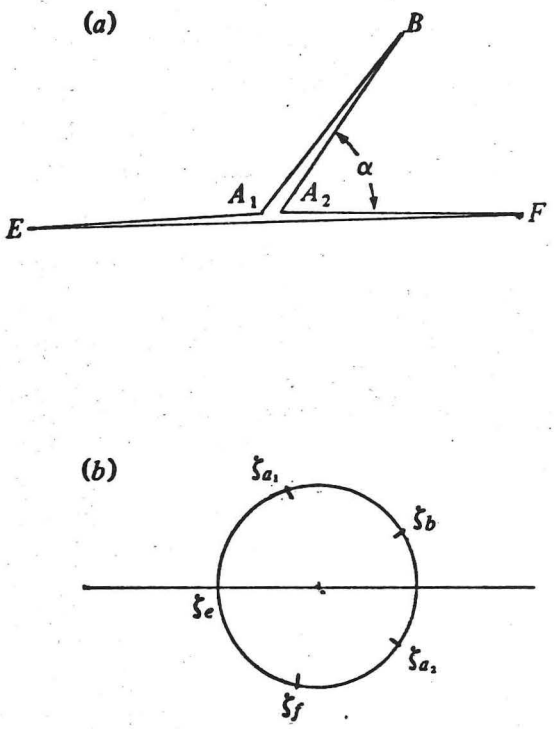

Figure 2.2. The conformal transformation. (a) The z-plane. The physical boundary may be thought of as a degenerate polygon. (b) The ζ-plane. The boundary conditions may be transformed onto the unit circle in the ζ-plane via equation (2.1).

the transformed vertices, and here we take $\zeta_e = -1$. Other values correspond to rotations of the boundary in the ζ-plane.

We may then take any values consistent with equation (2.2) for the other transformed vertices, in sequence around the unit circle, and use them to integrate equation (2.1) numerically to obtain the various lengths in the physical plane.

As the rotor moves across the stator the transformed vertices move round the unit circle in a manner which is hard to establish by any other than numerical methods.

The complex potential may be considered as the linear superposition of three components; the flow generated by the relative motion of the blades, that caused by an external stream, and that caused by a non-zero total circulation on the system. All three may be evaluated, and we look first at the component generated by the relative motion of the blades with zero total circulation and no flow at a large distance.

The motion of the rotor is represented by a normal velocity boundary condition in the physical plane, and, since the normal velocity is equal to the derivative along the boundary of the stream function Ψ, we may express the boundary condition as

$$\Psi = \begin{cases} -v \sin \alpha \; z \; e^{-i\alpha} & \text{on the rotor} \\ 0 & \text{on the stator} \end{cases} \qquad (2.3)$$

provided that we take the trailing edge of the rotor at $z = 0$.

The boundary conditions may be transferred into the ζ-plane, where they become

$$\Psi = \begin{cases} -v \sin\alpha \, e^{-i\alpha} z(e^{i\eta}) & \text{for } \eta_{a1} > \eta > \eta_{a2} \\ 0 & \text{otherwise,} \end{cases} \tag{2.4}$$

where $\zeta = e^{i\eta}$ on the unit circle. The corresponding complex potential is

$$w(\zeta) = -\frac{v\sin\alpha}{\pi} \int_{\eta_{a1}}^{\eta_{a2}} \frac{z(\zeta')e^{-i\alpha}}{(\zeta-\zeta')} d\zeta', \tag{2.5}$$

where the integration is to be taken clockwise round the unit circle, and the trailing edge of the rotor is taken at the origin in the physical plane, ie $z(\zeta_{a1}) = 0$.

This is the complex potential for the flow generated by the relative motion of the rotor and the stator. The total complex potential will include contributions representing an external flow and a non-zero total circulation. These are easily calculated, since the boundary in the ζ-plane is a circle. An external stream with velocity (U,V) at a large distance in the ζ-plane gives rise to a complex potential

$$w_e(\zeta) = (U+iV)\zeta K + (U-iV)\zeta^{-1}\bar{K}, \tag{2.6}$$

where the overbar denotes the complex conjugate, and a total circulation C adds

$$w_c(\zeta) = \frac{iC}{2\pi} \log \zeta. \tag{2.7}$$

Thus the complex potential is known for any flow conditions.

If in the z-plane an external stream is applied with the same velocity as the rotor, so (U,V) = (v,0), and C = 0, it is clear that a uniform flow parallel to the stator will result. Thus

$$\zeta K + \zeta^{-1}\bar{K} - \frac{\sin\alpha}{\pi}\int_{\eta_{a1}}^{\eta_{a2}} \frac{z\, e^{-i\alpha}}{(\zeta-\zeta')} d\zeta' = z. \tag{2.8}$$

Hence equation (2.5) may be written in the following form which is more convenient for computation:

$$w(\zeta) = v(z-\zeta K-\zeta^{-1}\bar{K}). \tag{2.9}$$

The complex potential with external flow (U,V) and circulation C is then

$$w_T = w + w_e + w_c$$

$$= vz + (U-v+iV)\zeta K + (U-v-iV)(\zeta^{-1}\bar{K}) + \frac{iC}{2\pi}\log\zeta. \tag{2.10}$$

We now have full information on the flow around our simple two blade model immersed in any external flow, for the period while the blades are in contact. This will enable us to calculate the forces on the blades, and see how the interaction will affect the blade circulations. We can then use the results to estimate the performance of cascades of interacting blades, treating each interaction between two blades in isolation as a first approximation, and compare with the performance of a conventional stage.

The complex potential in equation (2.10) may be used with the

conformal transformation [equations(2.1) and (2.2)] to calculate the streamlines for any geometry and flow condition. Since the conformal transformation is written in terms of ζ it is natural to start in the ζ-plane. The boundary in the ζ-plane is a circle, therefore polar co-ordinates with the origin at the centre of the circle were chosen. One hundred values of each co-ordinate were taken to cover an annular region from the boundary to a circle with six times the radius of the boundary, and figure 2.3(a) shows the co-ordinate system for every fifth value taken.

Suitable positions for the transformed vertices on the unit circle were then chosen to give a rotor of equal length to the stator, and inclined at 45 degrees to it, with the two blades about to separate (A and F coincident in figure 2.1). Equation (2.1) was integrated round the unit circle in the ζ-plane to give the value of z corresponding to each of the one hundred chosen values of ζ on the boundary. These values of z could then be used as starting points for integrating equation (2.1) along each of the radial lines in the ζ-plane, and the map of all the chosen values of ζ onto the z-plane found. The method of integration used for both of the preceding steps was that of taking the derivative midway between two adjacent points in the ζ-plane as an approximation to the gradient of the chord joining the two points, except near to A_1 and A_2 in figure 2.2 where a local approximation is needed to calculate adjacent points on the boundary. The results of this numerical mapping are shown in figure 2.3(b) which gives the transformation into the z-plane of the co-ordinate lines shown in figure 2.3(a) in the ζ-plane.

Once the corresponding values of z and ζ were known it was straightforward to calculate the value of the stream function Ψ = Im(w) from equation (2.10) at each position for any required flow condition. These values were then fed to a contour plotting routine, along with a set of z or ζ values, and the streamlines in the

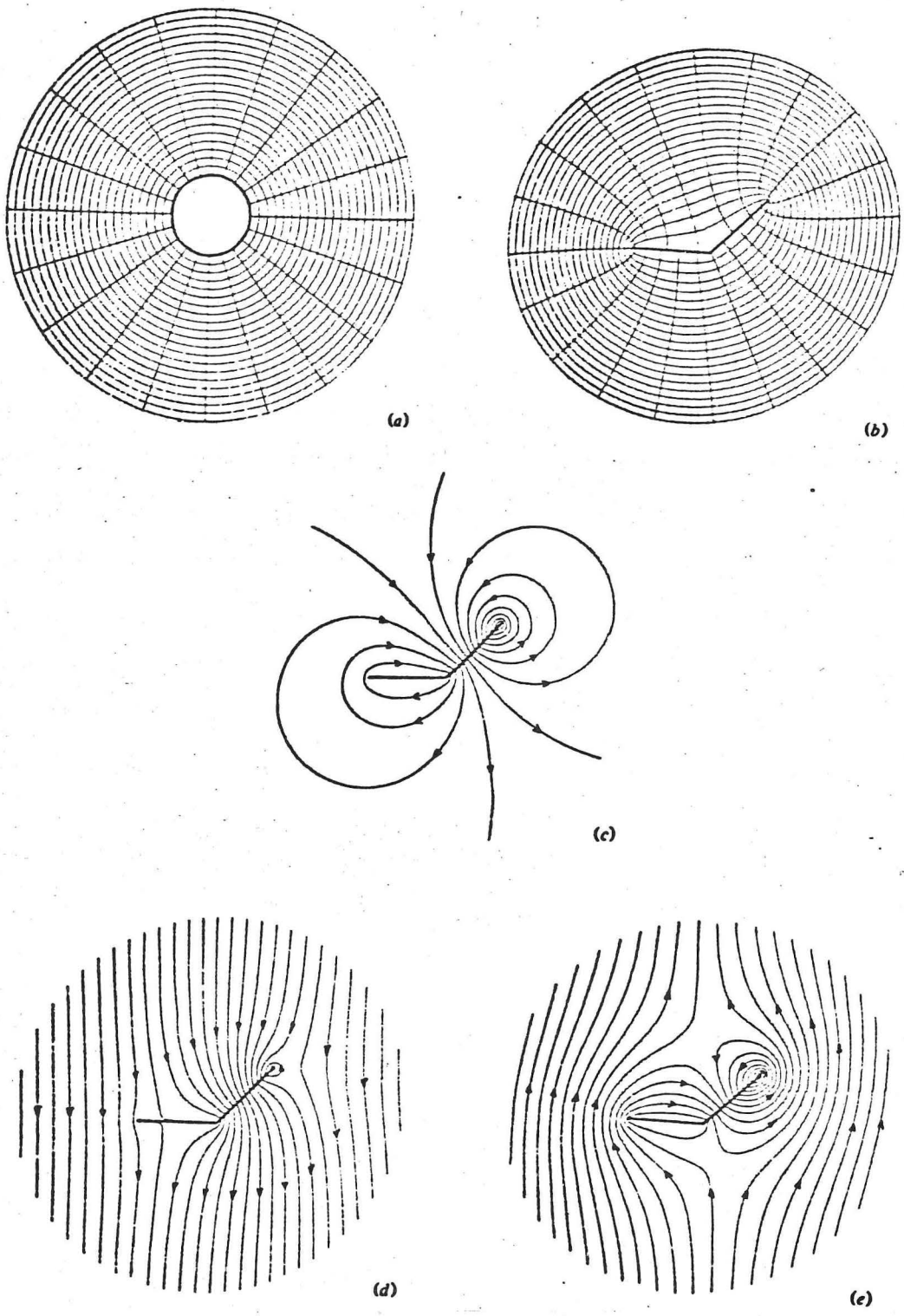

Figure 2.3. (a) The co-ordinate system in the ζ-plane, showing every fifth value. (b) The co-ordinate system of (a) transformed into the z-plane. (c) Streamlines for the flow generated by rotor motion alone, showing clearly the circulatory motion. (d) A descending stream with 1/4 of the rotor velocity has been added to the flow of (c), corresponding to an axial flow with no swirl in a conventional machine. (e) An ascending stream is added to the flow of (c), and the blade circulations are augmented.

corresponding plane were output.

Figure 2.3(c) gives the streamlines in the absence of any external flow or net circulation, and shows clearly the circulation developed around the rotor leading edge, and in the opposite direction around the stator. When an external stream approaches vertically from above with one quarter of the rotor's velocity, the streamlines are as shown in figure 2.3(d). The circulation on the rotor is partly cancelled by the streaming around the body, but some remains. This has been established by a procedure to be described later in this section. If the external flow approaches instead from vertically below, the circulation is enhanced. The streamlines for this flow are shown in figure 2.3(e). There are now two saddle-points in the flow away from the boundary.

The complex potential [equation (2.10)] also contains sufficient information to work out all the pressure distributions, but an evaluation of the overall lift generating performance may be obtained more directly from consideration of the blade circulations. We consider the case where there is no external stream, and the flow is generated solely by the rotor motion. We take also zero total circulation, corresponding to starting the motion from rest in a stationary fluid. Under these conditions, the circulations generated on the rotor and stator will be equal and opposite.

The velocity is the gradient of the velocity potential, so the circulation round a curve is the change in the potential going once round the curve. The circulation on the rotor is therefore the change in potential across the trailing edge

$$\Gamma = \mathrm{Re}[w(\zeta_{a_1}) - w(\zeta_{a_2})], \tag{2.11}$$

taking an anti-clockwise circulation in figure 2.1 as positive. Thus from equation (2.10)

$$\Gamma = v\ \mathrm{Re}[K(\zeta_{a_1}-\zeta_{a_2})+\bar{K}(\zeta_{a_1}^{-1}-\zeta_{a_2}^{-1})]. \tag{2.12}$$

This equation gives the circulation on the rotor at any time when the blades are in contact. What happens when the blades are not in contact ? We know from Kelvin's circulation theorem that the vorticity is conserved in incompressible inviscid two-dimensional flow, and it follows that the circulation on either blade cannot change once they are separated. Thus the circulations carried by the blades between contacts are determined entirely by the conditions around the blades at the time of separation. For our calculations we take the circulation after separation to be equal to that on the blade immediately prior to separation; we justify this in section 2.3.

At the moment of separation the geometry is determined by the angle of incidence of the rotor, the ratio of the length of the rotor to that of the stator, and a scale factor. The circulation on the rotor may be compared with the Kutta circulation at the same angle of incidence, and the ratio will depend only on the first two factors above. It may be calculated as follows.

At separation A and F coincide, so $\zeta_{a_2} = \zeta_f$ and equation (2.2) reduces to

$$\frac{\alpha}{\pi}(\zeta_{a_2}-\zeta_{a_1})+\zeta_b-1 = 0. \tag{2.13}$$

Since the transformed vertices are on the unit circle we may write

$$\zeta_b=\exp(i\eta_b),\ \zeta_{a_1}=\exp(i\eta_{a_1}),\ \zeta_{a_2}=\exp(i\eta_{a_2}),$$

(2.14)

whereupon equation (2.13) becomes two real equations

$$\begin{aligned}\frac{\alpha}{\pi}(\cos\eta_{a_2}-\cos\eta_{a_1})+\cos\eta_b-1 &= 0,\\ \frac{\alpha}{\pi}(\sin\eta_{a_2}-\sin\eta_{a_1})+\sin\eta_b &= 0.\end{aligned}\qquad(2.15)$$

We write equation (2.15) in terms of the half angles, and the requirement that the transformed vertices are in the correct sequence round the unit circle leads to

$$\eta_{a_1}+\eta_{a_2}=\eta_b$$

and that either

$$\eta_{a_1}-\eta_{a_2}=2\sin^{-1}((\pi/\alpha)\sin\tfrac{1}{2}\eta_b)$$

or (2.16)

$$\eta_{a_1}-\eta_{a_2}=2\{\pi-\sin^{-1}((\pi/\alpha)\sin\tfrac{1}{2}\eta_b)\}$$

Equations (2.16) have valid solutions only when $0 \leq \eta_b \leq 2\sin(\alpha/\pi)$ and when this is satisfied they yield two possible solutions for η_{a_1} and η_{a_2}.

On the unit circle $\zeta = e^{i\eta}$ we may write equation (2.1) in terms of the half angles:

$$\frac{dz}{d\eta}=K'\left(\frac{\sin\frac{1}{2}(\eta-\eta_{a_2})}{\sin\frac{1}{2}(\eta-\eta_{a_1})}\right)^{\alpha/\pi}\sin\tfrac{1}{2}(\eta-\eta_b)\cos\tfrac{1}{2}\eta,\qquad(2.17)$$

where

$$K'=4K\exp\left(\tfrac{1}{2}i[(\eta_{a_2}-\eta_{a_1})\alpha/\pi+\eta_b]\right),$$

which is real. Equation (2.17) may be integrated numerically using values for η_{a_1}, η_{a_2} and η_b found as described above to give the rotor and stator lengths. The circulation may be found from equation (2.12)

and compared with the Kutta circulation. The results of these calculations are shown in figure 2.4, which gives the ratio of the interaction circulation to the Kutta circulation against the ratio of the rotor length to the stator length for various values of α, the rotor angle of incidence.

Figure 2.5 gives the rotor lift coefficient against angle of incidence for various ratios of rotor to stator length near unity, and also, for comparison, the Kutta lift coefficient.

Although it was found necessary to use a computer to integrate equation (2.17) for general cases, the asymptotic behaviour of the ratio of circulations shown in figure 2.4 may be calculated for ratios of blade lengths either much greater or much less than unity, as may the slope of the lift curve in figure 2.5. These calculations are described in detail in the next section, and confirm the behaviour shown in these figures.

Figures 2.4 and 2.5 show that the circulations developed by this interaction under zero flow conditions are lower than those imposed by the Kutta condition at the same incidence, but they are of the same order of magnitude, and the Kutta circulation is not attainable at the higher incidences owing to flow separation. Encarsia formosa uses the interaction to generate circulations twice as high as those generated by hovering insects which rely on the Kutta condition, and it therefore seems reasonable to expect that higher circulations are possible with our machine also. What can be achieved in practice will be established only by experiment.

We have now established that the model geometry will generate a circulation of sufficient magnitude to be of interest, and we can calculate the effect of any of the external flow parameters. We have shown that the interaction principle employed by the wasp may be built

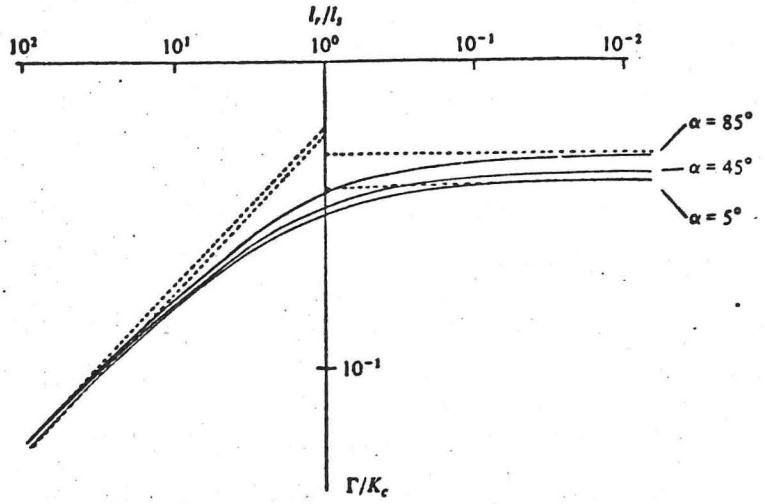

Figure 2.4. The results of the theoretical calculations. The ratio of the circulation Γ imparted by the interaction to that K_c imposed by the Kutta condition against the ratio of the rotor length l_r to the stator length l_s for various rotor angles of incidence α, with the asymptotic values for α=0° or 90° and $l_r/l_s >>$ or $<<1$ shown dotted.

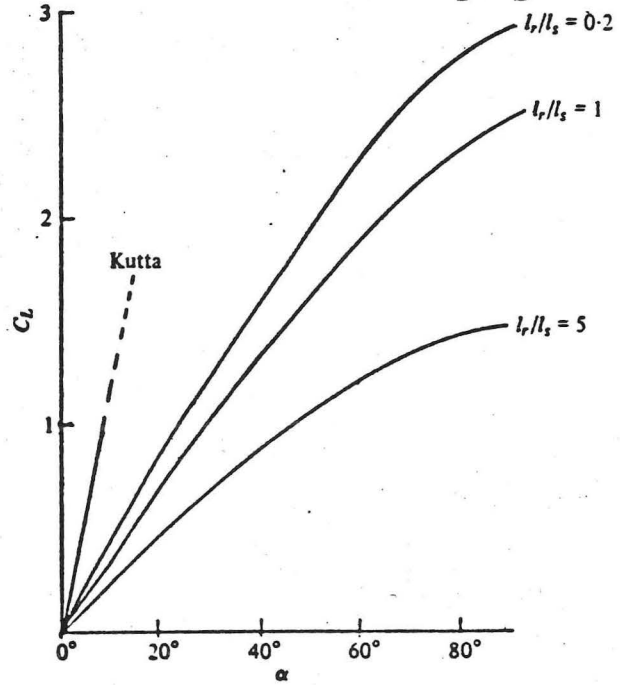

Figure 2.5. The rotor lift coefficient C_L generated by the interaction is plotted against the rotor angle of incidence α for various ratios of rotor length l_r to stator length l_s. The lift coefficient resulting from application of the Kutta condition in the absence of the stator is also shown.

into a different geometry more suitable for engineering applications, and we suggest that there will be such applications where blading designed to use interactions constructively will give a higher performance than conventional designs.

The calculation of the circulation just before separation that we have described here will apply equally to the case where the stator is not parallel to the direction of motion of the rotor. Returning to the expression for the complex potential in equation (2.5), we can see that only the component of the rotor velocity normal to its chord enters into the result. The rotor could have approached this position with any velocity component parallel to its chord. So long as α is set to the difference between the geometrical incidences of the rotor and stator, and v is considered to be the quantity making the normal velocity equal to $v \sin\alpha$, equation (2.12) may be applied to any pair of flat plates in purely translational relative motion which touch at their edges during the motion. We shall use this extension of the preceding theory in due course.

2.2 Asymptotic behaviour

The results in the previous section rely on extensive computation to find numerical values for the circulations. The methods outlined there have been successfully used to produce a computer program which will calculate the circulation under any conditions, but it is useful to be able to check the results in at least some of the cases by other methods. We shall also see that we can derive exactly the result required for modelling the experiment (section 2.6) from those already obtained, despite the fact that the geometry used in the experiment appears to be excluded from the set of geometries covered by the theory of the last section. But first let us see which special cases offer immediate results.

When the rotor is much smaller than the stator, equations (2.16) reduce to

$$\eta_{a1} + \eta_{a2} = \eta_b \ ,$$
$$\eta_{a1} - \eta_{a2} = (\pi/\alpha)\eta_b \ , \qquad (2.18a)$$

whereas when the stator is much smaller than the rotor they become

$$\eta_{a1} + \eta_{a2} = \eta_b \ ,$$
$$\eta_{a1} - \eta_{a2} = 2\pi - (\pi/\alpha)\eta_b \ . \qquad (2.18b)$$

In either case the length of the larger blade is approximately independent of the length of the smaller blade, and may be found by setting $\eta_{a1} = \eta_{a2} = 0$ in equation (2.17). Then

$$\frac{dz}{d\eta} = K' \tfrac{1}{2} \sin\eta \qquad (2.19)$$

and so the length of the larger blade is

$$\int_{\pi}^{o} \frac{dz}{d\eta} d\eta = K' \ . \tag{2.20}$$

The length of the smaller blade may be found by approximating (2.17) to

$$\frac{dz}{d\eta} = \tfrac{1}{2}K' \left(- \frac{\eta-\eta_{a2}}{\eta-\eta_{a1}}\right)^{\alpha/\pi} (\eta-\eta_b) \ , \tag{2.21}$$

which is valid for a small rotor over the range of integration necessary to find the rotor length:

$$l_r = - \int_{\eta_{a2}}^{\eta_b} \tfrac{1}{2}K' \left(- \frac{\eta-\eta_{a2}}{\eta-\eta_{a1}}\right)^{\alpha/\pi} (\eta-\eta_b) d\eta \ , \tag{2.22}$$

and a similar expression may be found for the stator length when it is much smaller than the rotor. Equations (2.18a,b) may be used to find the dependence in equation (2.22) of l_r on η_b, and this may be written as

$$l_r = \tfrac{1}{2}K' \eta_b^2 \int_t^1 \left(\frac{t-x}{x-u}\right)^{\alpha/\pi} (1-x) dx \ , \tag{2.23}$$

where $2t=(1-\pi/\alpha)$ and $2u=(1+\pi/\alpha)$, or more compactly as

$$l_r = \tfrac{1}{2}K' \eta_b^2 I(\alpha) \tag{2.24}$$

where $I(\alpha)$ will be described later.

Equation (2.12) gives the interaction-induced circulation, which

may be approximated when either blade is small.
For the small rotor

$$\arg K = 0 \tag{2.25a}$$

and for the small stator

$$\arg K = \alpha - \eta_b \ . \tag{2.25b}$$

So from equation (2.12) for the small rotor

$$\begin{aligned} \Gamma &= \tfrac{1}{2} vK'(\cos\eta_{a2} - \cos\eta_{a1}) \\ &= \tfrac{1}{4} vK'(\pi/\alpha)\eta_b^2 \ , \end{aligned} \tag{2.26a}$$

and similarly for the small stator

$$\Gamma = \tfrac{1}{4} vK'(\pi/\alpha)(\eta_b \cos\alpha + 2\sin\alpha)\eta_b . \tag{2.26b}$$

In all cases the Kutta circulation used for comparison is given by

$$K_c = \pi l_r v \sin\alpha \ . \tag{2.27}$$

We may now establish the asymptotic forms of the curves in figure 2.4. For $l_r \ll l_s$ from equations (2.24), (2.26a) and (2.27)

$$\Gamma/K_c = [2\alpha \sin\alpha\ I(\alpha)]^{-1},$$

(2.28a)

which depends only on α, and for $l_r >> l_s$ using equations (2.20), (2.24), (2.26b) and (2.27)

$$\Gamma/K_c = \frac{1}{\alpha}\,[2(l_r/l_s)I(\alpha)]^{-\frac{1}{2}}.$$

(2.28b)

These results give the gradients shown in figure 2.4 for the two asymptotic conditions. The values may be confirmed if the function

$$I(\alpha) = \int_t^1 \left(\frac{t-x}{x-u}\right)^{\alpha/\pi}(1-x)dx\ ,$$

(2.29)

where $t=\frac{1}{2}(1-\pi/\alpha)$ and $u=\frac{1}{2}(1+\pi/\alpha)$ is known. It can be shown that

$$I(\alpha)=\left(\frac{\pi}{\alpha}\right)^2\left(\frac{1+\alpha/\pi}{2}\right)^{(1+\alpha/\pi)}(2+\alpha/\pi)\,{}_2F_1\left(\frac{\alpha}{\pi},1+\frac{\pi}{\alpha};3+\frac{\pi}{\alpha};\tfrac{1}{2}(1+\frac{\pi}{\alpha})\right),$$

(2.30)

where ${}_2F_1(a,b;c;z)$ is the Gauss hypergeometric function (see Abramowitz & Stegun 1964, chapter 15). A particular case that may be calculated is the limit as α, the rotor angle of incidence, tends to zero. From equation (2.29) we obtain

$$I(0) = \tfrac{1}{8}\pi^2/\alpha^2$$

(2.31)

so for the small rotor $\quad \Gamma/K_c \to 4/\pi^2\ ,$ (2.32a)

and for the small stator $\quad \Gamma/K_c \to \frac{2}{\pi}(l_r/l_s)^{-\frac{1}{2}}\ .$ (2.32b)

In general the evaluation of $I(\alpha)$ must be done numerically, though

the work is considerably less than that involved in the general case, and the results are shown in figure 2.6, along with the corresponding asymptotic values from equation (2.28a), and the intersection with the $\log(l_r/l_s) = 0$ axis of equation (2.28b). The asymptotes for $\alpha = 0$ and 90 degrees are shown in figure 2.4. The closeness of these asymptotes reflects the nearly constant nature of $\alpha\sin\alpha I(\alpha)$ and $\alpha^2 I(\alpha)$ as shown in figure 2.6.

The lift coefficient in figure 2.5 is related to the blade circulation by

$$C_l = 2\Gamma/vl_r \tag{2.33}$$

and the dependence on α may be found for small α when the rotor and stator lengths are equal. When $l_r = l_s$,

$$\eta_b = 2\alpha/\pi \tag{2.34}$$

and so from equations (2.16)

$$\eta_{a_1} = \pi/2 + \alpha/\pi$$

and (2.35)

$$\eta_{a_2} = -\pi/2 + \alpha/\pi.$$

From equation (2.12) using the definition of K' in equation (2.17)

$$\Gamma = \tfrac{1}{2}vK'\mathrm{Re}\left(\exp[-\tfrac{1}{2}i(\{\eta_{a_2}-\eta_{a_1}\}\alpha/\pi+\eta_b)]\{\zeta_{a_2}-\zeta_{a_1}\}\right) \tag{2.36}$$

or in view of equations (2.34) and (2.35)

$$\Gamma = vK'\sin\tfrac{1}{2}\alpha. \tag{2.37}$$

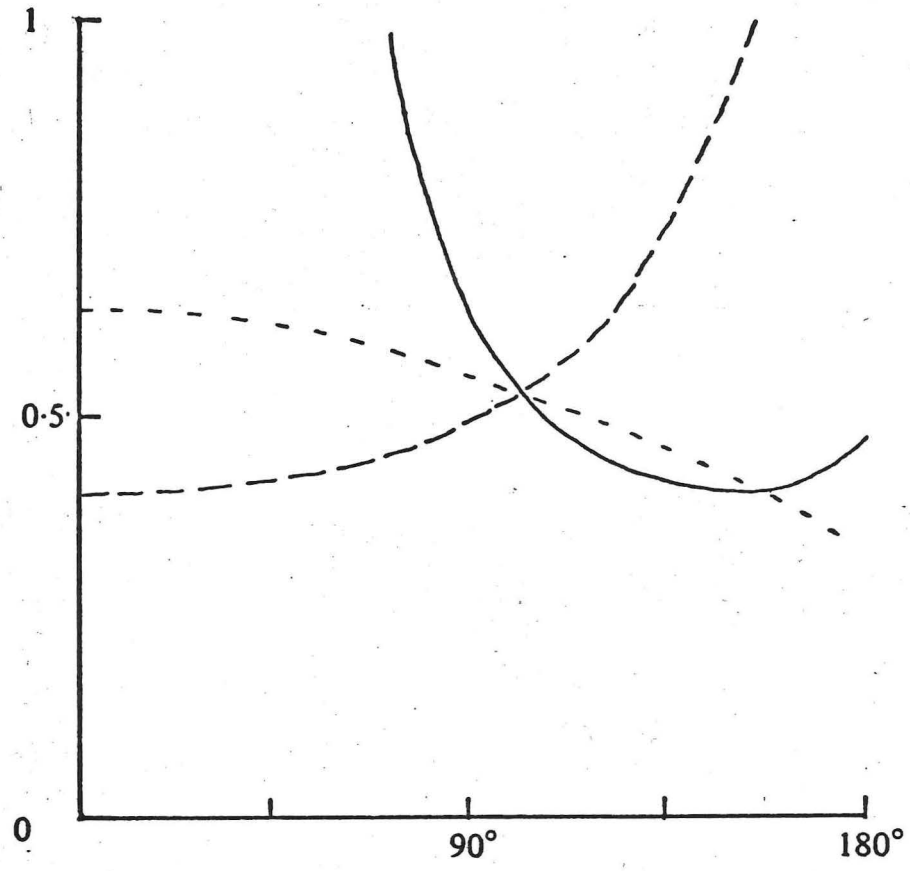

Figure 2.6. $I(\alpha)$ as defined in equation (2.29) is shown for values of α from 0° to 180°, together with $[2\alpha \sin\alpha\, I(\alpha)]^{-1}$ (broken line) and $[2\alpha^2 I(\alpha)]^{-\frac{1}{2}}$ (dotted). These last two curves represent the α dependence of the asymptotes given by equations (2.28a) and (2.28b).

For α near zero and $l_r = l_s$

$$l_r = l_s = \tfrac{1}{2}K' \tag{2.38}$$

and so equation (2.35) becomes

$$C_l = 2\alpha. \tag{2.39}$$

This is in agreement with the initial gradient of the appropriate curve in figure 2.5. When the rotor and stator lengths are not equal the calculation is more difficult. The model is symmetrical in $\alpha = 0$, so η_b/α will be stationary with respect to small variations in α near zero, and the following may be shown;

if

$$\eta_b = 2k\alpha/\pi \ ,$$

and l_r/l_s is denoted by R:

for $\alpha \ll 1$ and $R \leqslant 1$,

$$R = \frac{1-\sqrt{(1-k^2)}}{1+\sqrt{(1-k^2)}}$$

and (2.40)

$$C_l = \frac{4k \sin^{-1}k}{\pi[1-\sqrt{(1-k^2)}]}\ \alpha \ ;$$

for $\alpha \ll 1$ and $R \geqslant 1$

$$R = \frac{1+\sqrt{(1-k^2)}}{1-\sqrt{(1-k^2)}}$$

and (2.41)

$$C_l = \frac{4k(\pi-\sin^{-1}k)}{\pi[1+\sqrt{(1-k^2)}]}\ \alpha \ ;$$

Hence the initial gradients of all the curves in figure 2.5 may be found.

These calculations of asymptotes serve to confirm the results of the numerical calculations, and also yield directly the slope of the lift coefficient curve when this is plotted as a function of incidence. This slope is one of the important characteristics of an aerofoil shape.

Of particular interest to the model of the experiment described in section 2.6 is the result in equations (2.37) and (2.38). The experiment involves two blades of equal chord at zero relative incidence at the time of contact, and the moving blade travels perpendicularly to both their chords. The circulation left on the moving blade after contact resulting from their relative motion may be found from equations (2.37) and (2.38). Together they give the result that when the two blades have equal chord c and the relative incidence α is small, the circulation is $cv\alpha$, where v is the velocity of the moving blade parallel to the chord of the fixed blade. The only significant velocity for a moving flat plate is the component normal to its own chord, which is $v \sin\alpha \approx v\alpha$ here. Thus, if we call the normal component V, the circulation is Vc. This result holds for small α, and therefore continuity dictates that it must be true for $\alpha = 0$ also. The argument used to arrive at equation (2.8) cannot be applied when $\alpha = 0$, so the above discussion extends the theory of the last section, and is particularly convenient since it yields a result we shall require later.

The case when the relative incidence is zero may also be analysed at the time of contact by transforming the two plates, which at that time form one larger plate, into a circle using the standard conformal mapping. This gives the above result directly.

2.3 Blade separation

An unusual feature of the flow we are analysing here is that the boundary is not topologically continuous with respect to time. Before the blades touch there are two separate rigid bodies in relative motion, then there is one deforming body, and after separation two rigid bodies again. Unfortunately no way has been found of obtaining an exact solution to the problem when the bodies are not in contact, though we shall develop an approximate calculation method in section 2.6, but certain properties of the flows may be deduced directly from the laws of potential flow.

We shall demonstrate here that the assumption of section 2.1, namely that the rotor circulation is the same immediately after separation as it was before, is a reasonable one. But first let us consider what happens when a rotor approaches a stator.

Suppose that neither blade has any circulation on it, so the system may have been started from rest. While the blades are still some distance apart their flow fields will be approximately independent, and in the rest frame of the stator the total flow pattern will resemble figure 2.7(a). As the rotor approaches the stator its flow field will be deformed by the presence of the stator. The circulation on each blade cannot change, however, so a very high fluid velocity must be generated through the gap in the final moments before contact. The streamline pattern will be similar to that shown in figure 2.7(b). At contact the flow must suddenly be modified to that in figure 2.7(c) in which there is no flow between the blades. Accompanying this sudden change in the flow pattern is the generation of non-zero circulation on each of the blades, which may be calculated by the methods described previously.

Thus we see that at blade contact the effective blade circulations

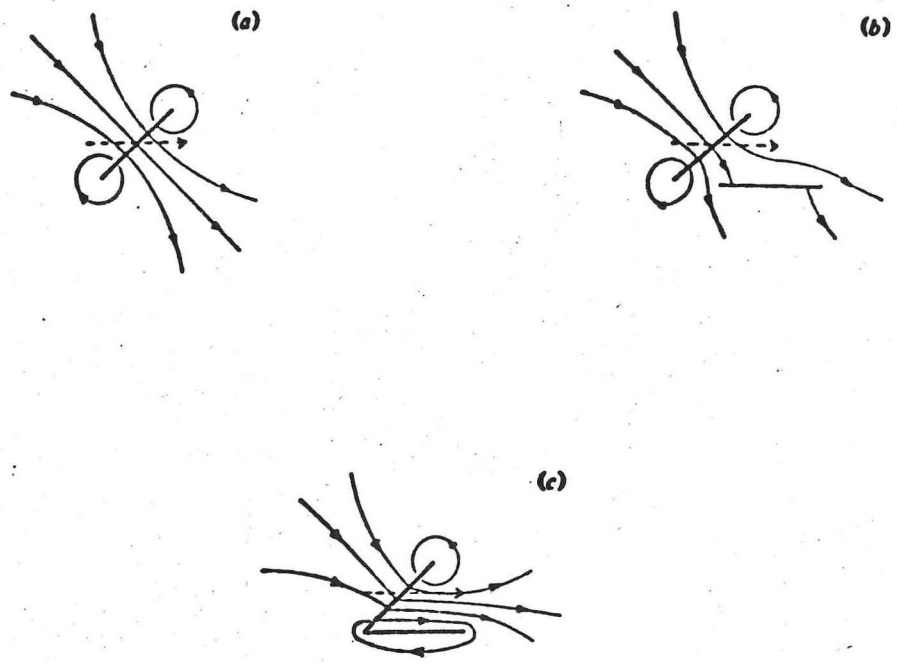

Figure 2.7. (a) The flow generated by a moving rotor distant from the stator with no circulation on either blade. (b) The flow of (a) modified by the proximity of the stator. There is still no circulation on either blade. (c) The flow after blade contact showing the circulations generated on the blades.

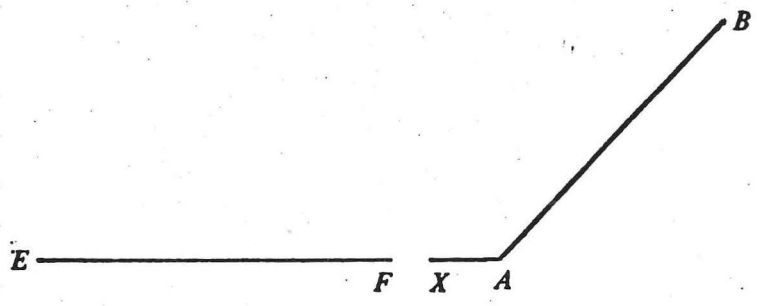

Figure 2.8. The modification for the continuity argument. A small horizontal section AX is added to the trailing edge of the rotor to move the pressure singularity at A away from the gap. The flow local to the initial, vanishingly small gap is then that through an aperture in an infinite plane boundary with the appropriate velocities parallel to the plane prescribed.

are suddenly changed as the irrotational flow of fluid between the blades is cut off. We now consider what happens to the blade circulations when they separate.

Once the blades are separated, by however small a gap, the conditions for Kelvin's circulation theorem are satisfied (Batchelor 1967, §5.2); but at the instant of separation they are not. In particular, the pressure is not single valued at the trailing edge of the rotor. The flow will therefore change instantaneously when a gap appears.

Not only is the pressure not single valued at the rotor trailing edge, but also it is singular on the lower side, as is always the case for flow round a sharp corner. To simplify analysis of the effect of a small gap on the flow, we move the gap away from the corner by adding a small horizontal section to the rotor at the trailing edge (figure 2.8). The flow near the vanishingly small gap is then approximately the flow through an aperture in a plane boundary with different fluid velocities parallel to the plane on either side. An analysis of the flow will show us how the circulation on each aerofoil is determined at the instant of separation by the asymptotic small gap local flow; once so determined it is preserved in accordance with Kelvin's theorem.

The complex potential for such a flow is

$$w = \tfrac{1}{2}(U_1+U_2)z+\tfrac{1}{2}(U_1-U_2)\sqrt{(z^2-\delta^2)}+A\log[z+\sqrt{(z^2-\delta^2)}] \qquad (2.42)$$

taking cuts in the z-plane from $-\infty$ to $-\delta$ and from δ to $+\infty$ along the real axis. This gives the potential flow caused by a gap of width 2δ in an infinite plane boundary between a stream of velocity U_1 above the plane and a stream of velocity U_2 below the plane. Note that the

constant A multiplying the only term which leads to a net flow through the gap is so far undetermined.

Each of the terms in equation (2.42) satisfies the boundary conditions on the plane exactly, and each is therefore a possible flow with this boundary. The first term is a uniform flow parallel to the boundary, and is not influenced by the presence of the gap. The second term describes the flow when the streams each side of the boundary are equal in magnitude but opposite in direction. A set of streamlines for such a flow is shown in figure 2.9(a). There is a stagnation point in the middle of the gap, and the fluxes through the gap either side of this point are equal and opposite.

These first two flows may be combined to produce any pair of stream velocities required. Figure 2.9(b) shows the streamlines for flow past a gap with stagnant fluid on the other side, while figure 2.9(c) has different velocities both in the same direction either side. All of these flows satisfy the boundary conditions and equations of motion without the third term in equation (2.42), so where does this term come in ? If we look again at figure 2.9(c) we see that there are two symmetrically positioned stagnation points near the gap, and singularities at the edges of the gap. The flow off the upstream edge of the gap is similar to that at the trailing edge of a flat plate aerofoil when the Kutta condition is not satisfied. For such an aerofoil, the attached circulation may be modified by vortex shedding to remove the singularity at the trailing edge. Similarly in the case of the flow past an aperture, we suggest that the physics of the flow will cause a flux through the gap sufficient to remove the singularity on the upstream plane. The flow will then leave this plane tangentially. When this condition is satisfied, which requires that $A=-\frac{1}{2}\delta(U_1-U_2)$ in equation (2.42), the flow in figure 2.9(c) becomes that in figure 2.9(d).

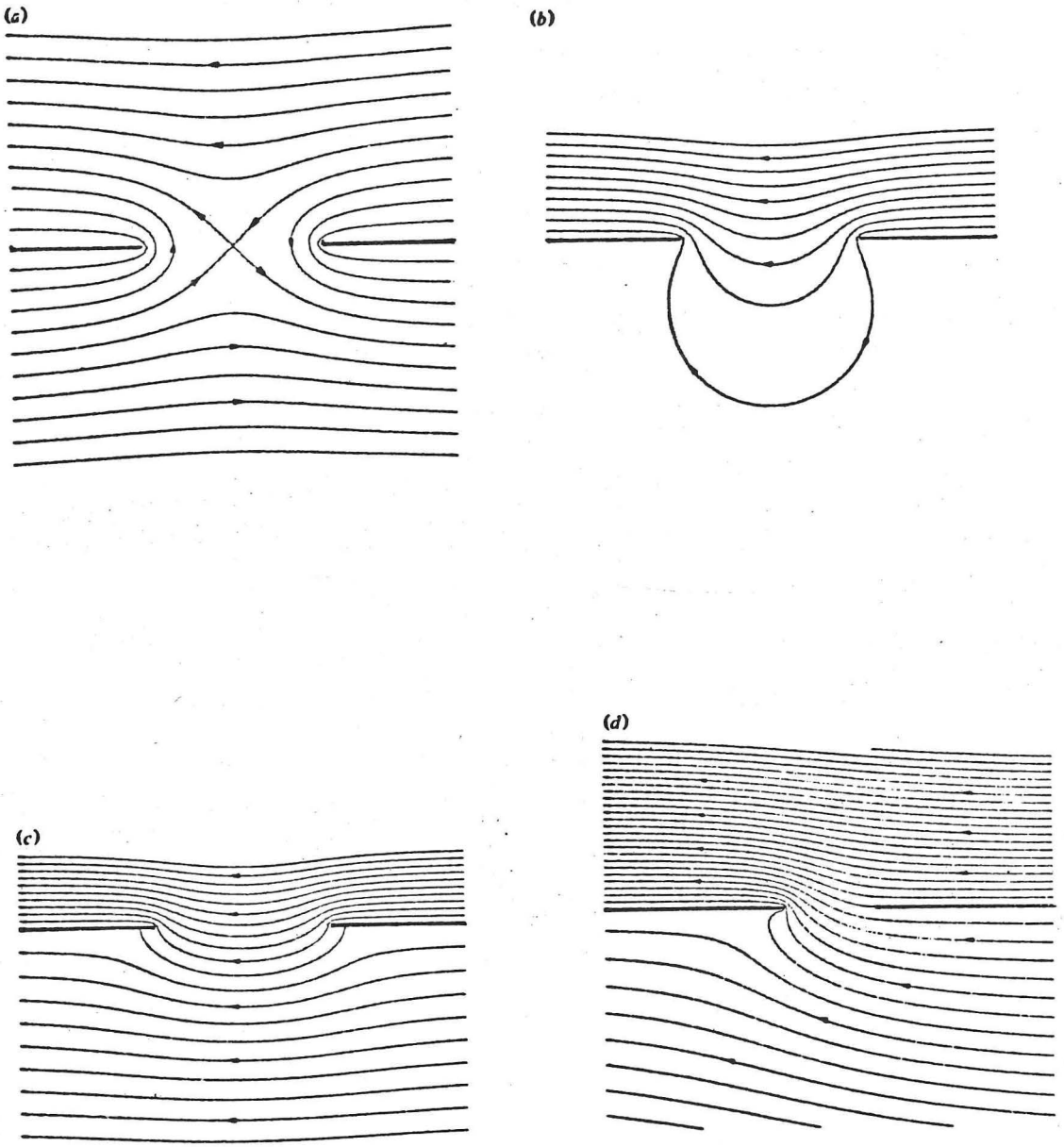

Figure 2.9. The flow near an aperture in a plane boundary: (a) with equal and opposite streams either side and no net flux through the aperture; (b) with stagnant fluid to one side and no net flux through the aperture; (c) with fluid of different velocities but in the same direction on either side, and no net flow through the aperture; (d) the flow of (c) modified by the addition of a flux through the aperture to remove the singularity on the upstream edge.

There will still be a singularity on the edge of the downstream plane, just as there is always a singularity on the leading edge of the flat-plate aerofoil.

The above argument will only apply if the flow is in the same direction either side of the gap. If the flow is in opposite directions, then we cannot say that one plane is upstream and the other downstream of the gap. It could be argued that the flux through the gap is likely to be from the high pressure side to the low pressure side, which allows the removal of the singularity on the plane upstream of the gap with respect to the faster moving fluid. The opposite flux would remove the singularity on the other plane. It seems reasonable to suggest that, whatever value the flux takes in practice, it will be of magnitude no greater than these limiting values, so, in equation (2.42),

$$|A| \leq \tfrac{1}{2}\delta|U_1-U_2| \qquad (2.43)$$

The flux through the gap may be calculated from the complex potential, and is found to be $A\pi$. This is consistent with the observation that in the far field to one side of the gap the term representing the flux approximates to a simple source of strength $A\pi$ placed next to a plane boundary, and in the far field to the other side of the gap it approximates to a simple sink of equal strength.

We have now found a description of the flow that will result when a gap appears in a plane boundary between two streams of differing velocities. As would be expected, the flow velocities are only changed significantly within a region of the same order of linear dimension as the gap, though as shown in figure 2.9(d) the streamlines may be displaced by a distance of the same scale as the gap everywhere downstream of the gap.

To estimate the effect of the appearance of the gap on the rotor circulation we must see whether letting the size of the gap tend to zero results in the limit in the same flow as is generated when there is no gap. Equation (2.42) shows that this is the case if we include the fact that A is $O(\delta)$.

Can the very small disturbance to the flow generated by an infinitesimal gap cause a finite change in the rotor circulation ? Consider the contribution to the circulation from the section of the half-plane between $(\delta,0)$ and $(x_1,0)$ on the positive real axis. The path for calculating the contribution is taken from $(x_1,i\varepsilon)$ along just above the real axis to the origin and then back below the real axis to $(x_1,-i\varepsilon)$. With no gap the integral of the velocity along the path is $x_1(U_2-U_1)$. With a gap of width 2δ it becomes $(U_2-U_1)\sqrt{(x_1^2-\delta^2)}-A\log[\delta^{-1}(x_1+\sqrt{(x_1^2-\delta^2)})]$; letting $\delta\to 0$ with $A=O(\delta)$ gives the same result. It follows that the appearance of an infinitesimal gap does not affect the rotor circulation, and thereafter Kelvin's circulation theorem ensures that no change can take place until the rotor makes contact with a subsequent stator.

It remains only to note that the addition of the small horizontal section to the rotor (AX in figure 2.8) has a small effect on the rotor circulation, in the sense that the change tends to zero with the size of the additional section. Thus it is reasonable to base our calculations on the original model as shown in figure 2.1 and to take the circulations immediately after blade separation to be the same as those just before.

2.4 Experimental apparatus

The preceding theory provides an estimate of how the circulations on two aerofoils will be affected if the blades touch while passing. The results will be modified to some extent by viscous effects. In his analysis of the wing interactions of Encarsia formosa, Lighthill (1973) considered the modification to his potential flow theory that would result from the action of viscosity. He found that the lift generating performance of the wings was actually improved by viscous effects. We wished to know how the behaviour of our model would be changed, so we decided to perform some experiments which we thought would answer this question. The results suggest that viscosity changes the mechanism and time scale of the circulation interchange, but the magnitude is not altered.

It would be ideal if an experiment could be designed to measure only this effect, and to exclude all others. Unfortunately if two blades are to touch they must also be close for a finite length of time, and during this time their potential flow fields will interact. Almost certainly this will result in a change in the conditions around their trailing edges, which will lead to vortex shedding, and hence to changes in attached circulation. These changes must be distinguished from the one we are trying to measure if the results are to tell us anything about the interaction.

One thing does distinguish the effect analysed in the previous sections from vortex shedding effects. In the idealized model the circulation changes take place instantaneously as the gap closes, whereas vortex shedding takes place on a finite time scale. The time scale used by Wagner (1925)and von Kármán and Sears (1938) to calculate the response of an aerofoil to unsteady conditions is the time for the free stream to travel one chord length past the aerofoil. This is the most obvious time scale for the potential flow view of

vortex shedding, based on satisfying the Kutta condition at all times. But vortex shedding is fundamentally a viscous phenomenon, and is therefore dependant on the behaviour of the boundary layers, which suggests that the time scale based on the free stream velocity and the boundary layer thickness might be relevant. Certainly the asymmetric thickening of the boundary layer on an aerofoil at incidence affects the application of the Kutta condition. The approach of von Kårmån and Sears has been found to give reasonable results in practice, however, and we shall be adopting their view of vortex shedding when we come to model the experiment, so we shall assume that the time scale based on the free stream velocity and the blade chord applies in our case.

In a real fluid the changes resulting from the closing gap will extend over the time the gap is being progressively closed by viscous effects, but it should not be difficult to ensure that this remains much shorter than this vortex shedding time scale.

The experiment should therefore be designed to incorporate at least two bodies capable of a relative motion which ensures that the gap between them can be closed very quickly on the vortex shedding timescale. It must also allow measurements related to the blade circulations to be made with sufficient resolution with respect to time that the two circulation changing mechanisms may be distinguished.

The apparatus specially constructed with the aim of providing this discrimination is shown in figure 2.10, and a photograph of it may be found at the end of the dissertation (plate 1). It takes the form of a wind tunnel working section, so that an external stream of known velocity may be applied. A fixed blade is mounted at zero incidence across the section, and incorporates a flexible trailing edge insert of Melinex to allow the moving blade to seal the gap without causing

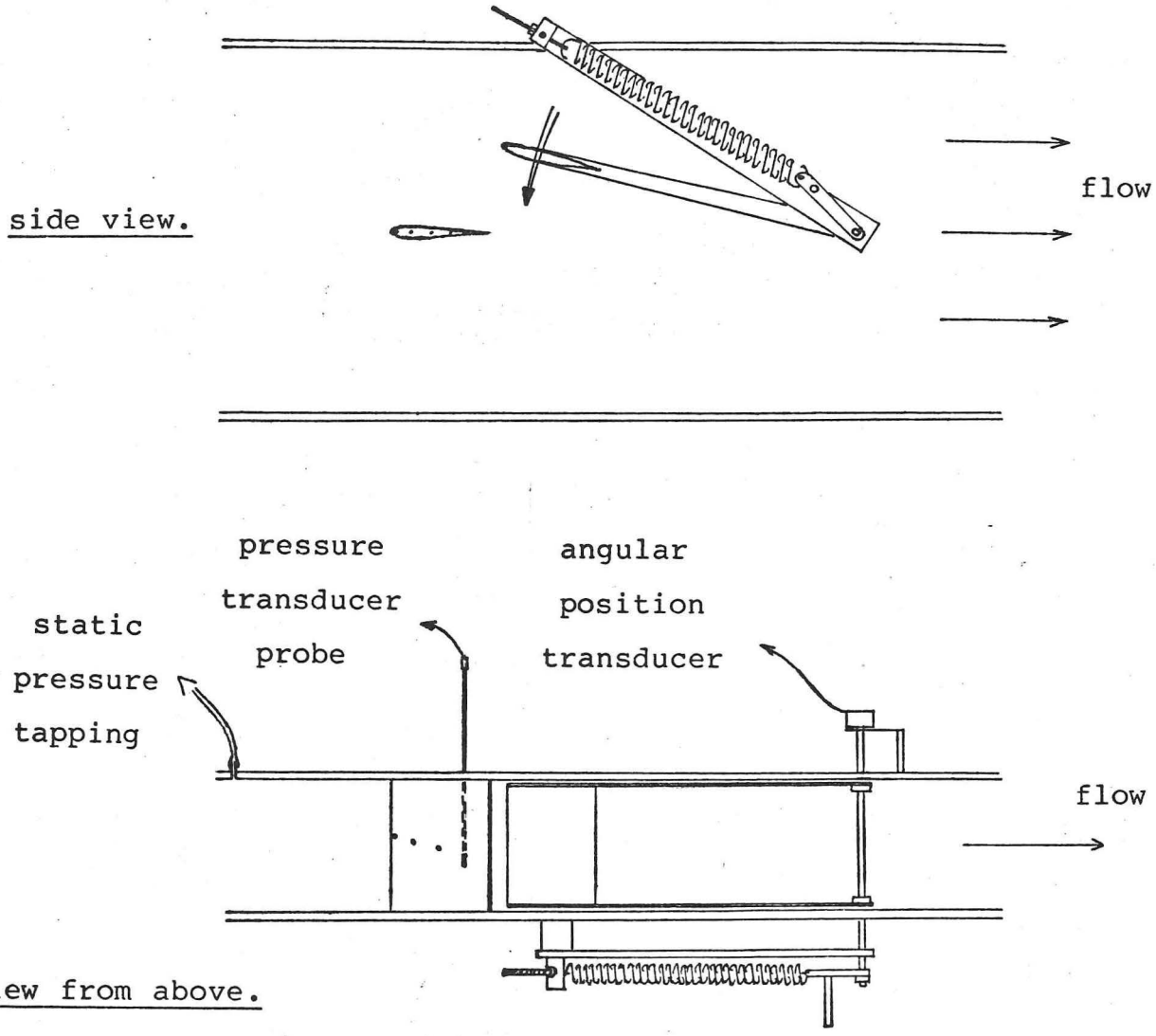

Figure 2.10. The experimental apparatus.

any damage, and minimising the mechanical noise. The moving blade is mounted on pivoted arms allowing it to swing across the tunnel behind the fixed blade. The geometry is such that the incidence of the moving blade is also zero when it is in contact with the fixed blade. The shaft on which the rotating arms are mounted is brought outside the tunnel on both sides. On one side there is an angular position transducer which supplies information on the position and velocity of the moving blade, and on the other side a lever is connected to the shaft with a handle and a large centering spring.

The fixed blade was formed with spanwise holes, and pressure tappings to the surface, positioned as shown in figure 2.11. The holes were 3 mm in diameter, allowing the insertion of the pressure transducers. The tappings were approximately 1 mm in diameter, ensuring that the frequency response would not be restricted by the constriction, and matching the aperture in the pressure transducer. The tappings were staggered down the aerofoil as shown in figure 2.11 to keep downstream tappings out of the wake of any upstream tapping.

The 'Gaeletic' pressure transducer consisted of a steel tube 18 inches long with one end closed and a 1 mm hole in the side near the closed end. Inside the tube opposite the 1 mm hole was a rectangular diaphragm with a strain-gauge sensor. The electrical connections to the sensor ran down the tube to the other end, which was open to atmospheric pressure. Thus the sensing element could be positioned immediately under a pressure tapping on the aerofoil, and the volume of enclosed air would be sufficiently small to ensure that with the size of aperture the frequency response of the transducer would be flat up to about 3 kHz. This was quite sufficient for our measurements.

The existing amplifier for the pressure transducer was DC coupled with a potentiometer for setting the zero level. The transducer output tended to drift over a period of time, making frequent adjustment

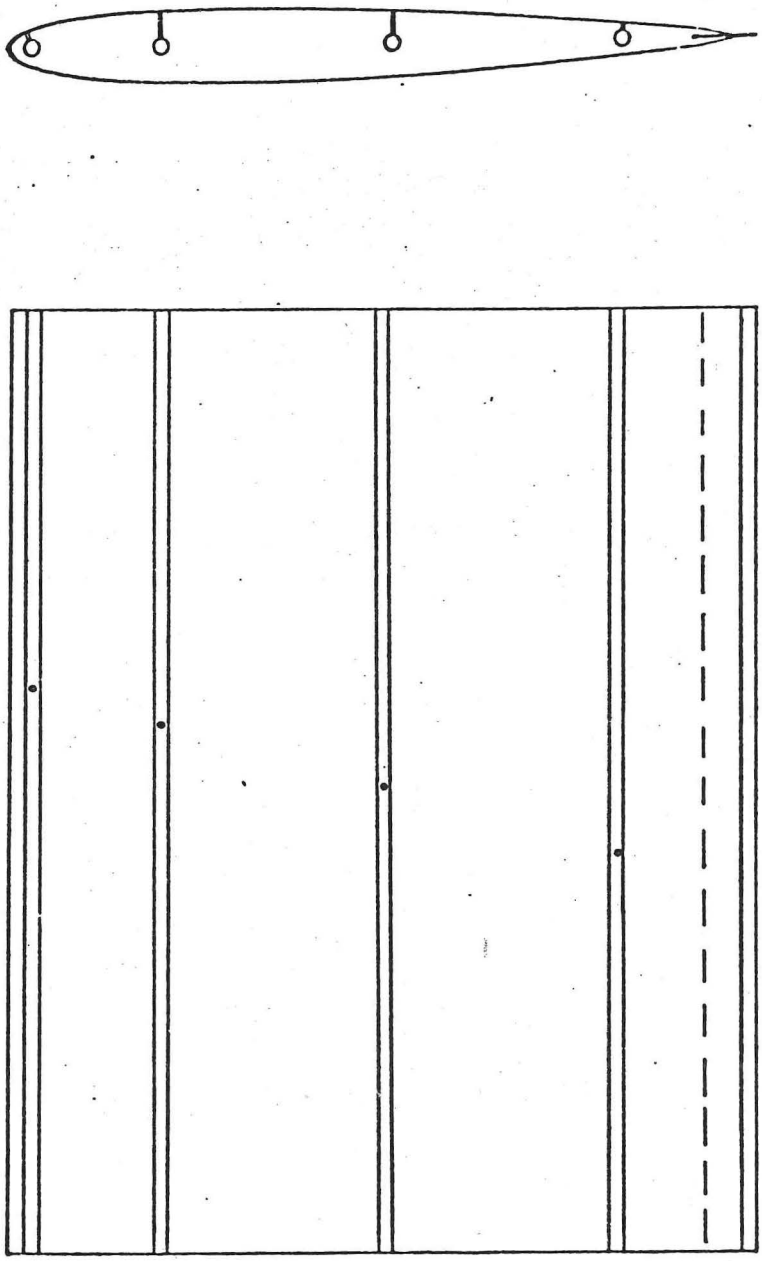

Figure 2.11. Details of the fixed aerofoil. The moving blade has the same section but no holes or tappings for the pressure transducer, and no flexible trailing edge insert.

of the zero necessary. Since we did not require a response down to DC, and the drift would have made calibration at DC impossible anyway, it was decided to build a new amplifier with a high pass filter at about .1 Hz and a low pass filter at about 1 kHz. The amplifier is described in detail in appendix 1, and was successful in making all adjustments unnecessary once the gain had been set to suit the particular transducer used.

The output from the pressure transducer amplifier was connected to an analogue-digital converter (ADC) on a microprocessor system built (as a hobby) by the author, as was the output from the angular position transducer. The microprocessor system is described in appendix 2, and with the ADC used was capable of logging data on one channel at up to 6 kHz. This rate was used only during pressure transducer calibration, as will be described later. During the tests the pressure and position voltages were logged every 1 ms. The values were held in memory for the duration of a test, then they were stored on floppy disk for later processing.

The original intention was to use a mechanical latch to hold the arm off centre against the spring. This latch would then be released and the arm would oscillate across the tunnel while readings were taken from the pressure and position transducers. Tests showed that the release generated too much mechanical noise which was picked up by the pressure transducer, so instead the moving blade was oscillated across the tunnel by hand. The natural resonance of the centering spring and blade mass ensured that the oscillations were closely periodic, and the position transducer information gave the exact position history of the system. This proved to be an effective experimental procedure.

The pressure transducer was inserted in the tube passing under the desired pressure tapping in the fixed aerofoil, and the output

was observed on an oscilloscope to check that all was well. The alignment of the hole in the pressure transducer tube with the tapping in the aerofoil surface was done visually, this being made straightforward by the relatively large size of the tappings and also because the aerofoil had been deliberately made of transparent material in the region around the tappings for this purpose.

Once the pressure transducer was in place the tunnel motor was started and the speed adjusted to the desired level. The speed was measured by comparing the static pressure at a tapping in the side of the working section at the upstream end with the laboratory atmospheric pressure using an inclined manometer filled with methylated spirits. The tunnel was of the open circuit type. The speed measurement was checked for validity after the tests by measuring the speed with a pitot-static tube mounted on a traverse. This was not possible with the working section used for the experiments described here, but an existing working section of the same dimensions already had the necessary traverse gear installed, and this was used for the tunnel calibration.

When the tunnel speed was satisfactory the oscillations of the moving blade were started. The pressure transducer output was monitored on an oscilloscope, and when all appeared to be working properly the data logging system was started. The two transducer outputs were then digitised and stored every 1 ms for 8 seconds, then the data logging system signalled that it had finished and the run was over.

The angular position transducer was calibrated statically by noting the digital output from the ADC at various positions and measuring these positions with a rule. The transducer specification was to a linearity of 0.5 percent of full scale.

The pressure transducer was more troublesome. The original specification of a flat frequency response to 3 kHz was reduced by the new amplifier to .1 to 1 kHz. Because the amplifier was not DC coupled calibration with static pressure was not possible though, for reasons stated previously, the DC drift of the transducer would have made this impossible even if the amplifier were DC coupled. What was required was a known source of oscillatory pressure. The device used was a Bruel and Kjaer pistonphone, intended for the calibration of B&K condenser microphones. This device contains a battery driven elecric motor which drives two pistons through a known volume displacement in an enclosure of known volume. Thus a repeatable pressure field is set up in the enclosure, which varies only with atmospheric pressure. Calibration data for the atmospheric pressure correction are provided with the instrument.

The pistonphone has adaptors for the various sizes of microphone to ensure that the enclosed volume is correct. Our special purpose pressure transducer was not catered for of course, so it was necessary to improvise. The end of the transducer was made to project through one of the microphone adaptors, and the gaps sealed with 'blue-tack'. The pressure transducer tube had to project about 2 cm beyond the adaptor to ensure that the hole above the sensor would be inside the chamber. This meant that the transducer would displace a volume of .2 cc inside the chamber, or somewhat less in fact since the tube was hollow and opened through the hole above the sensor. The capacity of the pistonphone enclosure was 20 cc according to the manufacturer's specification, so the volume change caused by the pressure transducer was less than 1 percent, and hence the calibration error would also be less than this value.

The pistonphone operated at a frequency of 250 Hz. The calibration of the pressure transducer was performed by mounting the transducer in the pistonphone as described above, turning on the pistonphone,

then recording the transducer output voltages on the data logging system at the maximum data logging rate of 6 kHz. This data was then stored for future analysis. Figure 2.12 shows one complete sample of the calibration data, and also gives an idea of the transducer noise level, which makes deducing the amplitude of the response to the 250 Hz signal more difficult than might at first be thought. The calibration tests were performed at various times throughout the tests, to see if the transducer sensitivity underwent any long term variation. This was not found to happen over the duration of the testing period.

The calibration data was processed by a spectral analysis program, and I am indebted to Colin Ross of the acoustics group for his assistance here. The problem is to establish the response of the transducer to a pure 250 Hz pressure from the output data, which contains a significant amount of noise. The program used produces a plot of the power spectrum of the data, and will calculate the total power in any frequency band specified. The input signal will produce a response with the power concentrated in a band around 250 Hz, whereas the noise will be spread more evenly over the whole frequency space. Thus if we calculate the power in a series of increasingly narrow bands around 250 Hz we expect to get all of the true signal, but less and less of the noise. This will continue until the band is so narrow that we start to exclude some of the signal.

It happens that for the calibration data the transducer noise at around 250 Hz is low enough to establish the signal power accurately, as can be seen from figure 2.13 whch has been normalised to adjust the signal power to its nominal value of 124 dB. The normalising factor gives us the calibration constant for the pressure transducer - amplifier combination as 71 Pascals per Volt.

The spectral analysis program can be used to calculate the total

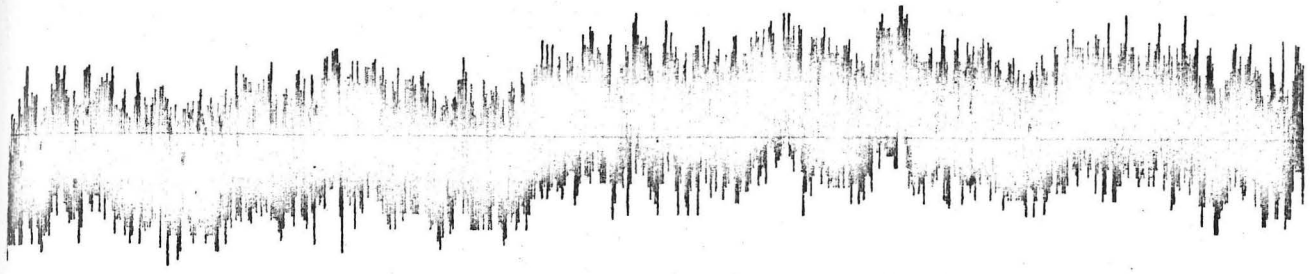

Figure 2.12. The raw pressure transducer calibration data.

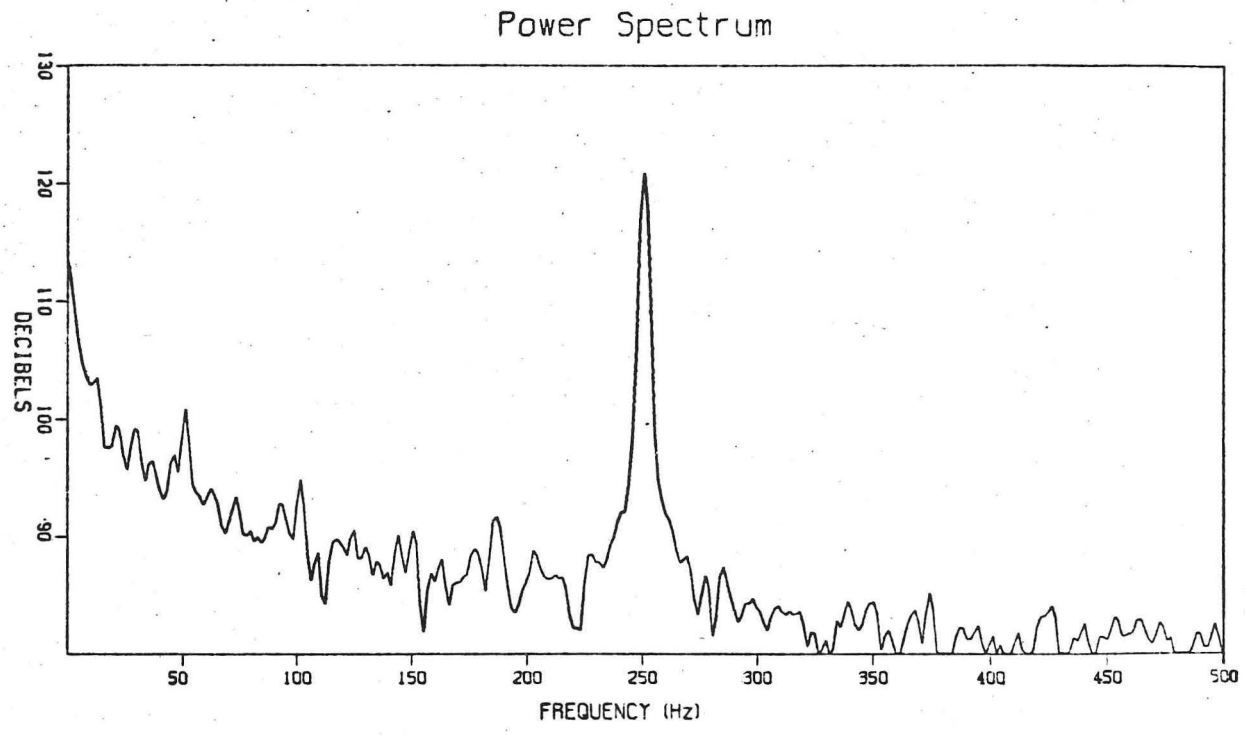

Figure 2.13. The power spectrum of the pressure transducer calibration data, normalised to give 124dB at the applied frequency.

power in the calibration signal, and the difference between this and the power in a narrow band around 250 Hz must be the noise power. The result is that the signal to noise ratio of the calibration data is about three, corresponding to a noise level of about half a volt, equivalent to a noise pressure of 35 Pascals. The spectral distribution of this noise power can be seen in figure 2.13.

This noise level is high, but not high enough to mask all the effects of interest. Some of the characteristics of the transducer output were visible on the oscilloscope during the experiments. The noise level need only be reduced by a factor of ten or so for all the effects to be visible, and with digitised and periodic data this can be achieved without much trouble, as we shall see in the next section.

2.5 Experimental results

The experiments described in the previous section produced as output sets of data giving the voltages from the pressure transducer amplifier and from the angular position transducer every 1 ms for just over 8 seconds, 16384 data values in all. An example of this crude data is shown plotted in figure 2.14, and of course looks exactly like the corresponding trace on the oscilloscope. The recordings were taken separately for each of the four pressure transducer positions on the top of the fixed blade, and under various flow conditions. As has been explained previously the noise level in the pressure transducer data is fairly high. The position transducer data can be seen to be close to sinusoidal.

In order to reduce the noise level in the pressure signal, it is useful to perform some averaging on the data. This is possible since the data is periodic. The point where we want highest resolution is that where the blades are in contact, or where the moving blade is at zero incidence. The output from the position transducer at this point may be found statically from the apparatus. The moving blade will pass through this position twice per cycle, once moving upwards past the stationary blade and once moving downwards. By treating these two cases separately we have information on the pressure on the same side as the approaching blade from the downwards motion, and on the opposite side from the upwards motion. Since the incidences of both blades have been chosen to ensure symmetry, the pressure on the top of the blade during the upward motion will be the same as that on the bottom during the downward motion. We may therefore infer the pressure on the bottom of the fixed blade, where measurements are not being taken, from those on the top measured during the other half of the cycle.

The pressure data sets are treated as follows. First the

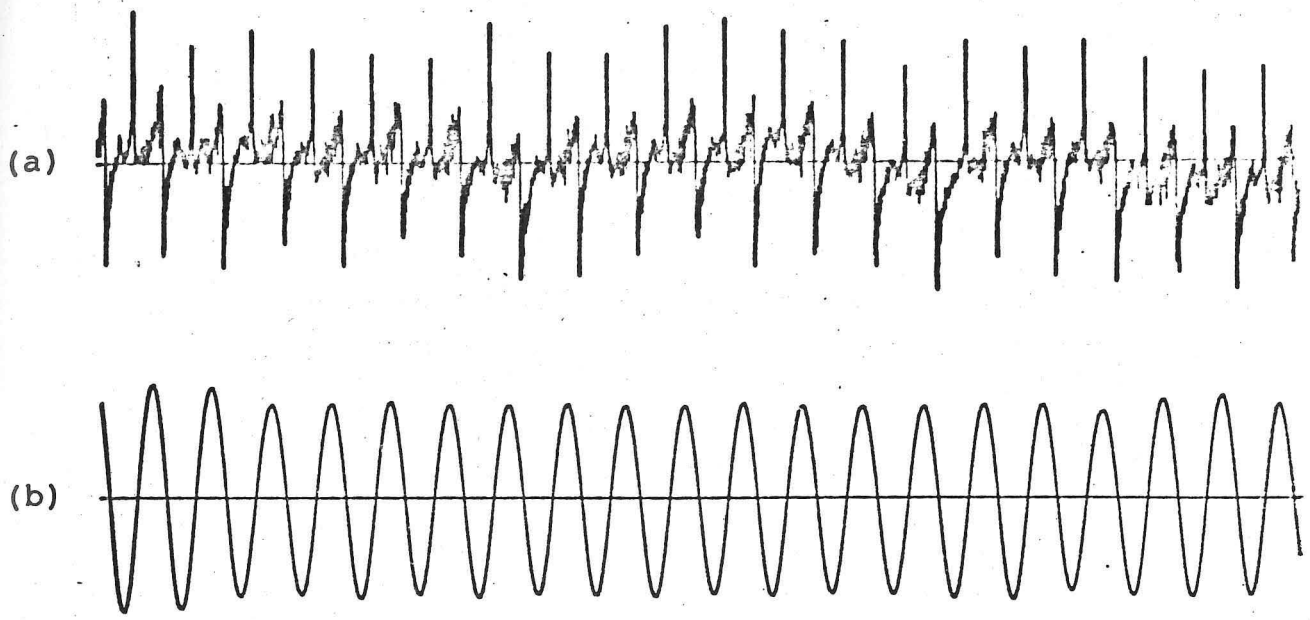

Figure 2.14. An example of the unprocessed data from the transducers. (a) The pressure transducer data. (b) The angular position transducer data.

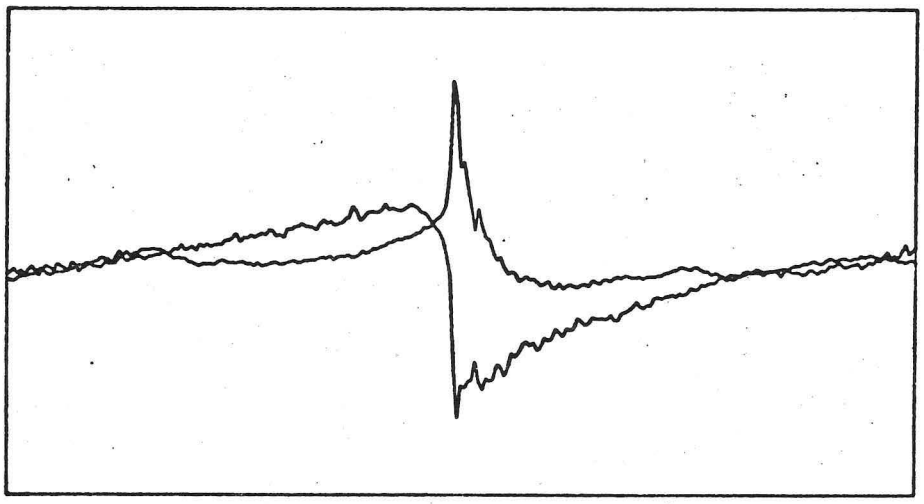

Figure 2.15. The pressure transducer data shown in figure 2.14 after averaging.

corresponding position data set is scanned to find the places where the moving blade passes through zero incidence. These places are remembered, and split alternately into two sets corresponding to upwards or downwards motion. All the upwards points are then taken, and the corresponding pressure values averaged. Then all the pressure values taken 1 ms before zero incidence during the upwards motion are averaged, and then all those 1 ms after, 2 ms before, 2 ms after, 3 ms before, 3 ms after, etc. The values taken during the downwards motion are treated similarly. The averaging is performed over a total span of data ensuring an overlap between the upwards and downwards curves, so that none of the information is lost.

An example of the results of this averaging can be seen in figure 2.15. Here the pressures recorded from the pressure tapping nearest the trailing edge are shown against time. This is the result of the averaging process applied to the raw data from figure 2.14. The noise is still visible, but no longer masks the major characteristics of the results. The total timespan shown on this figure is 250 ms, and the height of the box corresponds to the total range of the transducer amplifier output.

To prepare these results for presentation now requires only that they be normalised to some standard. The obvious normalisation for the pressure p is to convert to a pressure coefficient C_p based on the wind tunnel velocity U, where if ρ and p_a are the air density and pressure respectively, $C_p = (p-p_a)/\frac{1}{2}\rho U^2$. This will lead to values for C_p which may be compared with well known values for aerofoils at incidence. Unfortunately the pressure coefficient will not be independent of the stream velocity, as it is approximately for the isolated aerofoil, since the transverse velocity of the moving aerofoil influences the unsteady pressures. If the wind tunnel velocity is U and the moving aerofoil velocity scales on v, then the velocity disturbance on the surface of the fixed aerofoil caused by

the motion of the moving blade will scale on v also, and the pressure will vary like the square of U+kv. The unsteady part of the pressure (which is all that has been measured) will then vary like kUv, since v<<U in the experiment. The velocity disturbance on the fixed aerofoil generated by the circulation on the moving aerofoil at incidence will however scale on U, restoring the standard pressure coefficient as the natural normalisation. Since the latter effect is responsible for the larger part of the unsteady pressure, the standard pressure coefficient has been used for presentation of the results.

The normalisation of the other axis also presents some problems. This axis represents time, since the readings were recorded at fixed 1 ms time intervals. The predominant time related variable in the experiments is the period of oscillation, as can be seen from the raw data (figure 2.14). This time is not particularly relevant to the phenomena of interest to us, however, since the oscillation is just a convenient mechanism for generating the relative motion. It would have suited us better to have the blade pass at a steady velocity right across the wind tunnel, but no mechanism was found that would do this satisfactorily.

The circulation exchange takes place instantaneously, at least in the simple theory, so there is no time scale suggested there. The most convenient candidate is therefore the vortex shedding timescale, which we have taken to be the length of time it takes the free sream to travel one chord length past the aerofoil (see the disussion at the beginning of the last section). This will therefore be the timescale on which any deviation from the Kutta circulation, which may be caused by the circulation exchange mechanism, will decay. In our tests, where the tunnel speed was up to 20 m/s and the chord was 15 cm, this length of time is of the order of 10 milliseconds. The work of Wagner (1925) and von Kármán and Sears (1938) suggests that deviations from the Kutta circulation will take around five times

this long to reduce to a few percent of their initial value, depending on the circumstances in which they started. Thus any deviations arising in our tests should last for tens of milliseconds, and be clealy visible from samples taken at 1 ms intervals.

The results are therefore presented as shown in figure 2.16. 250 ms of calculated averages are shown, with the times marked corresponding to a particle in the mean stream being ten chords upstream, exactly at, and ten chords downstream of the fixed blade leading edge.

The results shown in figure 2.16 are those for a tunnel speed of 19.5 m/s. It can clearly be seen that all the pressures change very rapidly at the time the moving blade comes into contact with the fixed one. This change is what the simple theory would lead us to expect. Throughout the motion the boundary conditions on both blades must be satisfied, and the blades shed vorticity to prevent pressure singularities developing at their trailing edges. The rate of adjustment is limited, however, because the shed vorticity moves away from the trailing edge only at the velocity of the free stream. While it is still close to the trailing edge the shed vorticity generates a velocity field controlling the subsequent vortex shedding rate.

The approaching blade leading edge causes a high velocity flow through the space between the blades, which is suddenly cut off when the gap is sealed. Even though viscous effects will make this sealing of the gap take a finite time, it will be very fast on the vortex shedding timescale. The result will be a pressure impulse, slightly spread in reality. This will be associated with an instantaneous change in velocity, and not only the velocity through the gap. It has been shown how the velocity potential may be thought of as the pressure impulse required to set fluid into the corresponding motion from rest(see Batchelor 1967, section 6.10). It follows that a pressure impulse applied to a moving fluid is equal to the change

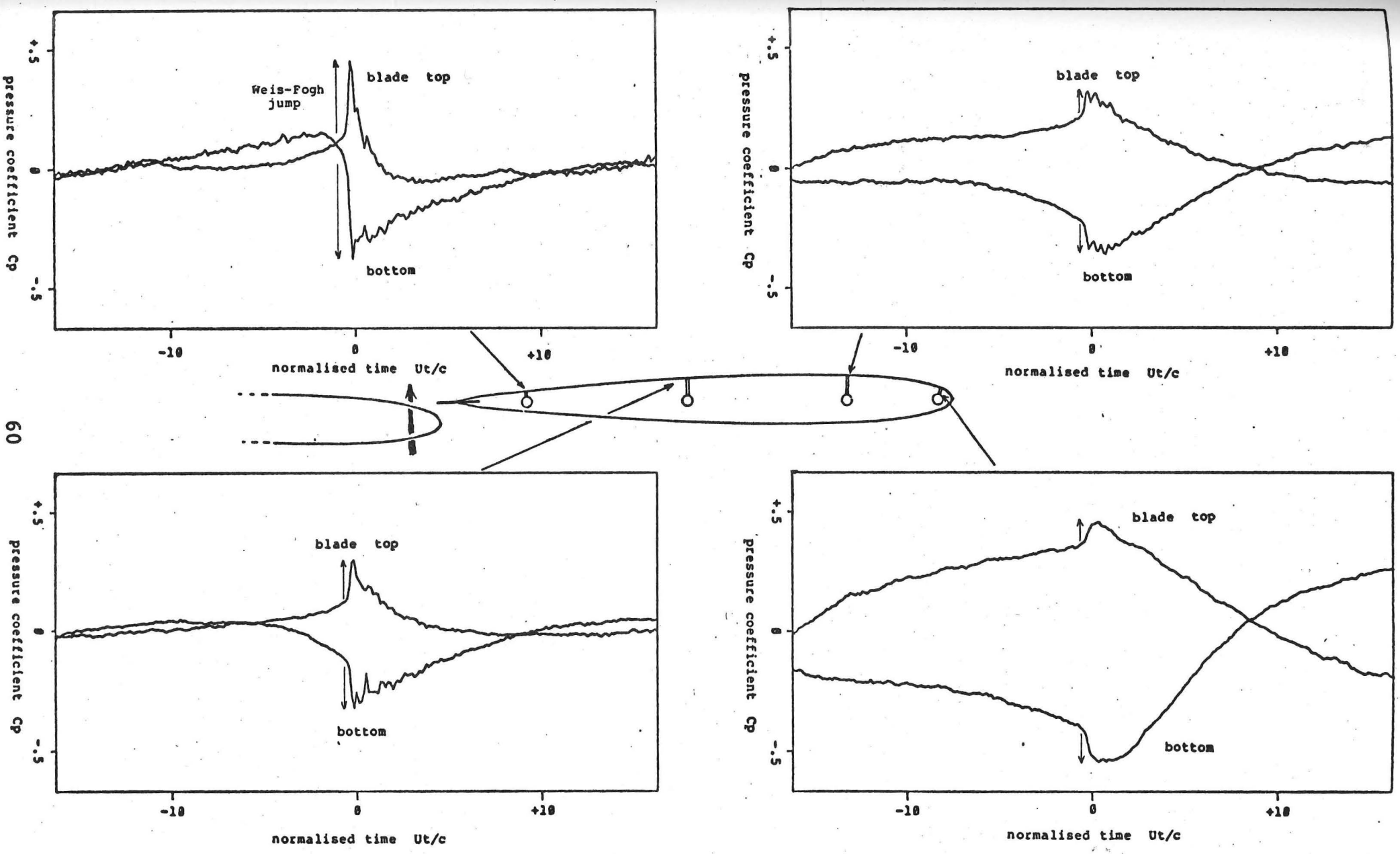

Figure 2.16. The averaged results at 19.5 metres per second.

t is time, c the blade chord, and U the free stream speed.

in velocity potential between two motions. The closing of the gap causes a pressure impulse by cutting off the flow through the gap, and it causes the fluid velocity to change not only through the gap, but elsewhere as well, and in particular along the surface of the aerofoil. A change in the fluid velocity along the aerofoil surface will result in a change in the pressure there, and this is what we see in the results shown in figure 2.16.

The pressure impulse itself will also register on the transducer. Ideally it should appear as a delta function, that is a spike of infinite height and zero thickness. The spreading out over time caused by viscous effects will make the spike finite in height and thickness. The limited frequency response of the transducer and amplifier would ensure that the measured value was finite in any case. The area under the theoretical delta function, or the change in the velocity potential, should not be affected by these smearing out processes, however, so we might expect to see some sort of spike on the final pressure curves. The high pressure curve in figure 2.15 resembles what we might expect. The pressures either side of the spike are roughly equal, and it is possible to conclude that the only thing that has happened is a pressure impulse at the time of contact. The same is not true of the low pressure curve in the same figure. There the pressure appears to change significantly across the time of contact, and then decay on the vortex shedding timescale back towards its original value. This looks most likely to be caused by a change in fluid velocity away from the value predicted by application of the Kutta condition, and the timing of the change suggests that this has been caused by the contact between the two blades.

Of course there are other possible explanations of the observed rapid pressure fluctuations in figure 2.15. The leading edge of the moving blade is passing very close to the trailing edge of the fixed blade, and the high velocities at the leading edge might cause

significant vortex shedding to take place. Alternatively the presence of the leading edge could affect the pressures by its blocking effect, or the motion of the blade might generate pressures through the virtual inertia term. Because it is not possible to separate all these effects in the experiment, a detailed break-down of the important contributions to the results must await the modelling of the experiment, which will be described in the next section.

The sets of measured pressure responses are presented for four test conditions. The first of these has already been introduced in figure 2.16, where the tunnel flow speed was 19.5 m/s.

The curves for all the transducer stations display the same rapid change in pressure at the time of contact, with the amplitude of the change reducing towards the leading edge of the blade. The pressure difference across the blade including all effects increases towards the leading edge, as would be expected since the vorticity distribution on an isolated aerofoil displays increasing vorticity towards the leading edge.

The curves look approximately symmetrical except for the one from the station nearest the trailing edge, in that the positive pressure deviation on one side of the blade is matched by the negative deviation on the other side. A vorticity distribution on the fixed aerofoil will generate a symmetrical velocity deviation, and this will lead to an approximately symmetrical pressure deviation except right at the leading edge where motion of the stagnation point will complicate matters. The asymmetry of the trailing edge pressures must therefore be caused by something other than the circulation on the fixed blade, and the only possibility is the circulation on the moving blade.

The blocking effect of the moving blade cannot be responsible since it would be symmetrical about the time of contact. We can see

at least in elementary terms how the moving circulation might cause the asymmetry at the trailing edge. When the moving blade is above the mid-point, its incidence causes a circulation to be set up which retards the flow beneath the blade and accelerates the flow above. The fixed blade is below, and the retardation will result in a pressure increase on both sides of the blade. As the moving blade passes through the mid-point its geometric incidence goes through zero, but the downward motion maintains a positive aerodynamic incidence for some time past the mid-point. Thus the circulation keeps the same sign through the centre, and the fixed aerofoil passes into the region of accelerated flow above the moving aerofoil. The pressures on both sides will then drop. The overall effect will be that the mean pressure will display a sawtooth behaviour, increasing steadily throughout the motion except when the blades pass when it will drop quite sharply. The effect will be most pronounced near the trailing edge of the fixed blade, as the test results show.

The second set of results were effectively a rerun of the first, and are shown in figure 2.17. The tunnel speed was 19.3 m/s. The noise level is significantly higher, for reasons which are not apparent. It is most likely that some electrically noisy equipment was being used nearby at the time of these tests. The curves are very similar to the earlier tests, as we would hope, but they also show some odd descrepancies. The most obvious of these is that the pressure difference across the blade during the period leading up to contact is not the same. The first tests (figure 2.16) displayed a pressure difference opposite in sign during this period to that after contact at the station nearest the trailing edge, whereas here the pressure difference is near zero. The second transducer position shows a similar discrepancy. The third curve shows a difference of the opposite sense, which suggests that these variations may be related to the motion of the moving blade. It should be remembered that each transducer position was recorded in a separate test, and the motion

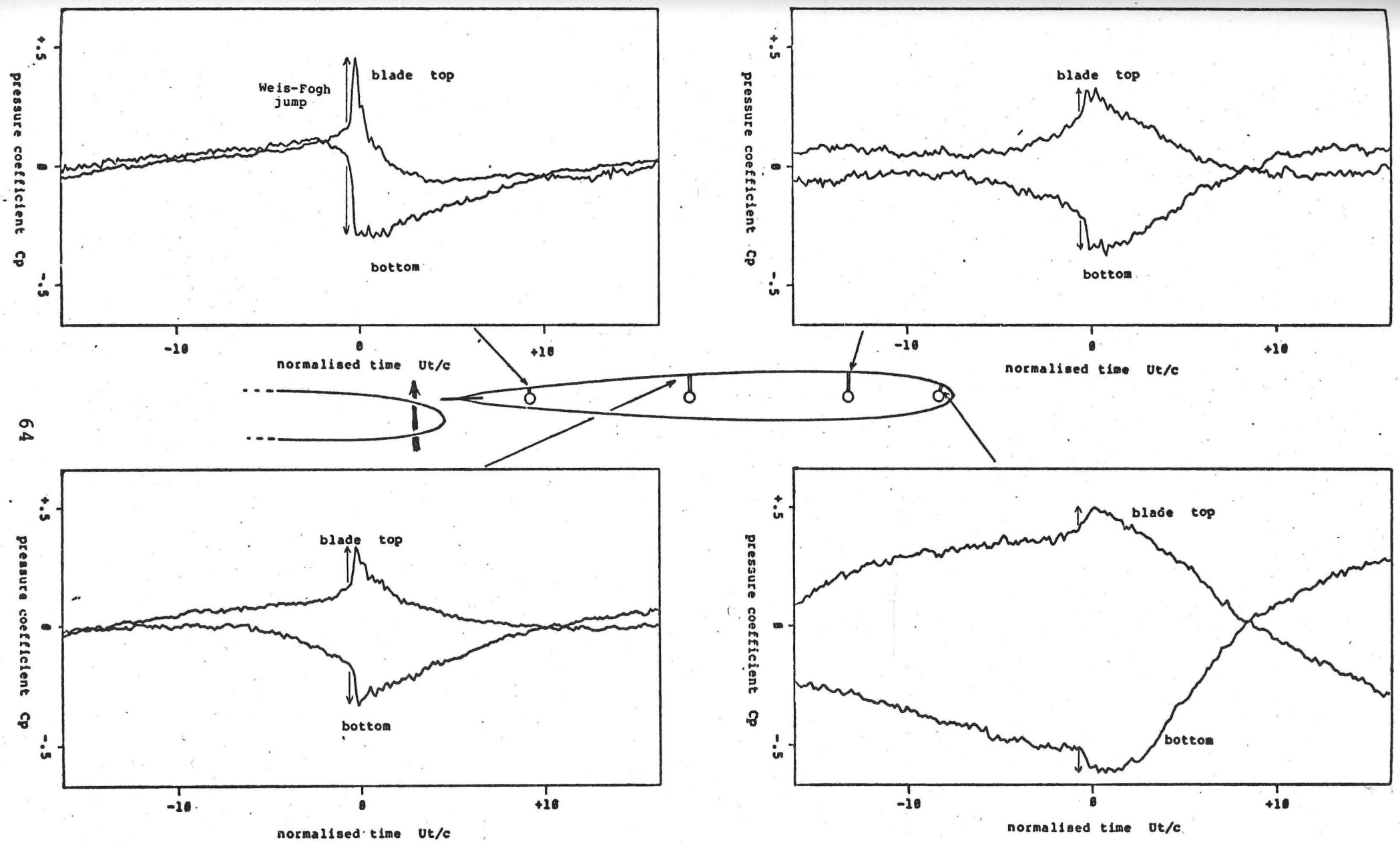

Figure 2.17. The results at a tunnel speed of 19.3 m/s. The conditions are similar to those in the previous test, and the differences are discussed in the text.

of the moving blade could not be repeated exactly for each test. The exact motion was recorded, however, and since a full interpretation of these curves requires theoretical modelling, this should not be considered to be too important.

The main features of figures 2.16 and 2.17 are not at variance, which are the shapes of the curves at and after the time of contact.

The third set of results are shown in figure 2.18. The tunnel speed here was 13 m/s, and the same effects are visible. The noise cancellation by averaging has not been so successful, since the actual pressures recorded were lower. The normalisation in terms of the pressure coefficient has increased the size of the curves, however, since the amplitude is related to the velocity of the moving aerofoil, which has not been significantly changed, as well as to the tunnel speed.

The curves retain the same points of interest, displaying the rapid pressure changes at contact. The frequency of oscillation has increased slightly, because the aerodynamic loads are reduced with the lower tunnel speed. These forces by and large operate away from the centre of oscillation, and therefore tend to increase the period.

Finally it was thought desirable to see what the influence of the flexible trailing edge insert was, by removing it and repeating the first test. This will have several consequences. Foremost from our point of view is that it would no longer be possible to seal the gap between the blades completely. The gap would be partially sealed by viscous effects if it were small enough however, and the presence of the wake from the fixed blade should increase this effect. Secondly, the streamwise separation of the two blades would be increased, reducing the interaction of their potential flow fields. Again a detailed model is necessary to interprete the results, which

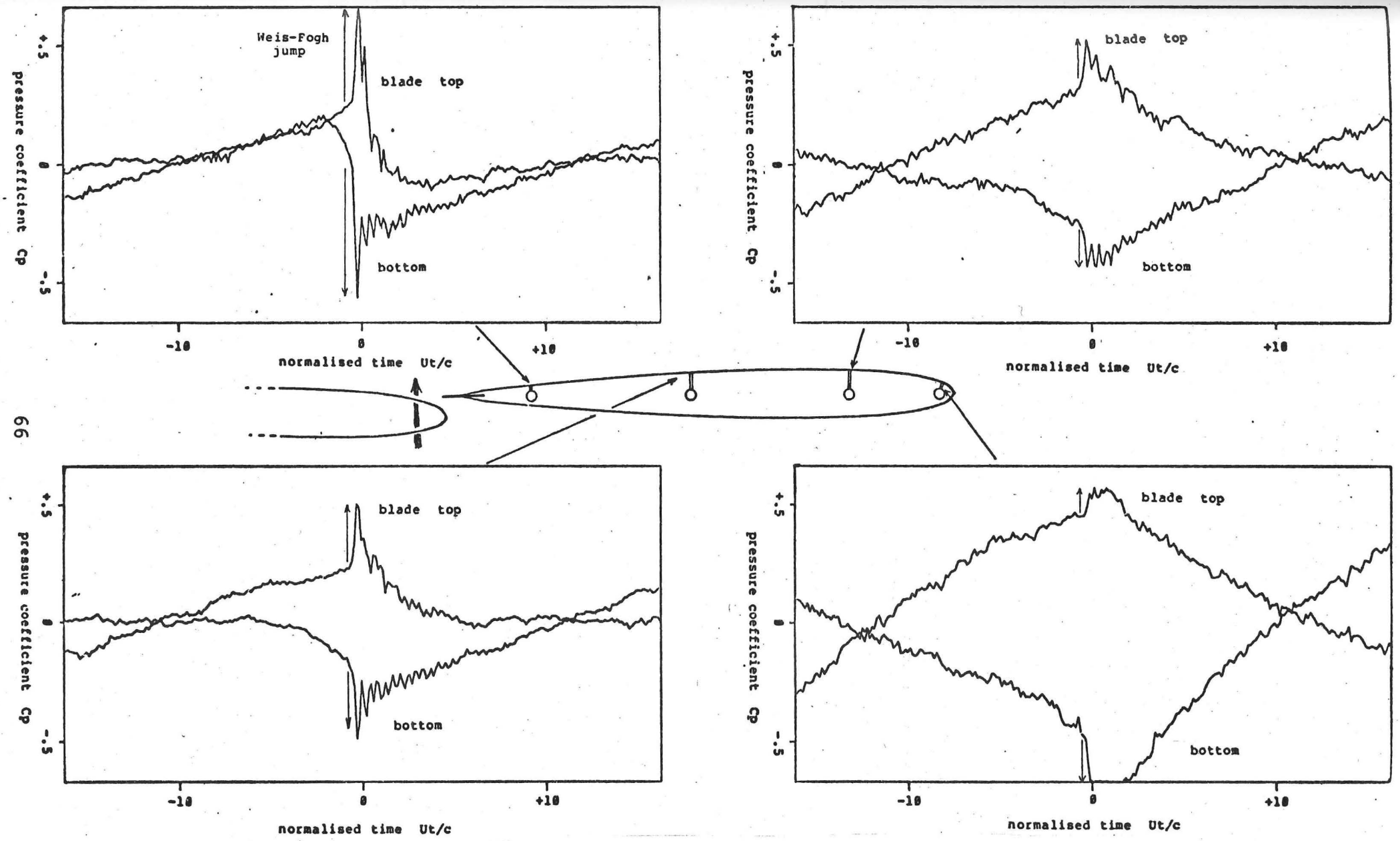

Figure 2.18. The results at a tunnel speed of 13 m/s.

t is time, c the blade chord, and U the free stream speed.

are shown in figure 2.19. The wind tunnel speed is 20 m/s, and the gap between the blades resulting from the removal ot the trailing edge was 2 mm.

The curves in figure 2.19 are not unexpected. They show similar behaviour to those in figure 2.16, but the amplitudes of the unsteady pressures are somewhat reduced. What is particularly interesting is that the pressures leading up to the closest position are changed very little compared with those just after this point. The circulation left on the fixed blade by the moving blade after passing the closest point is reduced much more than the effect of the disturbance created by the presence of the moving blade at other times.

We have stated during this section that a detailed model of the experiment is necessary to understand fully the results of these experiments, and such a model will be presented in the next section. The important factors will be introduced one at a time so that we can see how the features of the results given here arise. The new model will show how the Weis-Fogh principle operates in a machine based on our geometry, and also how viscous effects modify the mechanism of the circulation exchange.

The experiments show that very rapid circulation changes can take place on an aerofoil at high Reynolds number, and can arise from interactions like the one analysed in section 2.1. We shall see that the results confirm the validity of that analysis, and they also shed light on how the theory can be modified to allow for vortex shedding. We can therefore proceed in the knowledge that the effect is real and predictable, and that our theory gives at least the first approximation to the magnitude of the circulation change that we would find in a machine which had been designed to use the Weis-Fogh principle.

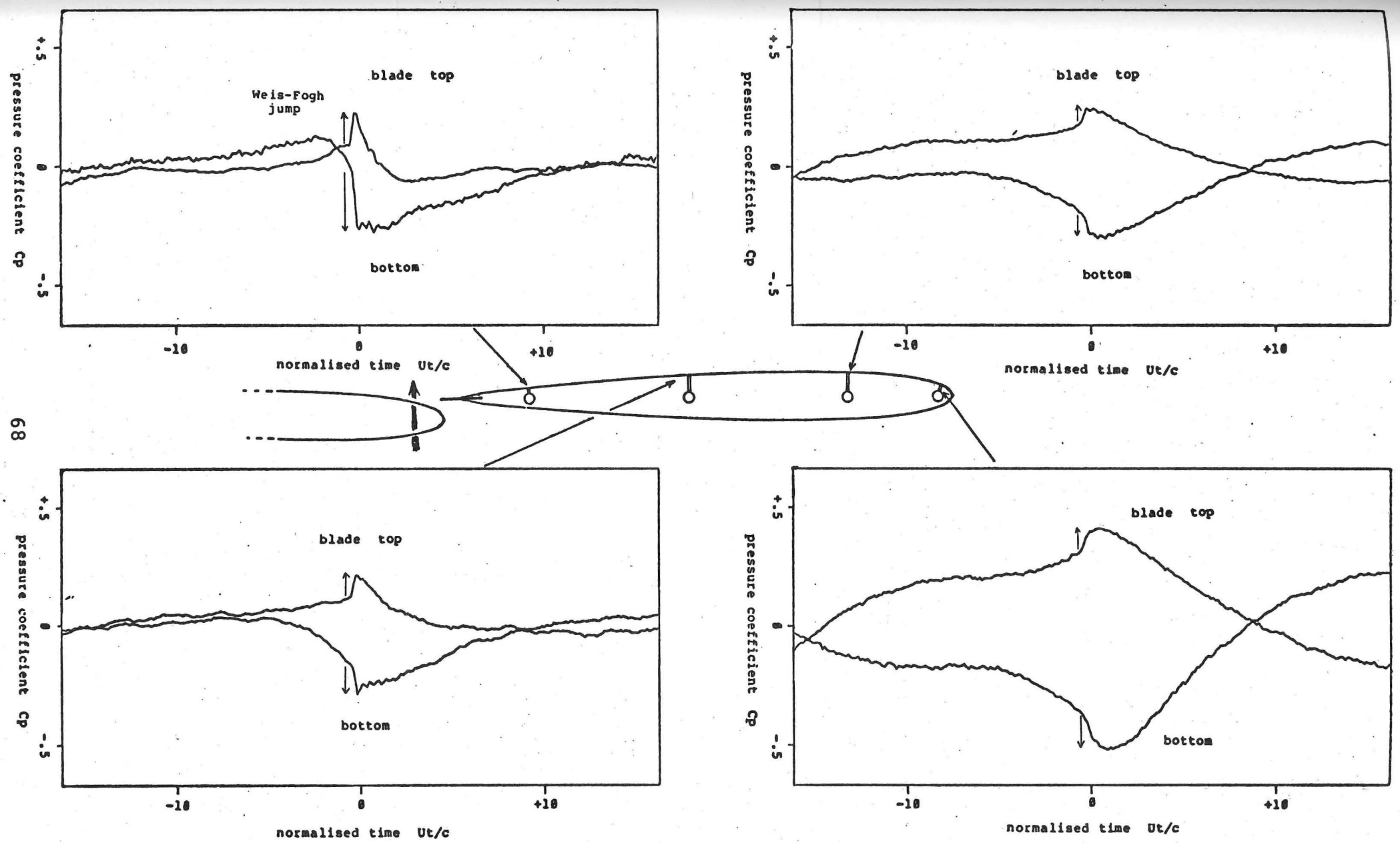

Figure 2.19. The results after the removal of the flexible trailing edge. The tunnel speed is 20 m/s.

2.6 Model of experiment

The generation of circulations by the interaction of two moving bodies must inevitably be accompanied by a more general disturbance of both of their flow fields. Thus the moving blade in the experiments just described will influence the pressure field not only at the time of contact, but at all other times as well. This means that it is necessary to be able to distinguish the various effects that are taking place in the experiments if we are to establish whether one of them in particular is working as predicted.

In a real fluid, the interaction between two aerofoils will usually have a significant effect on their circulations even when they are a chord apart, because the Kutta condition is so sensitive to the trailing edge conditions. In the experiments the two blades were never as much as one chord apart, so this will always be a consideration.

For these reasons, it is necessary to develop a much more complete model than was used for our initial calculations if we wish to be able to produce a theory which predicts the results of the last section. When we have a model which contains all the effects that appear to be important from the results we can then proceed to an evaluation of the original simple theory. In this section we shall develop the model and compare it with the experimental results. In the next section, in conclusion of the isolated interaction work, we shall see how useful the simple model is by comparing it with the model developed here.

In the experiments the only flow measurements taken were the unsteady pressures at four points on the surface of the fixed aerofoil. We therefore take this aerofoil as the central element in our model. The original aerofoil was a 10C4 section, and the thickness

to chord ratio was ten percent; we shall model it with a flat plate. We think that this is likely to be reasonable except near the leading edge, where the singularity on the flat plate will lead to an over-estimation of the velocities, and also therefore of the pressure variations.

The other elements which may be important are numerous. The wake of the fixed aerofoil controls its circulation, at least when the moving aerofoil is not very close. This wake will be driven downstream with the fluid in which it is embedded, and may also drift off sideways. The lateral velocities in the tunnel are at most around one tenth of the main stream velocity, so the wake will be modelled as rectilinear, parallel to the tunnel centreline.

The moving aerofoil will clearly be important, as without it the flow would be steady. We can model the motion and circulation simultaneously with a vortex distribution along the centreline. There will be a wake from this blade also, but it starts at the trailing edge, one chord downstream from the nearest point on the fixed blade. We therefore include the wake of the moving blade only in so far as it influences the circulation of that blade, and exclude its direct effect on the fixed blade.

The leading edge of the moving blade passes very close to the trailing edge of the fixed blade, in fact it touches it. The circulation on the fixed blade is very sensitive to conditions at its trailing edge, so it is important to model the leading edge of the moving blade accurately. It turns out that the thickness of the leading edge is important in determining the flow there, and this can be modelled by a source. The aerofoil thickness goes to zero at the trailing edge, so the source should be balanced by sinks there, but they are sufficiently far away from the fixed blade that they have little effect on it and can be ignored.

The only other effect that we have included is the reduction of incidence of the moving blade caused by the circulation on the fixed blade.

We shall now go on to see how all these effects are included in the calculations, and try to estimate the magnitudes of the effects left out.

We have decided to model the fixed aerofoil as a flat plate, and this enables us to transform it to a unit circle via the usual transformation

$$z = \zeta + \frac{1}{\zeta} , \tag{2.44}$$

where z is the physical co-ordinate, in terms of quarter chords, and ζ is the co-ordinate in the transformed plane.

If there is an external stream U parallel to the fixed aerofoil it will generate a complex potential

$$w = Uz \ . \tag{2.45}$$

We have described how all the effects that we wish to include may be represented by singularities or distributions of singularities. The distributions we shall represent by sets of discrete singularities, so all we need is the complex potential generated by a simple source or point vortex in the presence of a circular boundary. This may be obtained from the circle theorem (Batchelor 1967 page 422), or equivalently by the method of images. The complex potential for a source of strength s at $\zeta = \zeta_0$ is

$$w_s = \frac{s}{2\pi} \log \left(\frac{(\zeta-\zeta_0)(\zeta\bar{\zeta}_0-1)}{\zeta}\right) , \tag{2.46}$$

and for a point vortex of strength Γ at $\zeta = \zeta_0$ it is

$$w_\Gamma = \frac{i\Gamma}{2\pi} \log \left(\frac{(\zeta-\zeta_0)\zeta}{(1-\zeta\bar{\zeta}_0)}\right) , \tag{2.47}$$

taking a clockwise circulation as positive.We therefore know the complex potential, and hence full details of the flow field when we have determined the strengths and positions of all the singularities.

We shall build up the model bit by bit, and see how each contributing element affects the pressures. For our example we shall use the conditions which led to figure 2.15, which shows the pressure variations at the pressure tapping nearest to the trailing edge in the tests performed with a wind tunnel speed of 19.5 metres per second.

The major unsteady contribution to the flow comes from the moving and varying rotor circulation; indeed most of the other factors which we shall consider are secondary effects of this. The quasi-steady circulation on the moving blade, ignoring for now the presence of the stator, includes the effect of three parameters. The blade has a geometrical incidence relative to the wind tunnel stream, it is moving across the wind tunnel which increases the incidence, and it is also rotating about a spanwise axis. The incidence and transverse motion may be accounted for by conventional means, but the rotation is not so straightforward.

If we consider a flat plate aerofoil rotating about its centre-line with angular velocity Ω, then the relationship between the stream function Ψ and the normal velocity on the surface leads to

$$\Psi = \tfrac{1}{2}\Omega z^2 \ . \tag{2.48}$$

Using the usual transformation [equation (2.44)] of the flat plate into the unit circle in the ζ-plane, we obtain for the boundary condition in that plane

$$\Psi = \tfrac{1}{2}\Omega \left(\zeta + 1/\zeta\right)^2 \quad \text{on } \zeta = e^{i\eta} \ , \tag{2.49}$$

whence the complex potential may be derived

$$w = \frac{1}{2\pi} \int \frac{\Psi(\zeta_0)}{(\zeta - \zeta_0)} \, d\zeta_0 \ , \tag{2.50}$$

where the integral is to be taken around the unit circle. Only the term of order ζ_0^{-1} contributes to the integral, and on reducing this term to partial fractions the result may be found using Cauchy's theorem:

$$w = \frac{\Omega i}{\zeta^2} \ . \tag{2.51}$$

The derivative with respect to ζ gives the complex conjugate of the velocity in the transformed plane, and the circulation required to maintain the stagnation condition at the trailing edge is 2Ω. In our experiment this means that the circulation resulting from the transverse velocity of the blade, which is of course proportional to the angular velocity, is reduced by less than 2 percent. This is equivalent to reducing the length of the supporting arm by a similar amount, though the distibution of the vorticity on the aerofoil will not be the same. There are many effects which have been ignored that are this big, however, so we shall neglect the slight change in the

vorticity distribution. For our first calculation we take all the rotor circulation to be concentrated at the position one quarter of the way down the chord from the rotor leading edge.

The pressure fluctuations at the trailing edge position resulting from this effect alone are shown in figure 2.20. They do not resemble the experimental results very closely, but the change in mean pressure follows the right sort of line.

The curves in figure 2.20 show a significant pressure difference across the trailing edge of the stator, even when the rotor is not particularly close. If this condition exists for long vortex shedding will result, so we can find how this will affect the pressures. The Kutta condition states that the flow must come smoothly off the trailing edge of a flat plate, and this means that the corresponding point on the circle in the transformed plane must be a stagnation point. All the singularities in the flow field will affect the velocity at this point, and the vortex wake is the only thing that can be adjusted to ensure that the stagnation point remains exactly there. Even then, that part of the wake which has already been shed is fixed and drifting downstream. Only the vortex currently shedding may be called upon to maintain the smooth flow at the trailing edge. In the model we shall have one vortex shed at each timestep, and the size of each shed vortex will be determined so that it maintains the Kutta condition.

It is clear that the effect of a vortex placed close to the unit circle on the velocity at the circle will depend very much on just how close it is placed. It is important therefore to take care in determining this factor. We take the vortex shedding rate to be uniform over a small time interval, so that the vorticity density will be constant in the part of the wake shed during that interval. If the vorticity density is γ, the total vorticity between z and z+dz

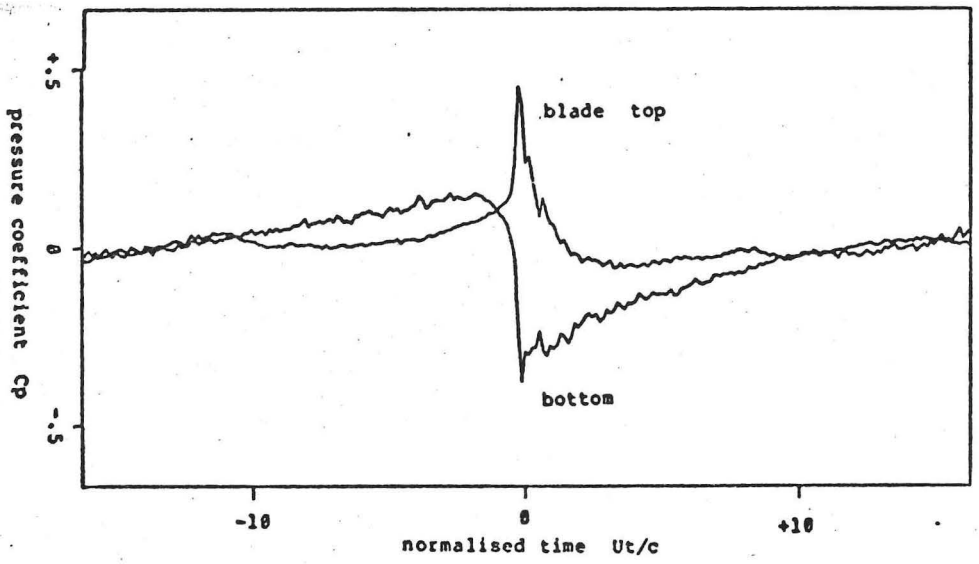

The experimental results in figure 2.15

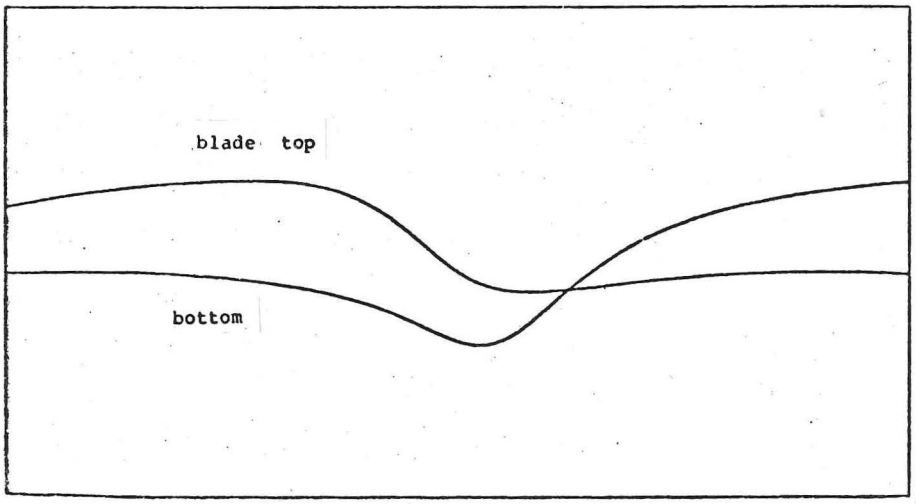

Figure 2.20. The pressures at the trailing edge tapping resulting from the rotor circulation alone, with no vortex shedding from the stator.

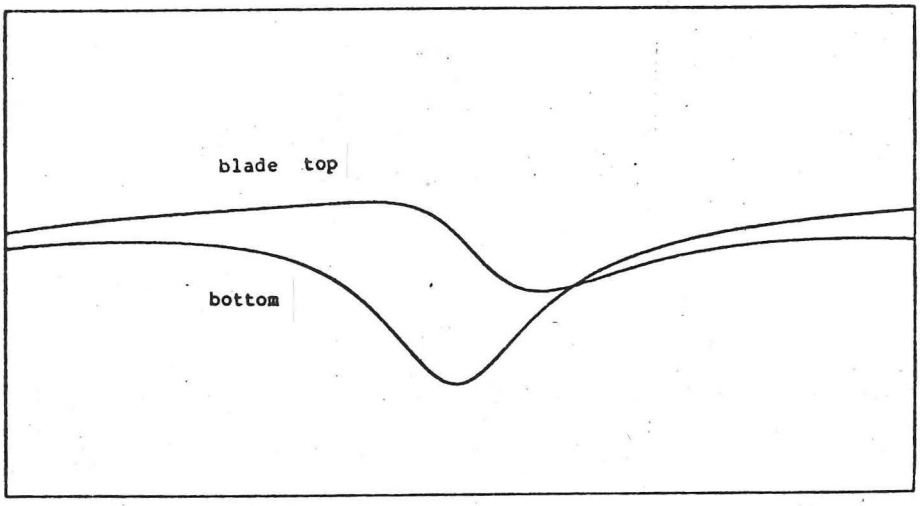

Figure 2.21. The pressure fluctuations of figure 2.20 when the stator is allowed to shed vorticity.

is γdz. At the end of an interval of length dt this vorticity extends down the wake from z = 2 to 2+Udt. The rest of the wake was determined during previous time intervals. The effect of this vorticity on the flow velocity at the point on the circle corresponding to the trailing edge, remembering that shed vorticity represents a reduction in the attached vorticity, is

$$\Delta V_\gamma = \int_1^{\zeta_1} \left(\frac{\zeta+1}{\zeta-1}\right) \frac{\gamma \, dz}{2\pi d\zeta} d\zeta \ , \tag{2.52}$$

where ζ_1 is the transformation of z = 2+Udt into the circle plane. The integral converges, and yields the result that the total shed vorticity Γ_s is related to the velocity excess ΔV at the trailing edge of the circle in the absence of any shed vorticity during this interval by

$$\Gamma_s = \Delta V \ 2\pi \ Udt\left((\zeta_1-1) + 2\log\zeta_1 + 1 - 1/\zeta_1\right)^{-1} \ . \tag{2.53}$$

The first vortex downstream of the trailing edge is thus determined. The vortices in the wake are all placed on the real axis, the nth being at z = 2+(n-.5)Udt, and they shunt one place downstream at each time step. The pressures resulting from including the stator wake in the calculation are shown in figure 2.21. The pressure difference at the trailing edge is now large only when the rotor is close, which is when the vortex shedding rate is also high.

Once we assume the Kutta condition at the trailing edge the vortex shedding rate becomes sensitive to the conditions there. The rotor circulation is not concentrated at the quarter chord position, and is in fact strong at the leading edge, which passes very close to the stator trailing edge. We therefore improve our representation of the rotor vorticity distribution by using several discrete

vortices instead of the one, and we calculate their strength and position as follows.

We use the quasi-steady vorticity distribution, given by

$$\gamma(x) = \frac{\Gamma}{\pi} \left(\frac{1+x}{1-x}\right)^{\frac{1}{2}} , \tag{2.54}$$

where Γ is the total vorticity on the aerofoil, and x goes from -1 at the trailing edge to +1 at the leading edge. We split the rotor up into nine sections, of size decreasing towards the leading edge of the blade. This non-uniform representation of the rotor vorticity is used for two reasons. Firstly the distribution given by equation (2.54) shows a strong concentration of the vorticity towards the leading edge, and secondly the leading edge is closest to the stator trailing edge, so the accurate modelling of the distribution is more important there.

The total vorticity in the section from x=a to x=b on the rotor may be found by integrating equation (2.54), and is

$$[\gamma]_b^a = \frac{\Gamma}{\pi}[\sin^{-1}b - \sin^{-1}a + \sqrt{(1-b^2)} - \sqrt{(1-a^2)}] . \tag{2.55}$$

In our model these proportions of the total rotor vorticity do not vary. The result of including this discrete vortex representation of the rotor in the previous calculation is shown in figure 2.22. We are now beginning to see the general shape of the experimental curves. We can also include a wake on the rotor calculated in the same way as that on the stator, to allow for the phase lag the actual circulation will show behind the quasi-steady value. This gives the curves shown in figure 2.23.

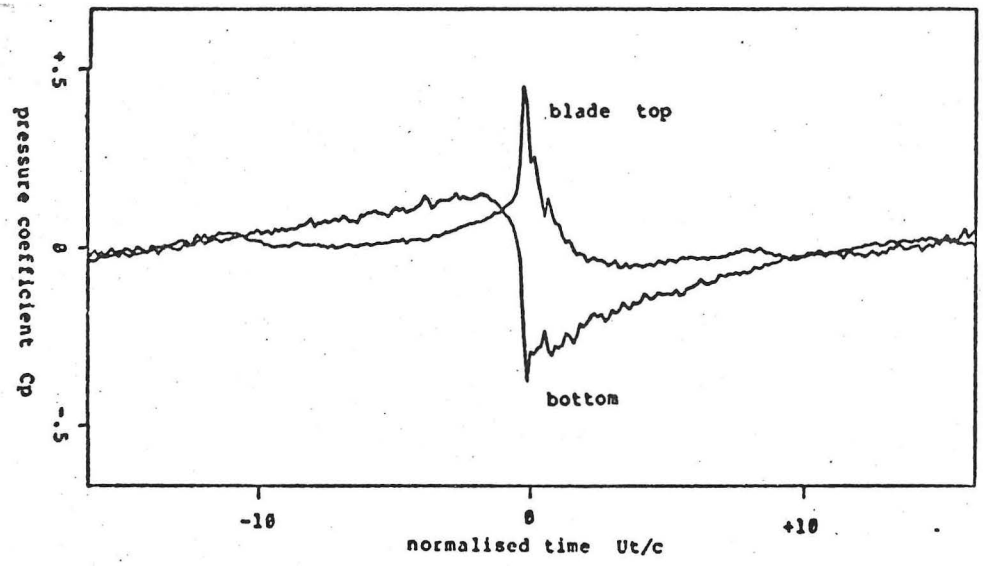

The experimental results in figure 2.15.

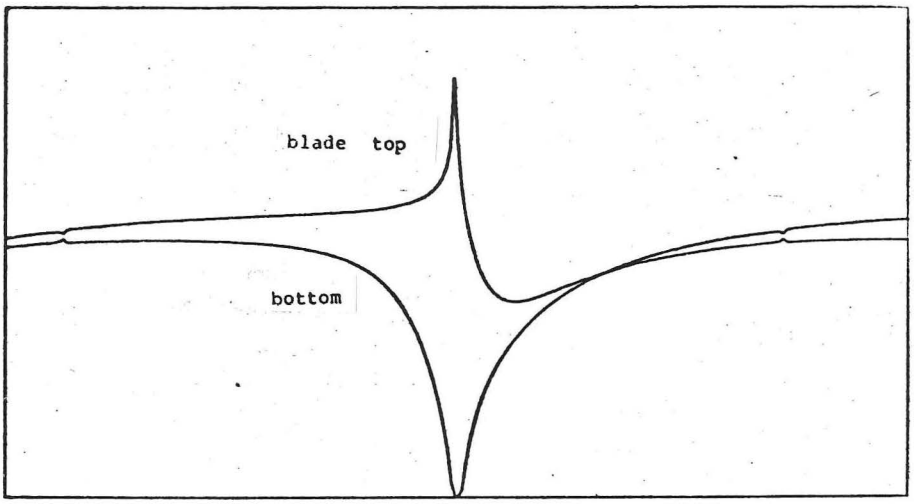

Figure 2.22. The pressure fluctuations at the trailing edge tapping position with the rotor represented by 9 discrete vortices and the stator shedding vorticity.

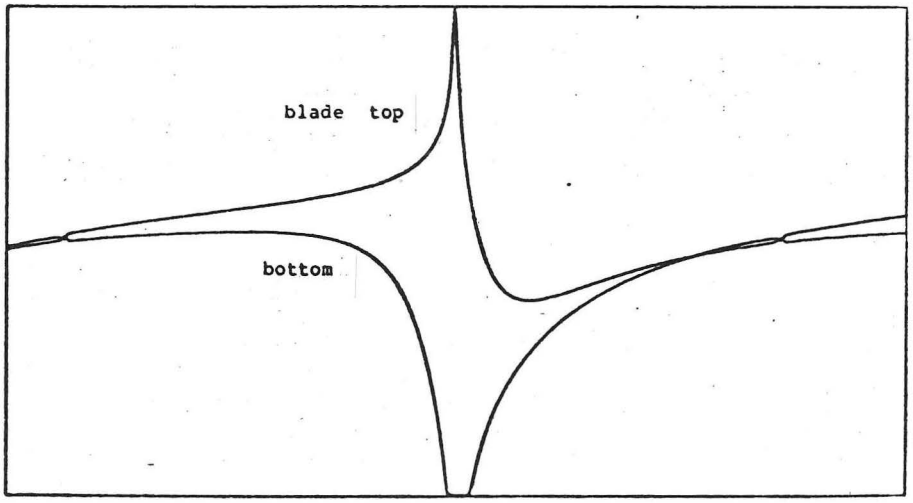

Figure 2.23. The pressure fluctuations when the rotor circulation is also controlled by vortex shedding.

The leading edge of the rotor passes close to the stator trailing edge, so we now include in our model the main effect of the leading edge thickness.A source of strength s placed in a stream of velocity U gives the flow equivalent to that past a semi-infinite body of thickness s/U. If this thickness is made equal to the maximum aerofoil thickness, which is one tenth of the chord, then the profile of the body is as shown in figure 2.24.There is a stagnation point upstream of the source at the leading edge of the body, and the distance of this from the source is easily calculated to be $s/2\pi U$. Positioning the source this far downstream from the aerofoil leading edge will, in the absence of any other boundaries, result in the leading edges of the aerofoil and the semi-infinite body coinciding and their maximum thicknesses being equal. Note that although the maximum thicknesses of the two bodies have been made equal, they do not occur at the same point downstream of the leading edge. The thickness of the semi-infinite body increases downstream, tending to its maximum at infinity. The maximum thickness of the aerofoil is at 30 percent of the chord, and the aerofoil is therefore thicker there than the semi-infinite body. The good matching of their general shapes near the leading edge can be seen in figure 2.25 where they have been superimposed. This is what leads us to hope that the representation of the rotor thickness by a simple source of the above strength and at the above position will be adequate, though of course the shape will not be so good when other boundaries are present. The inclusion of this source into the calculations gives the results shown in figure 2.26, which are now looking quite close to the experimental results.

It is often noted that aerofoils tested in wind tunnels generate less than their theoretical lift coefficient, due to the boundary layer thickness being different on the two surfaces thereby changing the effective incidence. This will occur also in our tests, and be manifested by a reduced circulation on the rotor. Also the rotor mounting allows some leakage between the ends of the aerofoil and

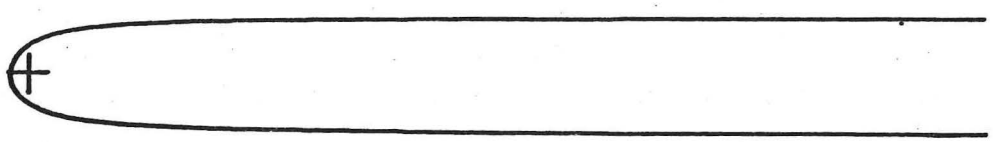

Figure 2.24. The shape of the semi-infinite body equivalent to placing a simple source in a uniform stream.

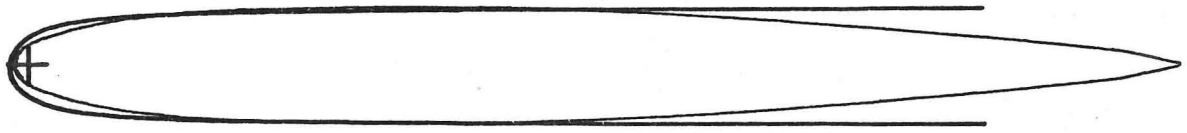

Figure 2.25. The body of figure 2.24 positioned so that its leading edge coincides with that of the aerofoil, and the source strength adjusted to give the same maximum thickness for both bodies.

the tunnel wall, which will affect the circulation further. For this reason the calculation procedure is designed so that in a steady state the blade circulations would tend to lower values than those predicted by potential flow incorporating the Kutta condition, and for the results presented here a reduction of 20 percent has been found to be about right, as shown in figure 2.27.

The procedure in the computations is to calculate the total circulation on the rotor from considerations of its incidence, wake, and the downwash from the stator. The rotor wake is calculated in exactly the same way as the stator wake, which we have described. The strength of each vortex in the representational distribution is then known from equation (2.55), as is its position in the z-plane from simple geometry. The position in the ζ-plane may be found by inverting the transformation [equation (2.44)]. The effect of each vortex on the velocity at the transformed trailing edge may be found from the complex potential in equation (2.47), enabling the stator wake to be established using equation (2.53). When the stator wake is known, all the details of the flow are available. The velocity and velocity potential at the four pressure transducer positions may then be found by summing the contributions from all the singularities.

The flow is determined uniquely if the boundary and singularity velocities and positions are known, but initially the strengths of the wake vortices are not known. The calculation must therefore be allowed to proceed for some time before the effects of the initial conditions become insignificant. The length of time is related to the vortex shedding timescale previously mentioned, and in practice the time taken for the wake to travel ten chords downstream was found to be sufficient, so long as the initial conditions were not too wild. The quasi-steady Kutta circulations were used as initial values in the calculations here.

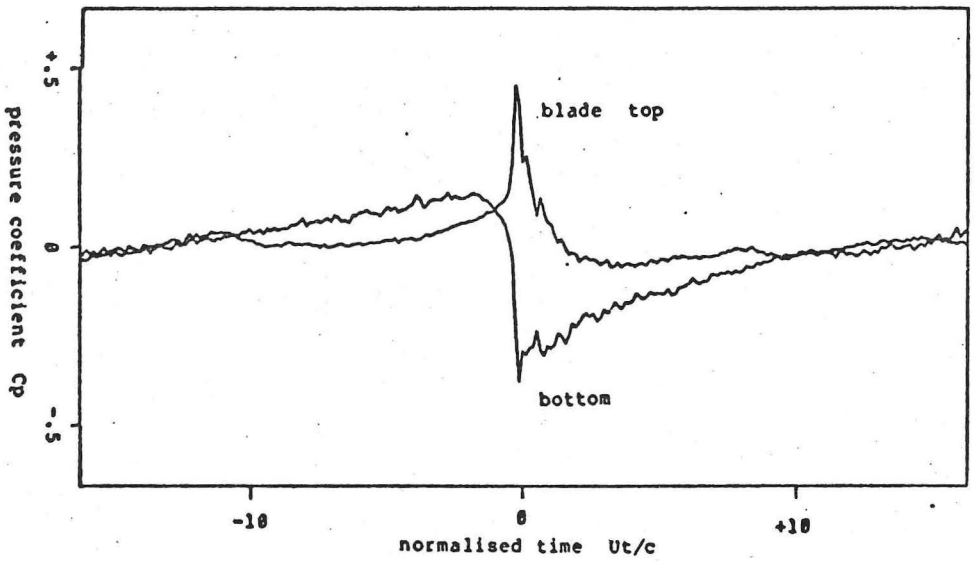

The experimental results in figure 2.15.

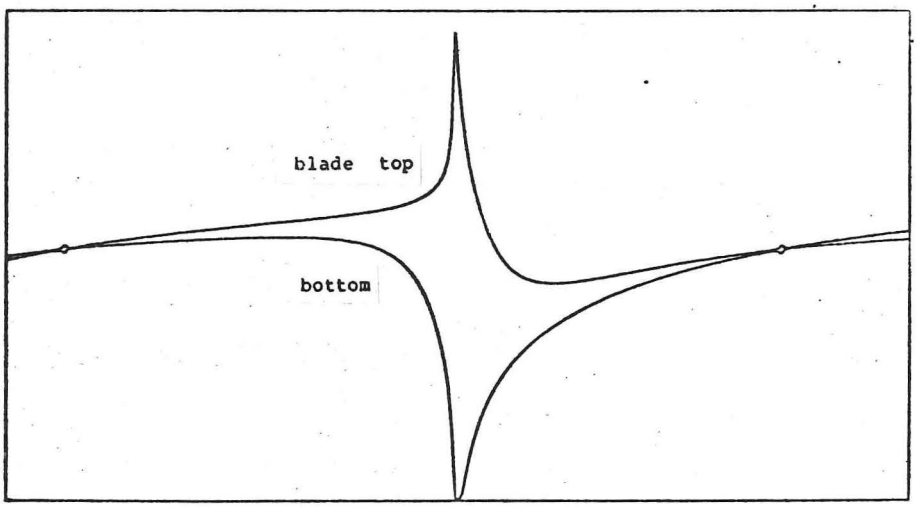

Figure 2.26. The pressure fluctuations at the trailing edge tapping position with a source representing the rotor leading edge thickness.

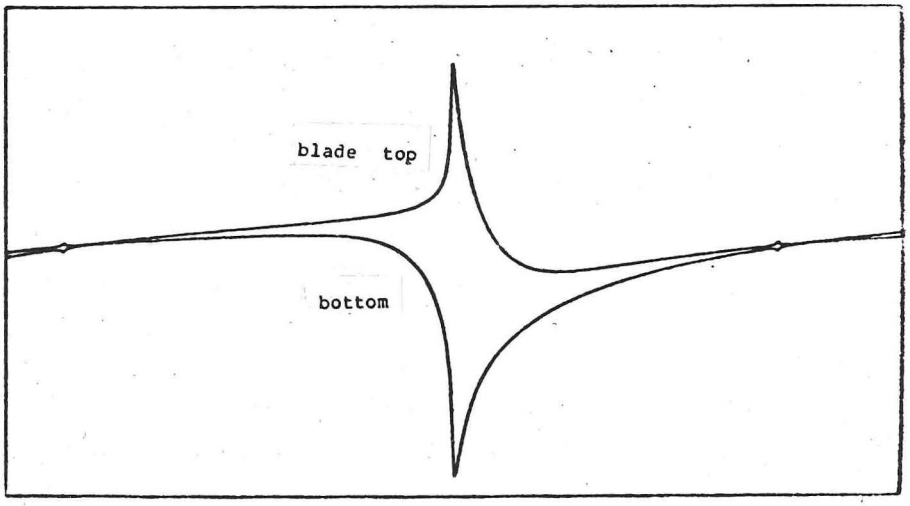

Figure 2.27. The pressure fluctuations with the rotor circulation reduced by 20 percent.

Once the velocities and velocity potentials have been found over the required time, the pressures may be obtained from the unsteady Bernoulli equation:

$$p + \tfrac{1}{2}\rho u^2 + \rho\frac{d\phi}{dt} = \text{constant} \ . \tag{2.56}$$

We may estimate $d\phi/dt$ by dividing the difference between the velocity potentials at consecutive time steps by the length of the time step. The difference between the calculated pressures and their average provides the unsteady pressure, which may be compared with the measured values.

In the experiment the oscillations of the moving blade were not exactly centred on the trailing edge of the fixed blade, nor was the period exactly consistent from one run to another. The output data from the angular position transducer was therefore used to provide the necessary offset and period inputs to the model calculations. The procedure used was to note all the places where the position output corresponded to the rotor being in contact with the stator, and then to equate the period to twice the average time between these points. The angle offset of the mean position from the contact position is related to the average difference between alternate times, and may be found from elementary consideration of the intersections of the line y=constant with the curve y=sin(x). The amplitude of the oscillations was found from the position data to be always close to .2 radians, and the motion of the blade is then fully determined.

The results of the calculations from the model including all the effects we consider, and which give a close representation of the experimental situation near the trailing edge (figure 2.27), are shown in detail in figures 2.28 to 2.30, where they are drawn in red over the corresponding experimental results which were described in

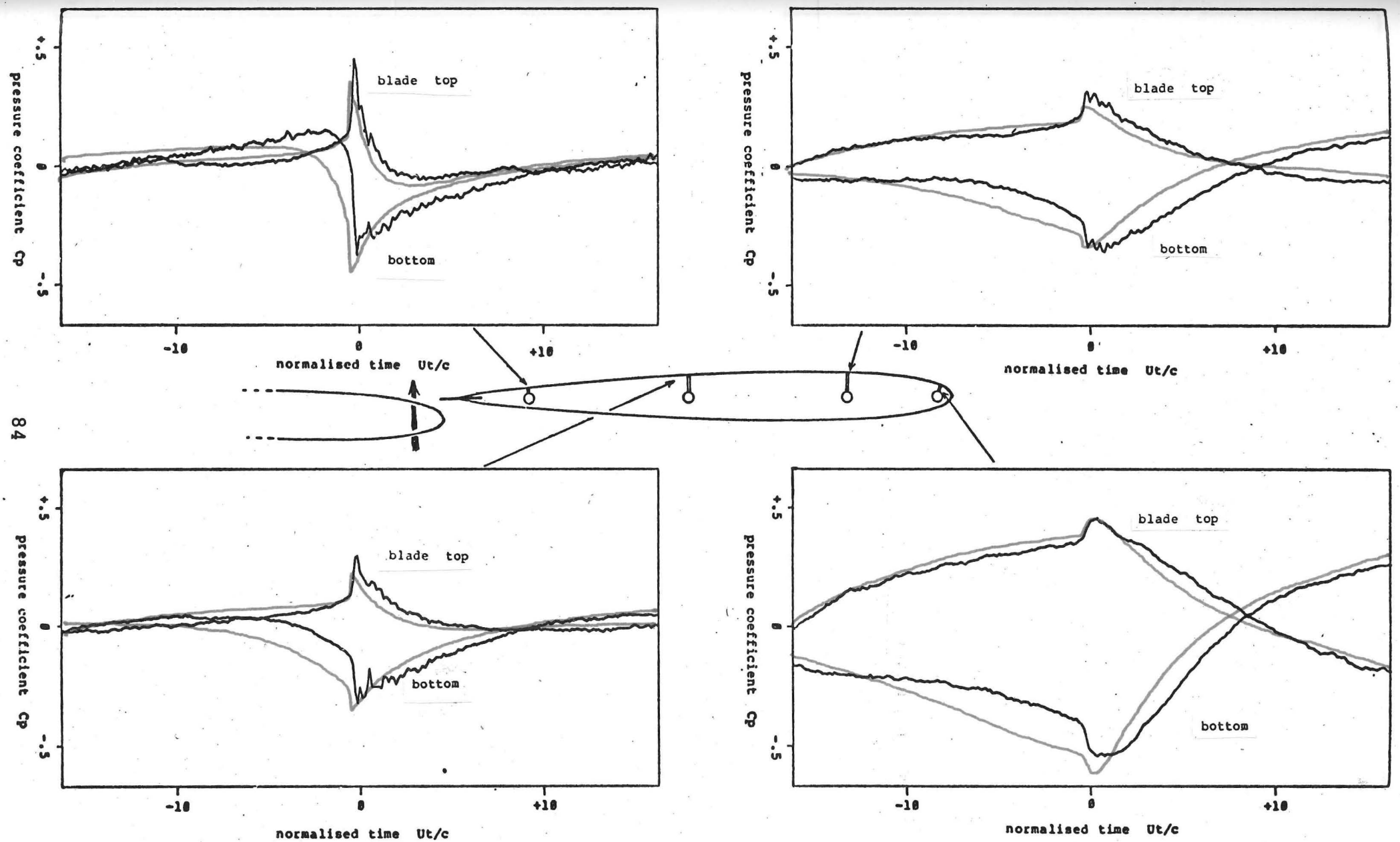

Figure 2.28. The theoretical results for the 19.5 m/s tests.

t is time, c the blade chord, and U the free stream speed.

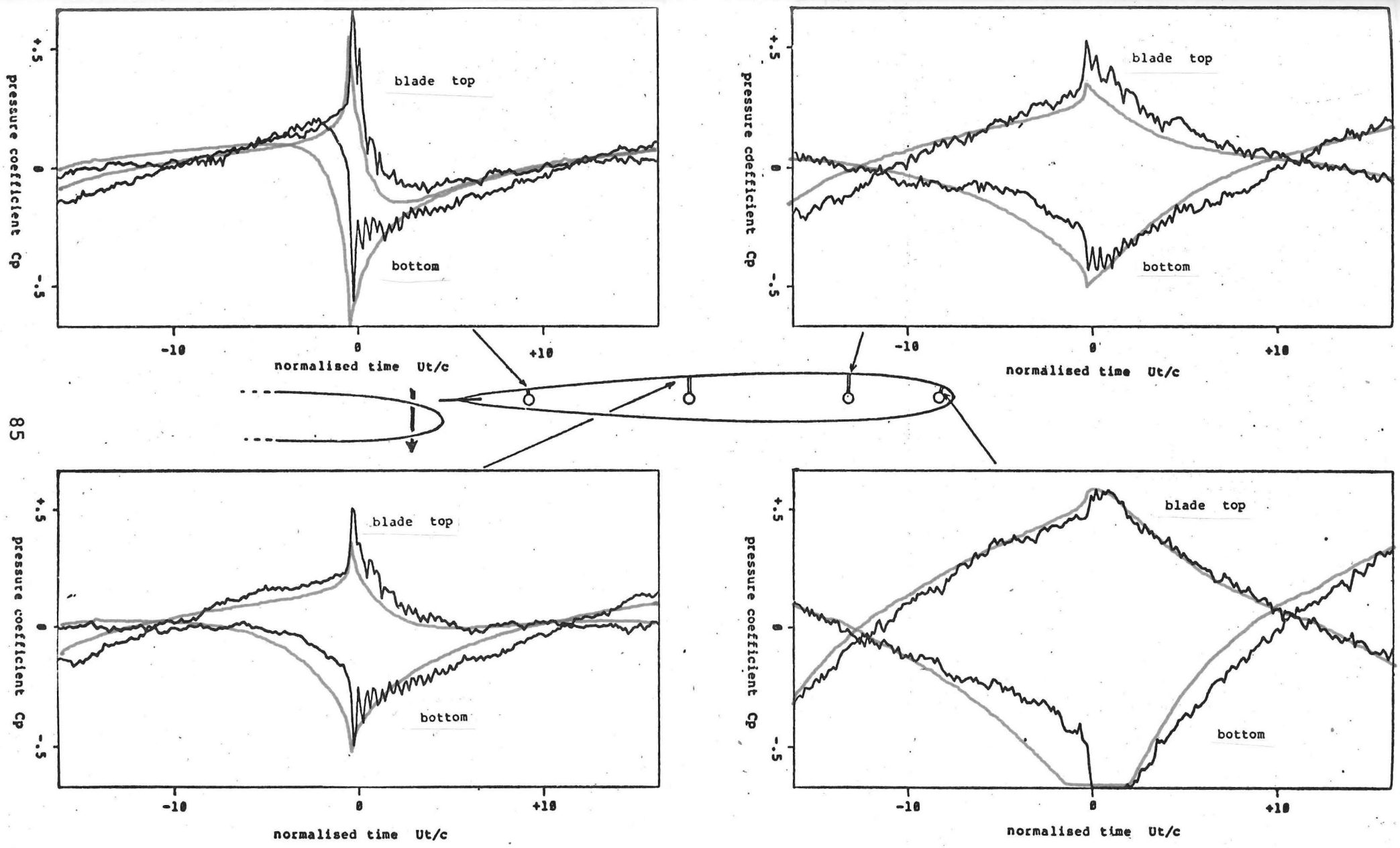

Figure 2.29. The theoretical results for the 13 m/s tests.

t is time, c the blade chord, and U the free stream speed.

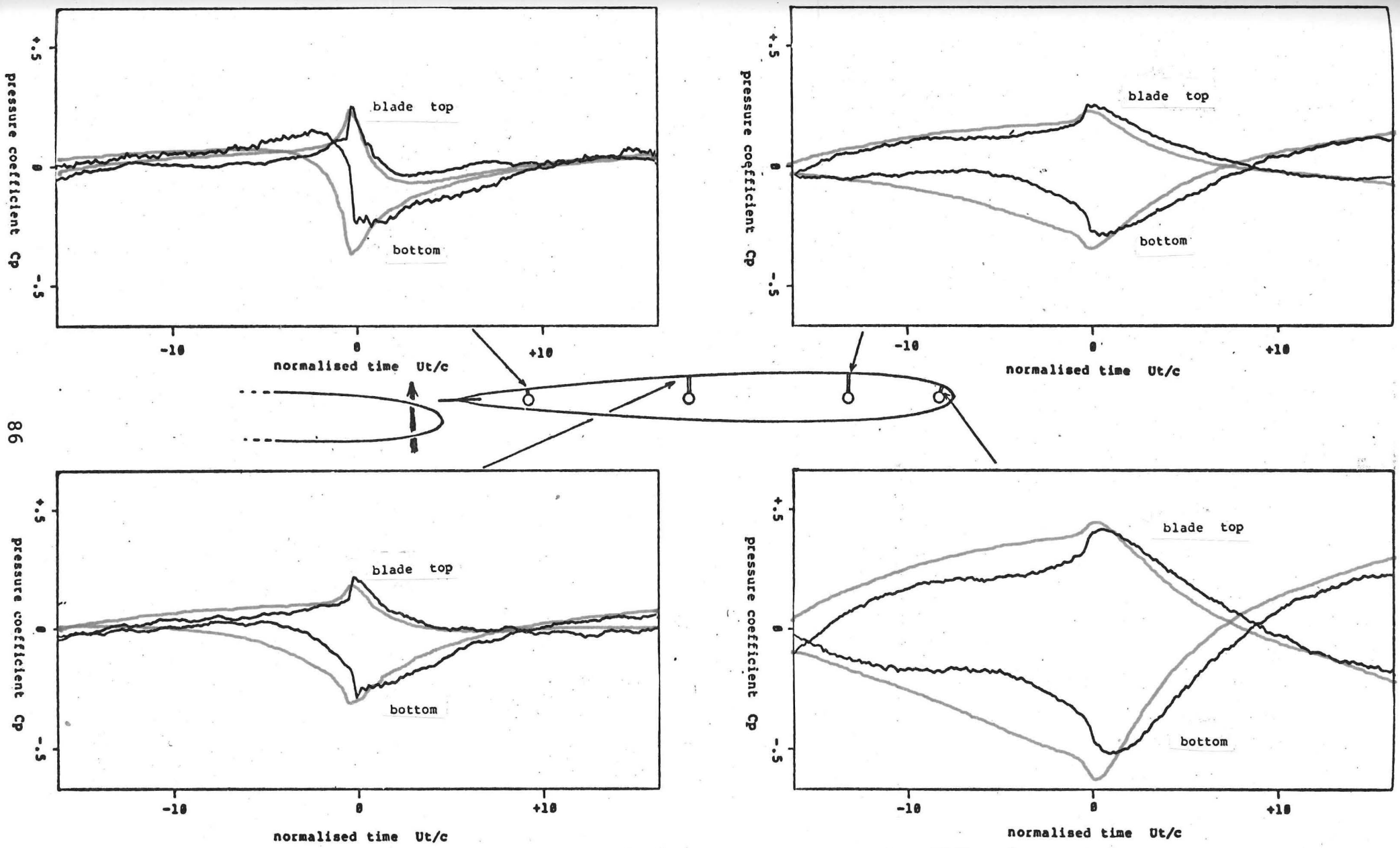

Figure 2.30. The theoretical results for the tests performed after removal of the flexible trailing edge.

the last section. The general agreement is reasonably good, in that the curves display the same phenomena and the magnitudes of the pressure fluctuations are roughly correct. A discrepancy common to all the predicted curves is that the pressure difference increases too much before the point of contact, and the size of the rapid change at contact is correspondingly reduced. The experiments seem to display greater transient pressure changes than the theoretical results, which is not perhaps what we usually expect.

It only remains to estimate the sizes of the many effects left out of these calculations. The blocking effect of the boundary layers on the tunnel walls are effectively allowed for in the calibration of the tunnel speed, but this calibration was carried out without the two aerofoils present. They both span the tunnel width, and have thickness of 1.5 cm compared with the tunnel height of 50.8 cm, so the velocity increase in their presence would be about 3 percent.

All the singularities representing circulations will have images in the top and bottom of the tunnel, and the images will themselves have further images. To find out how large the effects of all these images are we look at the first two. Since the succeeding images will be opposite in sign the whole series will converge to a sum less than the first terms in magnitude, and our estimate will be an upper limit. We are interested mainly in the pressure difference across the fixed blade, and it is sufficient to consider the effect of distant images on the blade circulation. Any variation in the local velocity which they cause will affect both sides of the blade equally, and not the pressure difference. The effect of an image vortex Γ_i at (x,y) in the ζ-plane may be found from the complex potential in equation (2.47). This tells us that the circulation required to maintain the Kutta condition is given by

$$C = -\Gamma_i \frac{2(x-1)}{(2x-[x^2+y^2+1])} , \qquad (2.57)$$

and when the vortex is an image in the tunnel top or bottom it is at approximately (0,h) where h is the tunnel height. This leads to a circulation of magnitude $\Gamma_i(2/h^2)$. Since Γ_i is the strength of the image, which will be the same but opposite in sign to the vortex already on the blade, and h is approximately 14 quarter chords, this amounts to a correction of about 1 percent.

The sources and sinks representing the blade thicknesses are relatively weak, and their images in the tunnel walls generate velocities of less than half a percent of the free stream velocity at the aerofoil surfaces.

The most difficult effect to estimate is that caused by the rotor moving through the vortex wake of the stator, and of course this wake is very strong at the time of passing. When the rotor is very near the wake the vortices will have images in the rotor approximately as though it was a plane boundary. The vortex and its image will be close and opposite in sign, and will therefore tend to cancel each others fields. They will also move in each others fields, and the signs are such that at this time their progress downstream will be slower. The total time involved is fairly small however, and the effect will be swamped by the presence of the rotor circulation, so although it is hard to put a figure on this effect we think that it is not very significant as far as the pressures on the stator are concerned. We shall see in the next section that the wake-rotor interaction is bound up in the role played by viscosity in the circulation interchange mechanism, and would be very significant if the pressures on the rotor were our concern.

In this model of the experiment we have not included any

instantaneous effects at the time when the blades touch. This might appear odd at first sight, since this dissertation is primarily concerned with just such contact effects. However the exchange of circulation at the time of blade contact described in previous sections is a simple consequence of the normal velocity conditions on the aerofoil surfaces, and the model described here satisfies these conditions (approximately) at all times because we have imposed the Kutta condition. That the instantaneous flow change observed in the experiments happens automatically in this model is confirmation that the Kutta condition was satisfied at all times in our experiment. At higher Reynolds numbers, however, we would not expect this to be the case, and the circulation would then be generated at the time of contact by the Weis-Fogh mechanism.

Our calculations were originally performed with an interchange of circulation at contact calculated as described in section 2.1, but it was noticed that previous vortex shedding caused the interchange to have little effect. The circulations adjusted themselves in the last few moments before contact to levels such that the total circulation change on the fixed blade was insignificant, and was a function only of stepwise modelling of the temporal development of the flow. The only visible differences on the theoretical curves shown in figures 2.28 to 2.30 were small spikes at the moment of contact, caused by sudden small changes in the velocity potential which gave rise to relatively large transient pressures due to its time derivative entering the unsteady Bernoulli equation [equation (2.56)]. We shall go into this matter more thoroughly in the next section, and just note here that since the circulation interchange only gave rise to these spikes which were probably just a spurious result of the approximations in the model, the curves presented here were the results of calculations performed with no discontinuous effects at the time of contact.

Vortex shedding according to constraints imposed by the Kutta condition inhibits the Weis-Fogh circulation change but, and this is most important, the Weis-Fogh mechanism will ensure that the stator blade acquires the correct circulation whether or not the Kutta condition is satisfied. The circulation acquired during the interaction by either vortex shedding or the Weis-Fogh mechanism will cause the stator to support aerodynamic loads in regimes where it is otherwise unloaded. It is this ability to drive circulation onto the stator in flows that are developing too quickly for the usual vortex shedding process to apply that gives the Weis-Fogh mechanism its potential application.

The rotor is similarly affected, and we shall see shortly that there is little dynamical difference between the Weis-Fogh interaction, where circulation is transferred onto the moving blade, and the more gradual vortex shedding into the flow where the vorticity is convected along the moving blade. The potential flow model is, of course, an idealisation of the viscous situation, and plays in this interaction problem the same role as does the concept of bound vorticity in steady aerofoil theory. That is well established as an effective idealisation that describes the dynamical effects of the vorticity in the aerofoil's viscous boundary layer.

We have then a model of our experiment which seems to contain all the most significant effects, and predicts the general behaviour of the measured parameters well. We originally set out to develop a useful blade circulation without vortex shedding, and we analysed a flow in terms of solutions known only when the blades were in contact. The experiment called for a theoretical modelling in which vorticity was also shed into the fluid prior to blade contact. That modelling had necessarily to be approximate, and our treatment of it is, we think, the crudest that can incorporate all the essential features. Both models generate the same kind of effect in that the

interaction causes the stator blade to acquire a load. In fact we shall see that both effects also cause the rotor to sustain a potentially useful load that is entirely caused by the blade interaction. The Weis-Fogh effect thus complements the usual vortex shedding in sustaining blade loads under conditions where the more conventional process has failed. Vortex shedding can take more time than is available between successive blade interactions. We need now to compare in detail the relative magnitudes of the effects caused by these two mechanisms, and put them in the proper relative perspective.

2.7 Conclusions

We started this study of the isolated interaction by examining a method of generating a circulation on a blade without recourse to vortex shedding, and developed a theory which predicted the circulations left on both blades after contact under any initial conditions. Then an experiment was devised to see what would happen in practice if we tried to fulfil the conditions of the theory. It was found to be impossible to get all the necessary conditions without including other effects, so we developed an approximate model of the experiments which was valid prior to the interaction and which included all the effects thought to be important. In this the simplicity of the original model got rather lost, so we now conclude our studies of the isolated interaction by seeing how the two models compare under circumstances where they should both apply.

The reason why the simple model did not work well under the conditions of the experiment is now clear. In the experiment the incidence of the moving blade changes considerably, and vortex shedding causes its circulation to change, even if the fixed blade is absent. The Weis-Fogh theory does not allow for any circulation changes between interactions, and therefore cannot be expected to produce an accurate modelling of the experiment. Even so both models give the same qualitative picture. We designed the experiment to see whether contact between two blades in relative motion would give rise to very rapid circulation changes as predicted by the Weis-Fogh theory, and the results show clearly that this did happen, but the same changes are also predicted by the approximate vortex shedding theory.

A mechanical change to the experiment would overcome the problem of varying blade incidence, though it is not one that is easily built into the test rig. If, instead of oscillating across the tunnel on

pivoted arms, the moving blade were to traverse the tunnel at fixed incidence and speed then in the absence of the fixed blade its circulation would be constant. This is a situation where simple theory stands most chance of giving reasonable results. It is that situation which we now treat by both our theoretical models to compare and contrast their individual features and aid the interpretation of our experimental results.

Figure 2.31 shows the model used for comparing the theories. The stator is a fixed flat plate aerofoil at zero incidence to a uniform stream with velocity U. The rotor is a flat plate aerofoil moving perpendicular to the stream with velocity v, at zero geometric incidence. The moving blade comes in from infinity on a trajectory such that its leading edge just touches the trailing edge of the fixed blade instantaneously as the blades pass, and it continues thereafter indefinitely downwards. The circulation on the fixed blade is zero when the blades are far apart, and that on the moving blade is πcv. As they get closer the circulation on the moving blade will influence the conditions at the trailing edge of the fixed blade, causing it to shed some vorticity and gain non-zero circulation. When the blades touch there will be an exchange of circulation between them, then, after contact, they will gradually return to their original configuration.

The elementary Weis-Fogh model does not include any of the vortex shedding effects, so the attached circulations cannot change except at the time of contact. They will alter by the amounts previously described, and if we give the approaching rotor its Kutta circulation πcv, it will be reduced to $cv(\pi/2 - 1)$ by the interaction. The circulation on the stator will increase from zero to $cv(\pi/2 + 1)$. We know of course that the actual values will eventually return to the initial levels, but what we wish to emphasise is that the simple theory should be valid for a short time after the interaction. In

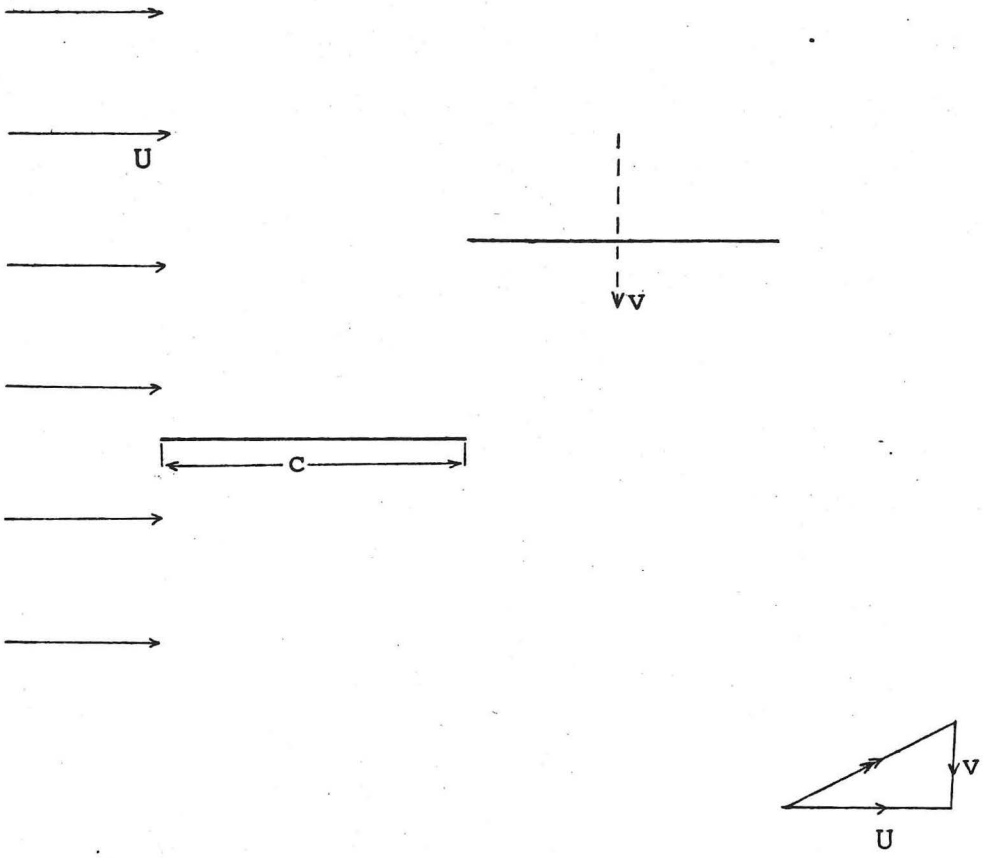

Figure 2.31. The model problem used to compare the simple potential theory and the more detailed but approximate theory developed to describe the experimental results.

a machine exploiting this interaction, consecutive blades would follow quickly, and the interaction generated circulations would not be required to last long.

The results of the two different approaches to the theory are shown in figure 2.32. The step function represents the potential theory involving no shed vorticity, and the smooth curve represents the results of the more detailed but approximate model used to predict the experimental results. The rotor speed is one tenth of the free stream speed, which corresponds closely to the conditions of the experiment. The Kutta condition requires that the circulation on the stator starts to build up when the rotor is still more than one chord length away, but the rate of increase grows markedly as the gap reduces. That circulation overshoots the Weis-Fogh value by about 50 percent at contact. All the circulation gained by the stator must be balanced by vorticity shed into the fluid. In the Weis-Fogh model this circulation is transferred to the rotor, and no vorticity is shed into the fluid. The circulations are of the same order of magnitude and represent respectively the result of 'slow' and 'fast' blade interactions. Both result in a blade loading not represented by isolated aerofoil theory.

Most of the vorticity is shed from the stator when the rotor is close. It is in practice convected by the stream along past the rotor. If it is close enough it will get caught in the aerofoil's boundary layer, and become indistinguishable from the vorticity usually represented by the bound vorticity on the rotor. We become involved in a rather arbitrary judgement of how close the vorticity has to be if we wish to know how much of the vorticity shed from the stator ends up effectively on the rotor. But we can analyse the detail of that problem to remove the arbitrariness, and that we now do.

Consider first an isolated vortex near a flate plate aerofoil.

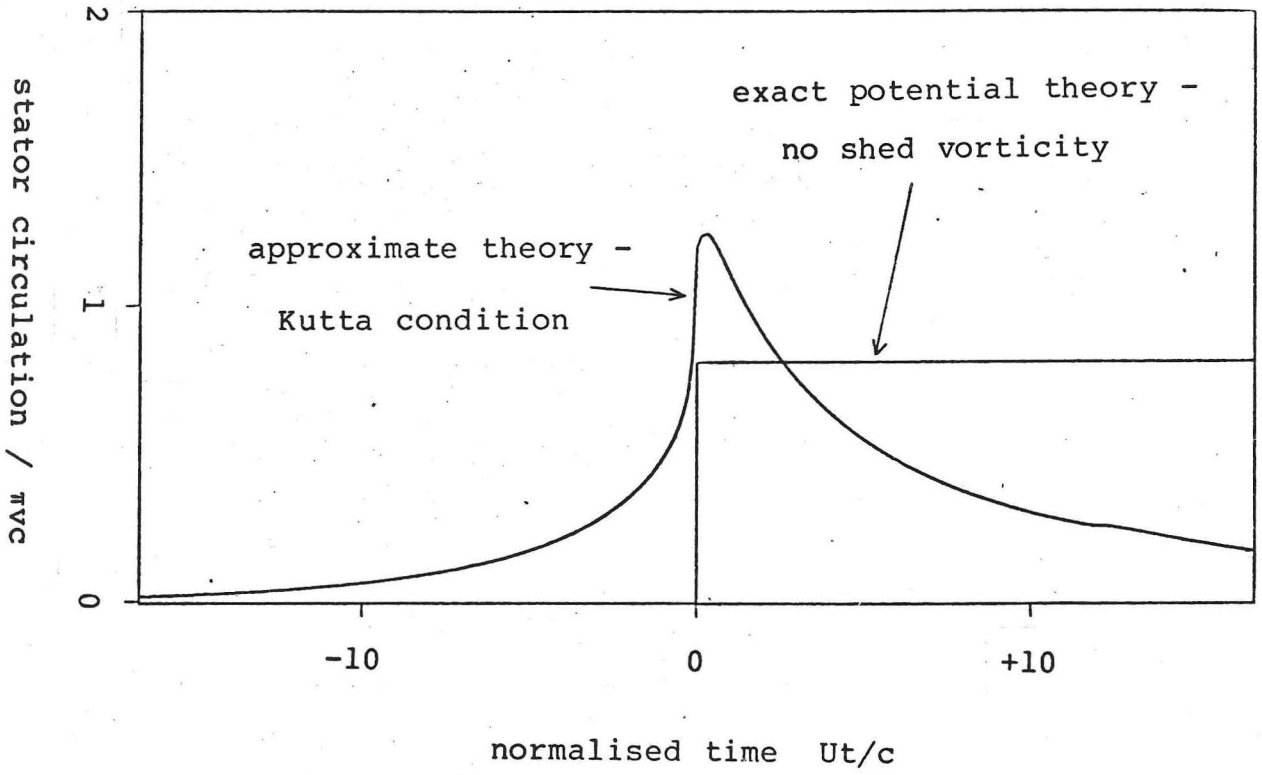

Figure 2.32. The comparison of the exact potential flow theory with the more detailed but approximate theory developed to describe the experimental results. The rotor speed is one tenth of the free stream speed.

If it is sufficiently close the flow field around the vortex will be that of a vortex near an infinite plane boundary, with an external stream. The vortex has an image in the boundary, of opposite sign and equal strength. It is a well known result that the vortex-image pair exerts no force on the boundary. The image represents a net circulation on the plate, and must therefore be balanced by an opposite circulation which is fixed in the plate. This fixed circulation, which is equal in strength to that of the original convecting vortex, will generate the same lift as though the convecting vortex were bound to the plate. Thus vorticity convecting near a flat plate causes that plate to attain the same lift as if the vorticity were attached to the plate. This is an important element of our model that is perhaps a little surprising. The result is not dependent on the boundary layer thickness, so we can rule out the boundary layer as providing the length scale that determines whether or not a vortex is near enough to the aerofoil to be effectively bound. We do not yet know the dependence of the lift on the distance of the vortex from the plate, but we can calculate that too.

The lift L on the aerofoil is the integral of the force exerted by the air pressure over the aerofoil surfaces:

$$L = \int_{-2}^{+2} (p_- - p_+) dx \ , \qquad (2.60)$$

where the suffices + and - denote the upper and lower surfaces of the aerofoil respectively. The length of the aerofoil is 4 in accordance with the usual transformation length scales. The pressure may be found from the unsteady Bernoulli equation [equation (2.56)]. The lift is then given by

$$L = \int_{-2}^{+2} \rho\left(\frac{d\phi_+}{dt} - \frac{d\phi_-}{dt} + \tfrac{1}{2}(u_+^2 - u_-^2)\right)dx \ . \tag{2.61}$$

The velocity and velocity potential may be found by conformal transformation of the boundary into a circle in the ζ-plane [equation (2.44)], whereupon the complex potential for a vortex of strength Γ at $\zeta=\zeta_0$ is given by equation (2.47). The velocity on the surface of the plate is

$$\frac{dw}{dz} = U + \frac{\Gamma}{2\pi\sin\eta}\,\frac{(1+\mu\sin\eta)}{(1+\mu^2+2\mu\sin\eta)} \ , \tag{2.62}$$

where $\zeta_0=-i\mu$ and $x=2\cos\eta$. The velocity potential is

$$\phi = Ux + \frac{\Gamma}{2\pi}\left[\pi-\eta+\tan^{-1}\left(\frac{\cos\eta}{\mu+\sin\eta}\right)-\tan^{-1}\left(\frac{\mu\cos\eta}{1+\mu\sin\eta}\right)\right] \ . \tag{2.63}$$

The pressure is influenced by the time derivative of the velocity potential, which may be related to the spatial derivative because the strengths of all the singularities are constant.

$$\frac{d\phi}{dt} = \frac{d\phi}{d\zeta_0}\,\frac{d\zeta_0}{dt} \ . \tag{2.64}$$

Of course the rate of change of ζ_0 is not the same as the fluid velocity in the transformed plane. It should be found by direct reference to the position in the physical plane:

$$\frac{d\zeta_0}{dt} = \frac{d\zeta_0}{dz_0}\,\frac{dz_0}{dt} \ ,$$

$$= \frac{U}{1+1/\mu^2} + \frac{\Gamma}{2\pi}\,\frac{\mu^3}{(\mu^2-1)(\mu^2+1)^2} \ . \tag{2.65}$$

The rate of change of the transformed position of a fluid particle near the centre of the flat plate is thus U/2, whereas the fluid velocity in the transformed plane at the same position is 2U.

The contribution to the lift from the virtual inertia term in equation (2.61) is then

$$-\rho\frac{\Gamma}{\pi}(\mu-1/\mu)\frac{d\zeta_0}{dt}\int_0^{2\pi}\frac{\sin\eta}{1+\mu^2+2\mu\sin\eta}\,d\eta\,, \tag{2.66}$$

which may be integrated by substitution of $t=\tan\eta/2$ to give

$$2\rho\Gamma\left(\frac{U}{1+\mu^2}+\frac{\Gamma}{2\pi}\frac{\mu}{(\mu^2-1)(\mu^2+1)^2}\right)\,. \tag{2.67}$$

The contribution from the velocity term is

$$\rho\int_0^{2\pi}\frac{\Gamma^2}{4\pi^2\sin\eta}\frac{(1+\mu\sin\eta)^2}{(1+\mu^2+2\mu\sin\eta)^2}\,d\eta\,, \tag{2.68}$$

which may be integrated by the same substitution, and after considerable algebraic manipulation gives

$$-\frac{\rho\Gamma^2}{\pi}\frac{\mu}{(\mu^2-1)(\mu^2+1)^2}\,. \tag{2.69}$$

The total lift when the vortex is equidistant from the leading and trailing edges of the aerofoil is thus

$$L=\frac{2\rho\Gamma U}{1+\mu^2}\,. \tag{2.70}$$

We confirm that when the vortex is very near the plate ($\mu\sim1$) then

the lift is $\rho\Gamma U$, the same as if the vorticity were attached to the plate. Furthermore we can now see how the lift reduces as the vortex position moves away. Figure 2.33 shows the reduction in lift as the vortex moves away from the blade. A vortex within one third of a chord gives more than half the lift which it would give if it were attached. It makes no difference whether the vortex is above or below the blade, the lift function is symmetrical about the zero point. It will affect the length of time that the lift acts, however. The velocity of the vortex relative to the flat plate is

$$\frac{dz_0}{dt} = U + \frac{\Gamma}{2\pi} \frac{\mu}{(\mu^2-1)(\mu^2+1)} , \qquad (2.71)$$

which is the free stream velocity U, plus a term representing the self-induced velocity of the vortex; that is anti-symmetric with respect to μ. A clockwise vortex above the plate will flow past at less than the free stream velocity, and the lift will therefore act for longer than would the lift induced by an anti-clockwise vortex which travels with more than the stream velocity. The opposite is true for motion below the plate. For a small vortex the change in lift impulse is second order in the vortex strength, and therefore no more important than the deviations of the vortices from the rectilinear wake. A strong clockwise vortex above the plate (or anti-clockwise below) may actually travel against the stream if it is near the plate. If no other boundary was present it would progress round the leading edge and downstream on the other side of the blade. The path in the presence of the other blade is beyond the scope of the work presented here, but could be found approximately with a full computer model, and the total lift impulse estimated.

Most of the vorticity shed by the stator in figure 2.32 passed within a third of a chord length of the rotor, and the greater part of this was therefore effectively attached. The circulation change

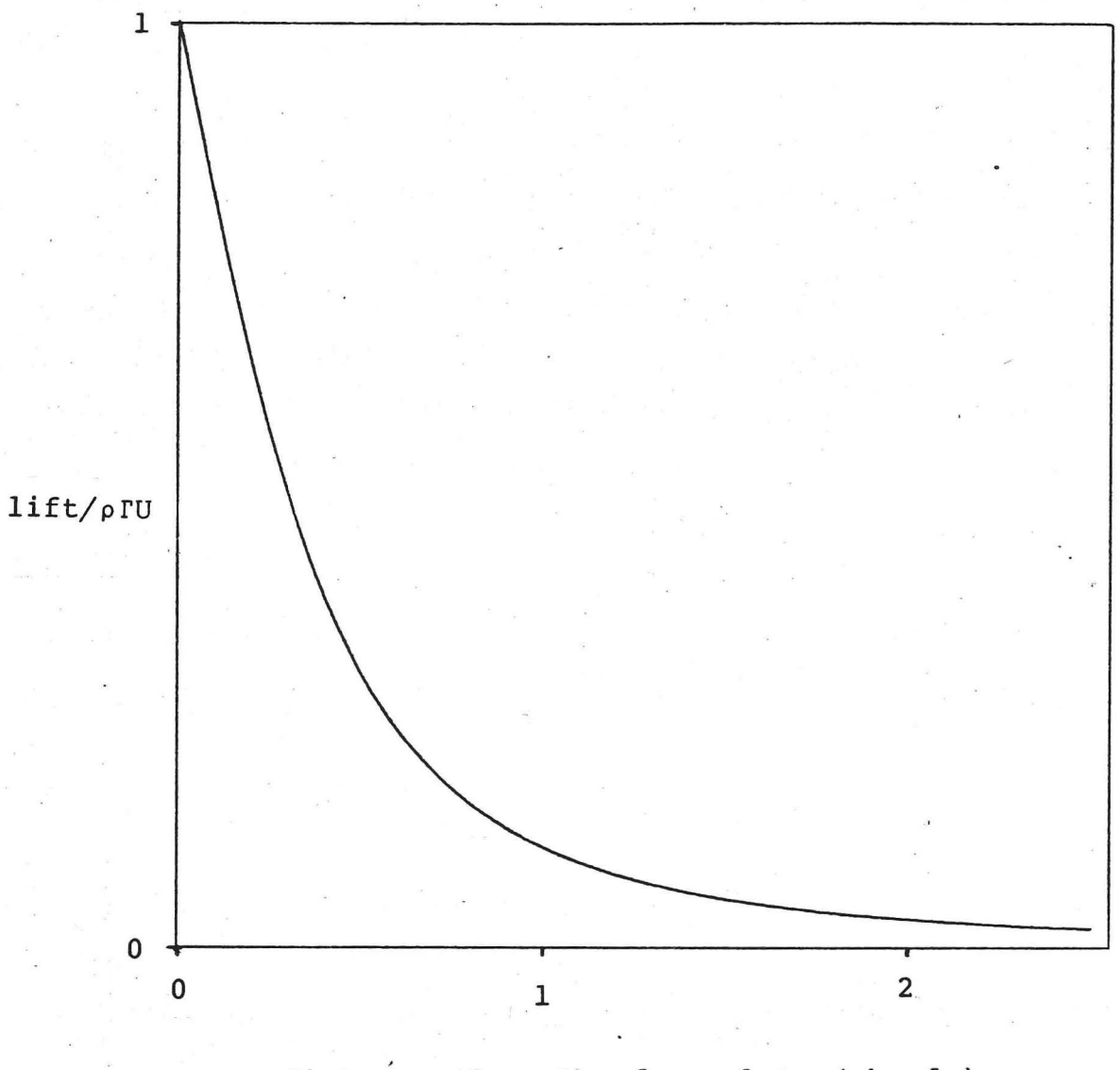

Figure 2.33. The dependence of the lift on a flat plate at zero incidence on the distance of the convecting vortex generating the lift. The vortex is on the line passing perpendicularly through the mid point of the plate.

on the rotor was probably less, but only a little less, than that predicted by the Weis-Fogh modelling.

In this example, and in the experiment, the rotor approaches the stator with one tenth of the free stream speed. In turbomachinery these speeds are usually approximately equal, and therefore less of the vorticity shed from the upstream blade will be convected downstream without passing close to the second blade. The lift on the downstream blade resulting from this convecting vorticity will be nearer the value predicted by the Weis-Fogh theory. As the rotor velocity increases relative to the free stream velocity, the time in which vortex shedding can act gets lower, and the closer the final circulation levels will become to those predicted by that potential theory, which is of course exact in the limiting case of no vortex shedding.

This concludes the examination of the isolated interaction between two blades which touch in passing. We have a potential flow model which ignores vortex shedding, and we have seen both theoretically and experimentally how vortex shedding modifies the results of this model. Our conclusion is that the Weis-Fogh type of model is a good first approximation to the real phenemenon for a known time around and after the interaction, particularly when the velocity of the moving blade is of the same order as, or greater than, the free stream velocity. This condition usually applies in turbomachinery, and it is therefore with some confidence that we now go on to examine the performance of the interaction in cascade.

3 INTERACTING CASCADES

3.1 Theoretical predictions

We now know that a pair of interacting aerofoils can generate circulations comparable with those on steady aerofoils resulting from application of the Kutta condition, and we suspect that the interactions can sustain a useful flow at effective incidences beyond the conventional stalling condition. We wish to build the interaction into a turbomachinery stage, and estimate the performance in comparison with a conventional stage. The problem arises here that there are many different parameters which will affect the results of the calculation. We have therefore chosen to base our model on a geometry close to to that used in one of our experiments (see figure 3.1).

The stage used in the following calculations has rotor and stator blades which are flat plates of equal chord, with the blade spacing also equal to the chord. The conventional two-dimensional cascade representation is used with infinite blade sets along the x-axis, and flow down the y-axis representing axial inflow with no swirl. The blade staggers are 45 and 30 degrees for the rotor and stator respectively. For the conventional cascade performance we have used the results of Weinig (1935) for the exact potential flow through a cascade of flat plates, the relevant sections of which are summarized by Horlock (1958). The rotor and stator are treated separately, though the entry conditions at the stator are of course determined by the flow deflection through the rotor.

The interacting cascade results were obtained by treating each rotor-stator interaction in isolation. The blade circulations were calculated by methods outlined earlier, and the rotor blade lift was assumed to be that resulting from the movement of this circulation

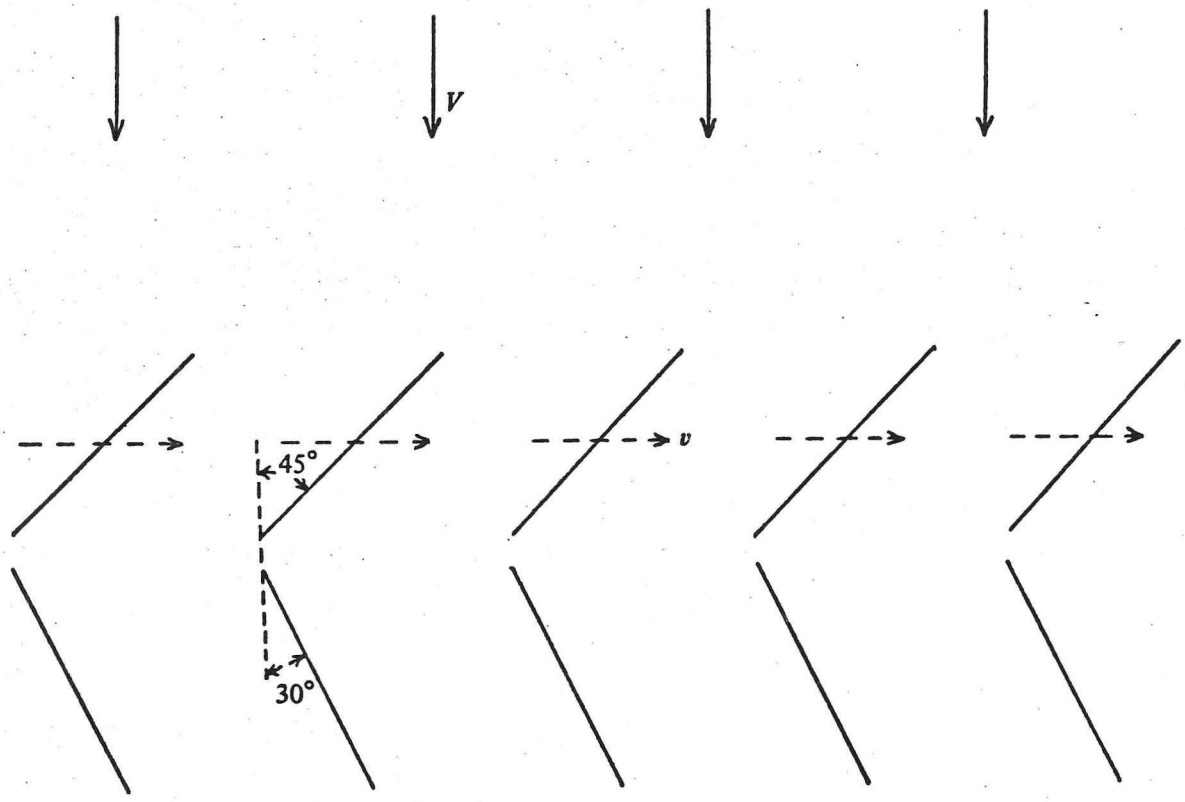

Figure 3.1. The geometry used for the stage calculations.

relative to the inflow. The rotor circulation also causes a deflection of the main stream which will then generate lift on the stator. Since the rotor and stator circulations are equal, the outflow from the stator will be axial, at least outside the disturbed area.

It is worth noting here that, since the rotor and stator circulations are equal but opposite in sign, when the blades touch subsequently the total circulations on each rotor-stator pair will be zero, as we assumed for the starting condition, so the solution does represent the steady state.

In any machine which exploits this high interaction loading in a real fluid, the generation of excess circulation over that required by the Kutta condition would result in vortex shedding and gradual return to the Kutta level. Each interaction would then return the circulations to their previous high value, so that the mean circulation would be above the Kutta value. Thus we should expect a real machine to work somewhere between these two possible conditions; detailed calculation of the actual level would require the extension of the theory along the lines we used to model the isolated interaction experiment, the results of which were qualitatively similar to the idealised case and justify our use here of the Weis-Fogh modelling which is more easily handled.

The results of these calculations are presented in figures 3.2 and 3.3. Figure 3.2 gives the stage loading ($\Delta p/\frac{1}{2}\rho v^2$ where Δp is the pressure rise and v the rotor velocity) against the flow coefficient (V/v, V being the axial fluid velocity). Figure 3.3 breaks the total stage loading down into separate rotor and stator loadings. We have also marked on figure 3.3 the lift coefficients of the conventional rotor and stator at various loading conditions, to give some impression of where stall will occur, since our calculations do not allow for flow separation. The results show that the

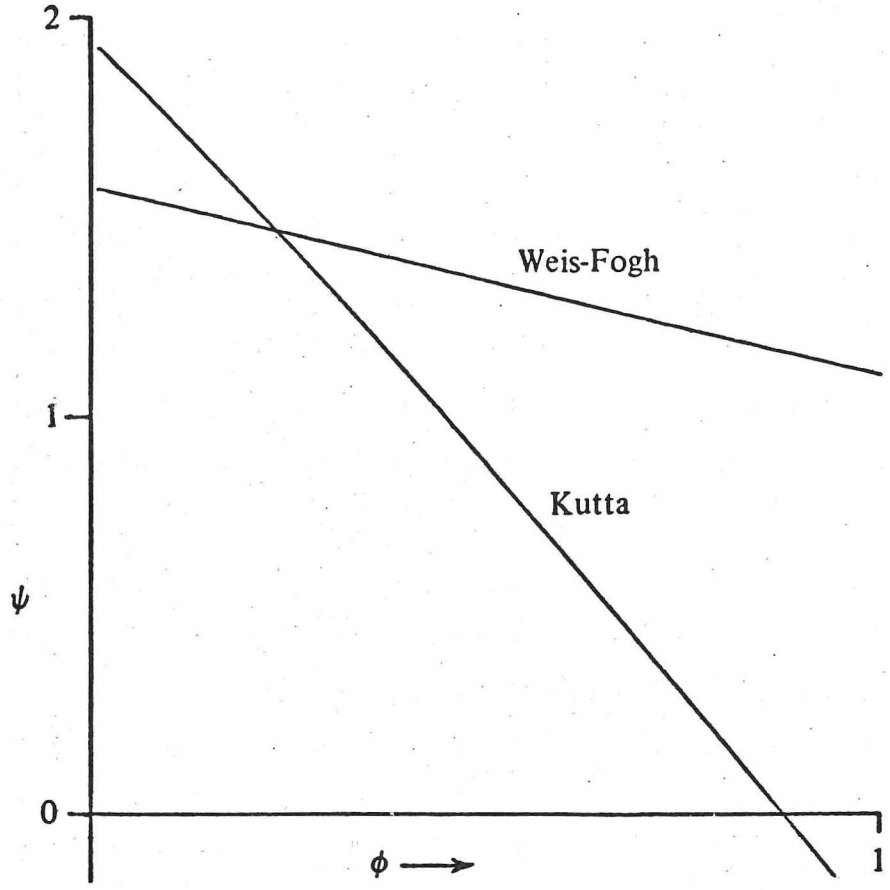

Figure 3.2. The overall performance of a stage operating under Kutta or Weis-Fogh conditions. The stage loading Ψ ($=\Delta p/\frac{1}{2}\rho v^2$) is shown against flow coefficient Φ ($=V/v$).

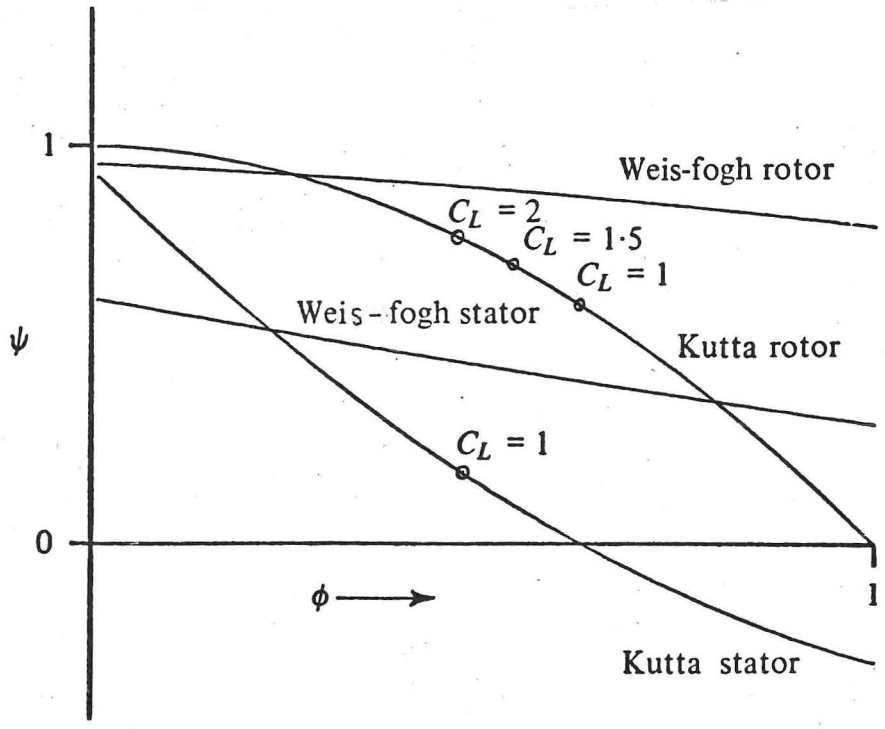

Figure 3.3. The rotor and stator stage loadings Ψ ($=\Delta p/\frac{1}{2}\rho v^2$) for flow coefficients between 0 and 1. The lift coefficients are shown for the Kutta blading to indicate where stall may be expected.

interaction blading has a very similar performance to the conventional blading at the peak operating condition, but the stage pressure rise reduces much more slowly as the flow increases. Thus the interaction stage may be expected to produce useful pressure rises over a significantly wider range of operating conditions. The relative peak performance may vary from one geometry to another, but in the case considered here the interaction stage appears to produce a somewhat higher pressure rise.

It should be said here that our potential flow models do not enable us to make any estimate of the relative efficiences of the two stages, and for many applications the efficiency is at least as important as the stage pressure rise. Realistic estimates of the effect of the interaction on efficiency are most easily found by experiment. We describe below a small scale rig operated at conditions in which the interacting stages could be studied experimentally. Tests on this rig confirm our hopes for improved performance from the interaction, and indicate also a slight efficiency advantage.

3.2 Experimental apparatus

The theoretical work presented in the last section indicated that there might be practical benefits from the use of the Weis-Fogh principle in turbomachinery. To demonstrate that performance advantages were realisable in practice would require that tests be performed on a suitable stage. The problem then arises that the model geometry used for the calculations does not give sufficient information to design an optimal interacting stage, any more than a flat plate leads to an optimal conventional cascade. We were consequently faced with the prospect of having to compare the performance of a prototype interacting stage, of aerofoils designed mainly by intuition, with a conventional stage which was the result of quarter of a century of intense development. In addition, the construction of a stage to obtain maximum performance requires working to very low tolerances in tip clearance, and in our case rotor-stator clearance, and running at speeds that demand high precision equipment. All of this adds up to great expense, especially when there is uncertainty about the exact blade shapes, and it might be necessary to construct more than one set.

It was decided, therefore, that this series of tests would not be intended to study the absolute characteristics of the interaction stage vis-a-vis the conventional stage, but rather to demonstrate that increasing the rotor-stator interaction in a particular stage could significantly improve its performance. This we have done.

Once the aim of the experiment was restricted to comparing the performance of one stage under differing conditions, it became possible to proceed in a much more economical manner. Instead of requiring minimum losses it was necessary only to ensure that the losses associated with the test-rig were the same for all configurations. The tests could be performed in water, so the rotational

speeds could be kept down and the accuracy requirements on the machine relaxed.

The tests were performed on an apparatus at the Whittle Laboratory, Madingley Road, Cambridge. The apparatus is used for practical work by third year students at the University Engineering Department, and is fully instrumented and designed for rapid access to the working section for blade changes and so on. It is manufactured by Tecquipment Limited, of Nottingham, England. Figure 3.4 shows the general layout of the apparatus, and there is a photograph of it at the back of the dissertation (plate 3). It is a closed cycle, water filled rig. There is a tank (bottom left of figure 3.4) into which the water may be drained for access to the working section. The circuit is refilled by pressurising the air in the top of the tank and releasing the air in the circuit through the vent at the highest point. There is an electric motor for driving the rotor with direct torque and speed measurements, and an auxiliary (centrifugal) pump for overcoming the circuit resistance at high flow rates, or for driving the fluid when the apparatus is used in its alternative role for testing turbine blading. A Venturi tube and manometer give a direct reading of the flow rate, and a second manometer is used for comparing static pressures at different points in the circuit. Various valves control the flow rate and include or exclude the auxiliary pump from the circuit.

The working section (figure 3.5) has stations for one row of inlet guide vanes, a rotor, and a stator downstream of the rotor. Any of these could be replaced by a blank ring, and in our case inlet guide vanes were not used. Each row consisted of twelve blades made of polycarbonate and mounted in a metal ring. The ring was designed to allow the blades to be rotated to any stagger before being clamped, though a change in stagger would alter the tip clearance and either increase the losses or require that the blades be further turned down.

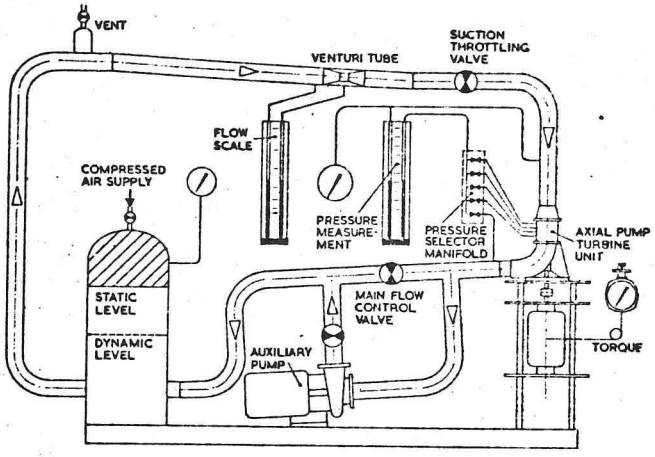

Figure 3.4. The Tecquipment axial flow pump/turbine H26. The general layout of the apparatus used for investigating the behaviour of axial stages at low rotor-stator clearances.

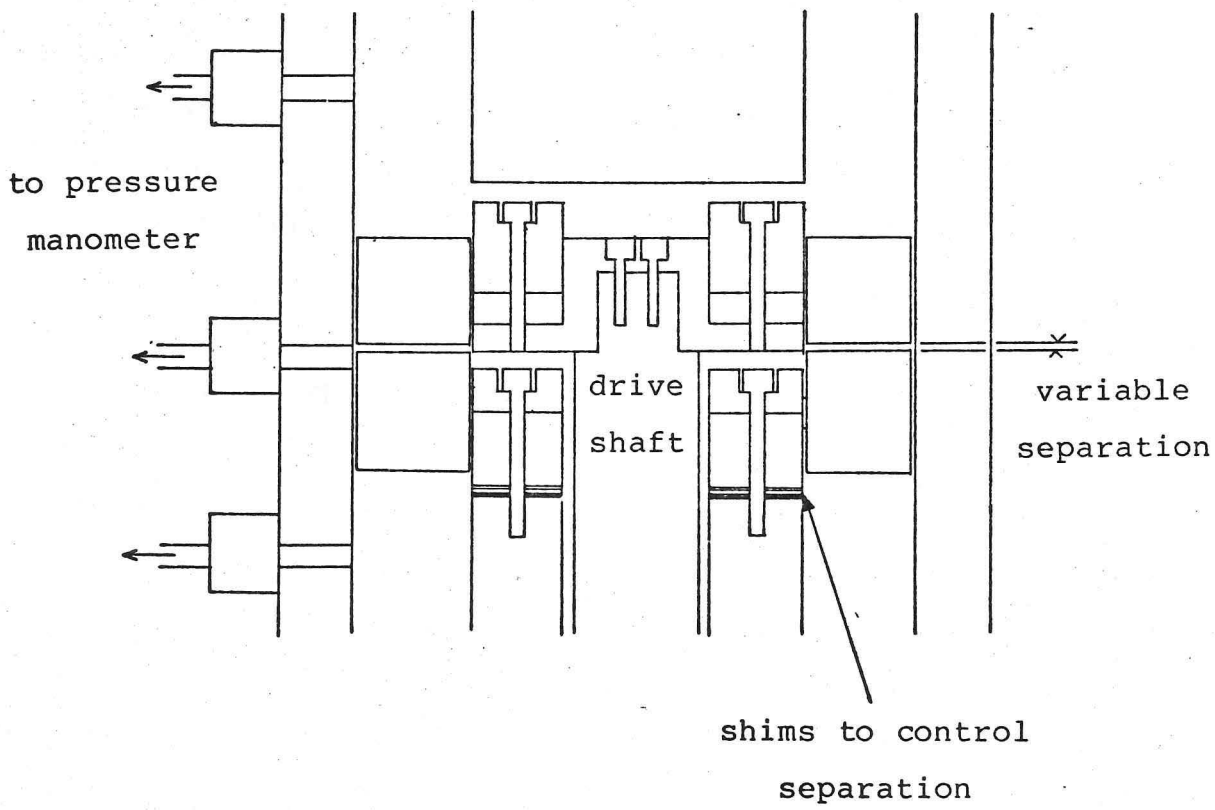

Figure 3.5. The working section of the apparatus, showing the blade mounting system and the arrangement for varying the rotor-stator clearance by use of shims.

For this reason normal practice was to set new blades to a predetermined stagger, turn them down on a lathe to give the standard tip clearance, and then use them just at that stagger.

Since the object of our tests was to examine the performance of blades running with very little rotor-stator separation, and the apparatus was not designed with this in mind, it was necessary to modify various components in the working section to reduce the minimum distance between the rotor and stator mounting points. This was fairly straightforward, and involved reducing the thickness of some of the components which determine this separation. Then a set of shims were made, to be placed between the rotor or stator mounting rings and their supports. These shims were the only items varied between tests, and they were used to control the rotor-stator separation.

The tests were performed with two different sets of blades. One set was designed to maintain the principle of the first theoretical model, and have effective rotor-stator contact for a finite time at each interaction. A conventional aerofoil could be used for the rotor, but the stator required a flat upper surface parallel to the direction of motion of the rotor. It was necessary, therefore, to have a new set of blades made. The blades previously used in ths apparatus were 'two-dimensional', and although the hub to tip ratio is not large enough to ensure a two-dimensional flow, this economy seemed reasonable enough for our comparative tests. The stator could then be specified by a single aerofoil section, about which little was known except that it should have a flat upper surface. A suitable profile was drawn 'by eye' using a computer aided design program at the Engineering Department design office. The program ensured a smooth fairing in of the flat surface with the rest of the profile, and generated output suitable for input to a numerically controlled milling machine to produce the mould in which the blades were formed. Figure 3.6 shows the resulting section, together with that of the

rotor, with the spacing corresponding to that at mid-span.

The second set of blades was more conventional, and is the set on which the model for the theoretical cascade analysis was based. The aerofoils were both of the section used for the rotor in the first set, and were known to give among the highest efficiences achieved by any blading in this rig. The sections and mid-span spacing are shown in figure 3.7.

Other data relevant to the tests are presented in appendix 3.

The test procedure was as follows. The blades were mounted on the appropriate rings at the desired stagger, and then the rings were mounted in the working section, using shims to obtain the desired axial clearance. The test at the lowest clearance (about .1 mm) was performed first, as some adjustment or trimming of a few blades was necessary to prevent catching. No further adjustment would be necessary for the tests at higher clearance, so we could be sure that this would not contribute to any differences.

The working section was then reassembled and the circuit filled with water. The valves were all opened fully and the stage used to drive the water round the circuit so that all the remaining air would collect at the top to be bled off. The connecting pipes to the manometers were similarly bled. Then the rotor was run up to speed (2,500 rpm) for the measurements. The valves were used to control the flow rate which was measured directly on the manometer connected to the Venturi tube. The torque required to maintain the rotor speed was indicated by a spring balance attached to the motor casing, and the speed itself was measured electrically. The static pressure rise across the stage was measured by a second manometer. When readings had been taken over the range of flow rates that did not require the auxiliary pump, this was switched on and readings taken for the higher

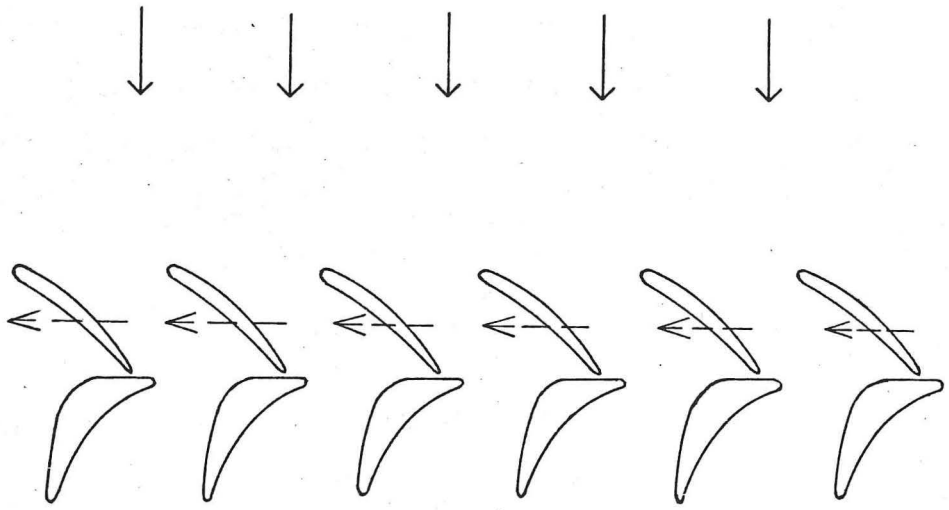

Figure 3.6. The blading designed to emphasise the interaction effects, shown at the spacing corresponding to that at mid-span in the apparatus. Note particularly the flat upper surface of the stators.

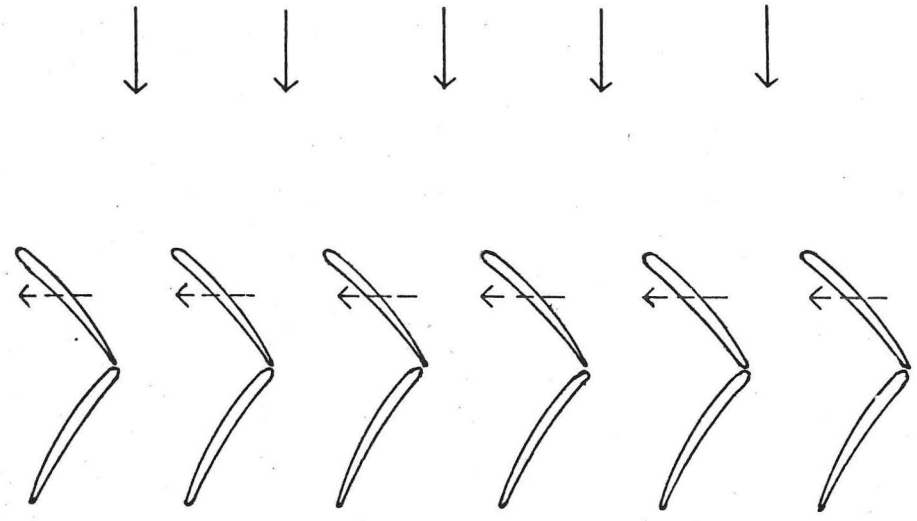

Figure 3.7. The conventional blading tested at low rotor-stator clearances, shown at the spacing corresponding to that at mid-span in the apparatus.

flow rates then attainable.

This completes the procedure for one rotor-stator separation. The working section can then be stripped down (after draining !) and the shims changed to give an increased separation. Only in the case of the test at 5 mm separation did the shims not give sufficient variation in the separation. For this final test it was necessary to mount the stator ring the other way up, having first rotated the blades through 180 degrees relative to the ring so that they retained the same orientation. This made use of the fact that the blade mounting positions were not vertically central on the mounting rings.

3.3 Experimental results.

The results of the tests described in the last section are shown in figures 3.8 to 3.11. Figures 3.8 and 3.9 are the results of the tests on the special stage with the stator designed to give a rotor-stator seal for a finite time at each interaction, and figures 3.10 and 3.11 are the results from operating a conventional stage at reduced clearances.

Two figures are given for each stage, one showing the stage pressure rise and the other showing the overall efficiency at various flow rates. Each figure has a number of curves, corresponding to the different clearances tested with each stage.

The results for the special stage show a clear increase in the stage pressure rise and efficiency as the clearance is reduced over most of the range of flow rates covered by the tests. At the highest flow rate the pressure rise and efficiency at the smallest clearance are almost double their value at the highest clearance, and the peak efficiency and pressure rise are increased by 10 and 20 percent respectively by reducing the clearance.

Readers familiar with the performance of current axial flow compressors will have noticed that the peak efficiencies achieved in these tests are much lower than those obtainable from conventional stages built to the highest standards. However the efficiences obtained here are not untypical of those achieved with conventional blading in this apparatus. The best conventional blades for the apparatus have been found by experiment, and can operate at efficiences up to 70 percent as we shall see in the tests with the conventional blading, but earlier conventional blading had a lower performance than our interaction stage.

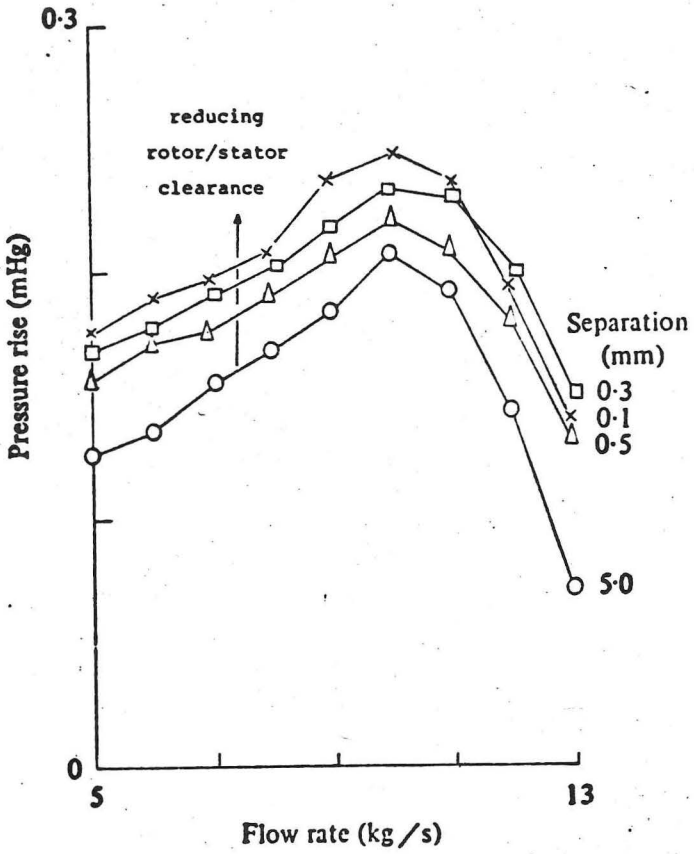

Figure 3.8. The pressure rise across the stage designed to emphasise interaction effects.

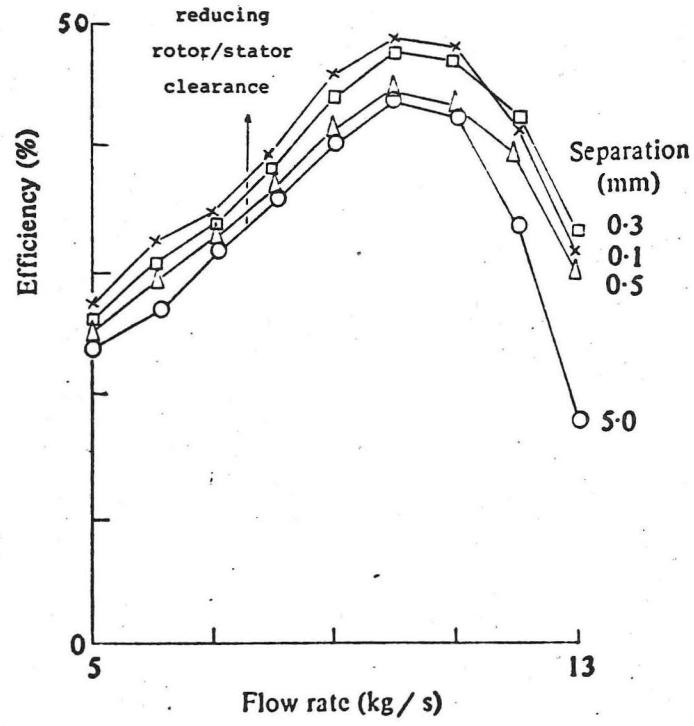

Figure 3.9. The efficiency of the stage designed to emphasise interaction effects.

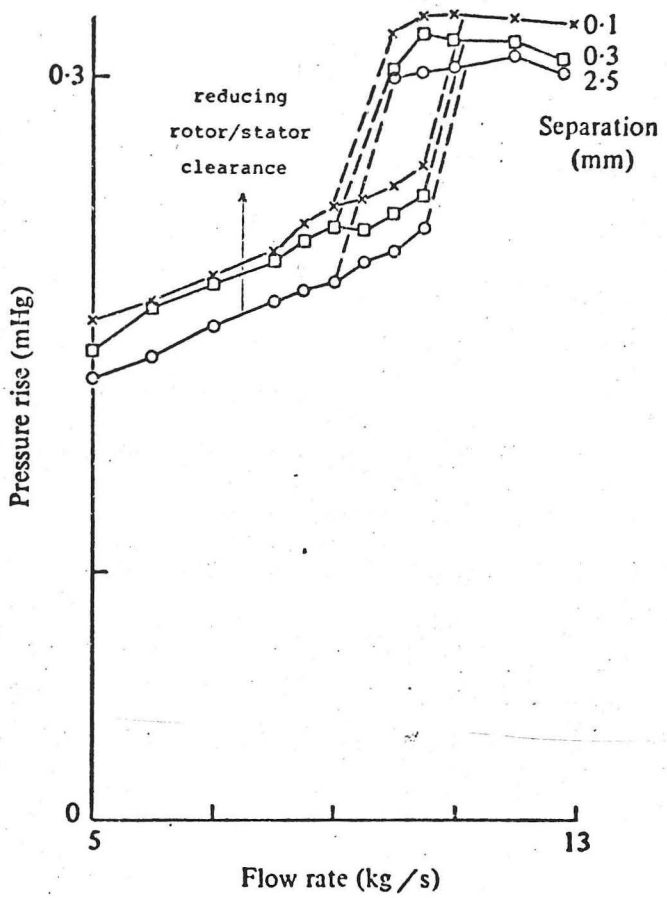

Figure 3.10. The pressure rise across the conventional stage.

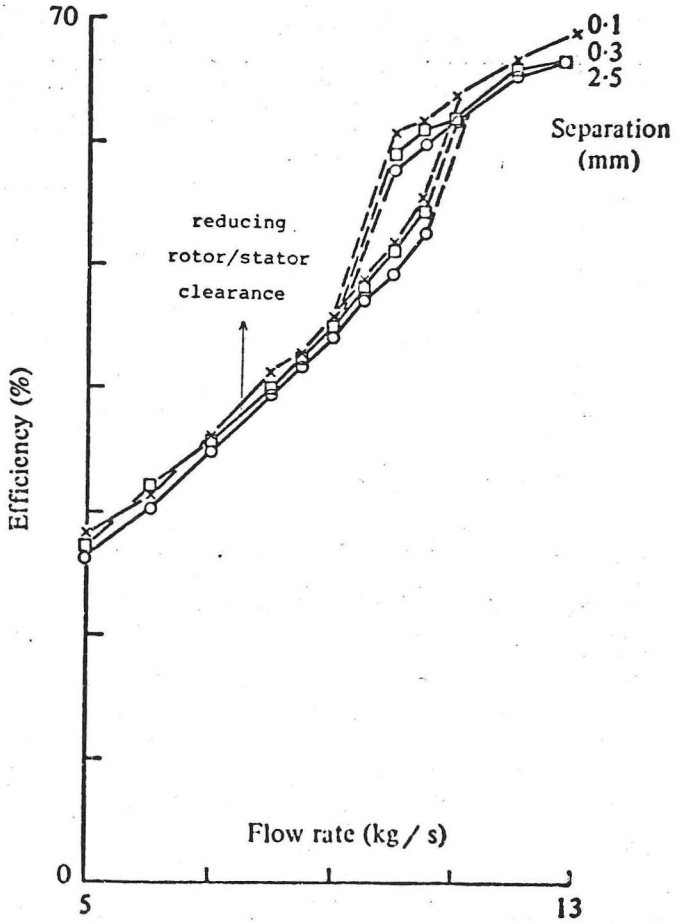

Figure 3.11. The efficiency of the conventional stage.

The results of the tests on conventional blading are shown in figures 3.10 and 3.11. Again there is a measurable increase in the stage pressure rise at all flow rates with decreasing separation, together with a smaller improvement in efficiency. These changes can be seen both above and below the stalling point. The flow rate at which the stage stalls does not seem to be affected by the separation, though the combined effect of unsteadiness in the flow and the hysteresis at the stall point made this hard to check with good accuracy. The pressure rise at stall is certainly higher at the lowest clearance.

The interaction, therefore, appears to enhance the performance of both the special and the conventional blading, at least under some operating conditions. The improvement is large enough to be of interest, and if a similar improvement were possible in an engineering application then the added difficulty of manufacturing the blade rows so that they could be run safely with a sufficiently low rotor-stator clearance may be justified.

3.4 Previous work

In recent years much work has been done to investigate the relative importance of the many geometric factors that determine a complete compressor design, but only during the last fifteen years has much attention been paid to the effect of axial clearance. We have found no reference to tests at the low axial clearances we used in our experiments, but nevertheless some published results are worth mentioning since they display similar trends which support our results.

Aschenbrenner (1966) performed tests on several different sets of blading in a closed cycle single stage axial pump rig at Brunswick Technical University in Germany. The axial spacings used varied between 2.6 percent and 40 percent of the rotor chord (our tests went down to half a percent), and improvements in the head coefficient and hydraulic efficiency were observed with reduction of the clearance for all blade sets. The efficiency improved by one or two percent, and the head coefficient went up by one to five percent. Flow visualisation indicated a reduction in flow separation, and it was suspected that not only the boundary layer flow but also the potential flow was affected by the interference between the blade rows at the lowest clearances.

Jenny (1976) notes similar improvements in efficiency resulting from reducing the axial clearance between an upstream rotor and a downstream stator, though the clearances used here are all above ten percent. The efficiency is lower, however, when the clearance between an upstream stator and a downstream rotor is reduced.

Smith (1970) was primarily interested in the effect of the various geometric parameters on the end-wall boundary layer thickness. He used a four stage low speed compressor which allowed independent

variation of the tip clearance, the aspect ratio, and the axial clearance. The axial clearance went down to 1.5 percent of the chord, and the pressure rise at this clearance was ten percent higher than at a clearance of seven percent of the chord. The peak efficiency was about one percent higher also.

Miller (1971) summarises the available evidence of the effect of axial gaps on compressor performance, including details of some industrial compressors where aerodynamic problems have been overcome by the reduction of these gaps.

The general picture seems to be surprisingly consistent. In our tests, and in the other references, we have found that reducing the axial gaps always seems to result in a higher surge pressure rise. The pressure rise for very low gaps (1 percent of the chord) is usually around ten percent higher than for large gaps (30 percent of the chord). The efficiency is increased by one or two percent at the low clearances, with the exception of Jenny's results on a single stage where the rotor was downstream of the stator. There are also reports that reduced gaps can supress surge and rotating stall (eg Miller, 1971).

Overall there is strong evidence that low axial clearances are beneficial to the aerodynamic performance of axial compressors, and particularly in that the surge pressure rise is significantly increased. Many of the results when plotted as a function of axial clearance show increasing improvements at the smallest gaps, suggesting that even lower clearances would give further gains. Our results support this. With our conventional stage, the increase in pressure rise resulting from reducing the gap from 1.5 percent of chord to .5 percent was as great as that from 12 percent to 1.5 percent. This suggests to us that the principal effect is the partial blocking of the flow through the gap when the blades pass, which must result

in the useful potential flow change we have described. There may be other effects involved at the higher clearances, such as the variations in the thickness of the casing boundary layer described by Smith, but it is hard to believe that this will be significant in cases with the smallest clearances. It is certainly not the major effect. We therefore conclude that the interaction takes place in conventional machines at very low axial clearances, and is probably responsible for the increased pressure rise and the postponement of surge and rotating stall. The improvements in efficiency are not so obviously the result of blade interaction, but are consistent with it in that the generation of strong circulation by the Weis-Fogh method would tend to reduce regions of separation, and thereby reduce losses, in exactly the same way as it suppresses stall.

4. ENGINEERING APPLICATIONS.

4.1 Axial flow fans.

We have described how interactions of the type used by Encarsia formosa may be built into geometries suitable for turbomachinery applications, and we have shown how the performance of such machines may be predicted. Our tests encourage us to think that the prediction methods are valid, and therefore the calculated performance advantages should be available for exploitation in production machines. We have suggested that some of the improvements found to result from reducing the axial spacing in conventional machines are due to the potential flow interactions which we have described, so the Weis-Fogh effect may already be in use. These unintentional applications of the effect were found before the view of the interaction that we have formed was available, and it is likely that a machine designed from the outset to make full use of the principle would find even greater performance advantages.

Designing a machine to make full use of the Weis-Fogh effect will introduce new problems. The axial clearances must be very low, and this may result in increased noise and susceptibility to damage from ingested contaminants, as well as the obvious difficulty of maintaining the clearances without causing mechanical damage as the blades deflect under cyclic load. The noise problem is sufficiently important that we devote the next section of this dissertation to it, and we shall leave further discussion of it until then. The ingestion and mechanical damage problems are related. The small axial gap between blade sets can be closed either by the blades bending or by contaminants passing through it. We used a flexible trailing edge in our tests on the isolated pair of aerofoils, and the axial stage rig, in which the blades were slightly flexible, had a contaminant filter. The use of some sort of flexible material on one

of the opposing surfaces would have to be given serious consideration.

How would the design be carried out ? We have not provided sufficient information to design optimal interacting stages, and further work is required in this area. It has been demonstrated that conventional stages can work better under conditions of high interaction, but the blading for these stages has been designed from isolated cascade data. It seems most likely that a stage designed from the outset to exploit the interaction would work better than two blade sets designed to work on their own which are then operated in a high interaction mode. Our initial attempt at a specially designed stage did not perform well in the tests, except that the improvements under high interaction conditions were far more pronounced than those observed in tests on conventional stages. We increased the interaction effects at the expense of the conventional performance, and lost out overall. The losses due to the flat upper surface would be smaller for lower flow coefficients, and it is possible that the special stage would extend the useful range of operating conditions if the stator camber were lower. The flat upper surface might be a valid feature of axial compressors designed to operate at high pressure rises and low flow coefficients.

Stages designed to use the Weis-Fogh effect would probably not look radically different from conventional designs, with the possible exception of the low flow rate stage mentioned above, but for high performance applications a reappraisal of the necessary compromise between aerodynamic performance and structural rigidity may be necessary. The constraint on the axial gap will inevitably introduce new difficulties for the designer, and these must be weighed against the performance advantages that will result from full exploitation of the principle.

4.2 Sound generation.

Although conventional axial compressors are designed from cascade data, which give details of blade performance under steady entry and exit conditions, the flows in actual machines are far from steady. The unsteady forces on the blades give rise to noise, and the transmission of this noise to the environment outside the machine may be found by establishing the appropriate Green's function and convoluting this with the source terms. We can get some idea of the likely noise generating performance of a compressor designed to use the Weis-Fogh principle without going through these calculations because the geometry is not very different from that of a conventional machine. The similar geometry means that the Green's functions can be the same, and so the relative sound generating performances will just be related to the relative source strengths. Thus we shall not attempt to present the absolute noise performance of our machine, but rather compare it with that of a conventional machine. The known performance of conventional machines will then enable us to estimate the absolute performance without any detailed calculation.

Unsteady forces on acoustically compact blades give rise to dipole sources in comparison with which all quadrupoles are negligible. Goldstein (1976) gives the necessary development of the expression for the acoustic density disturbance in a free space far field. His development is based on the work of Curle's (1955) extension of Lighthill's (1952) acoustic analogy.

$$\rho' \sim \frac{-x_i}{4\pi c_s^3 x^2} \frac{\partial F_i}{\partial t}(t-x/c_s) \qquad (4.1)$$

Here F_i is the total force acting on the sound producing surface, c_s is the velocity of sound in air, and the x_i are the coordinates of the observer relative to the source. This expression for the sound

field is valid when the source is compact. This will be the case at low enough frequency, and we will describe a different calculation method for the non-compact case. Of course, the sound produced inside an engine casing is modified by the appropriate transfer function, but we can anticipate that the unsteady blade loads would still play a critical part in determining the wave amplitudes. The field will be proportional to the unsteady loads on compact blading in most of the situations that we can envisage. We can therefore compare the sound generating performance of Weis-Fogh and conventional machines by looking at the ratio of typical unsteady forces in them.

Kemp and Sears (1953) give an approximate theoretical prediction of the unsteady forces in a conventional stage, and show that they may be twenty percent of the mean steady values. We would not expect the Weis-Fogh principle to be used to increase the pressure ratio of a stage by much more than twenty percent, but how is this related to the unsteady forces on the blades ? Also, the expression (4.1) for the sound density variations contains a derivative with respect to time of the forces. We must be careful therefore to see that we do not ignore the higher harmonics of the blade passing frequency, since they could be significant even if they contribute little to the force.

Let us consider the case of a conventional stage in which the axial clearance has been reduced to take advantage of the increased pressure rise resulting from the interaction. The circulation on each blade is boosted each time it passes a member of the adjacent row, and then the circulation decays on the vortex shedding timescale. The lift on the blade will decay until the next member of the adjacent row passes, when it will return to the high level. The time history of the lift will therefore resemble a sawtooth (figure 4.1). The proportion of the excess circulation which will be shed between interactions depends on the vortex shedding mechanism, and if we

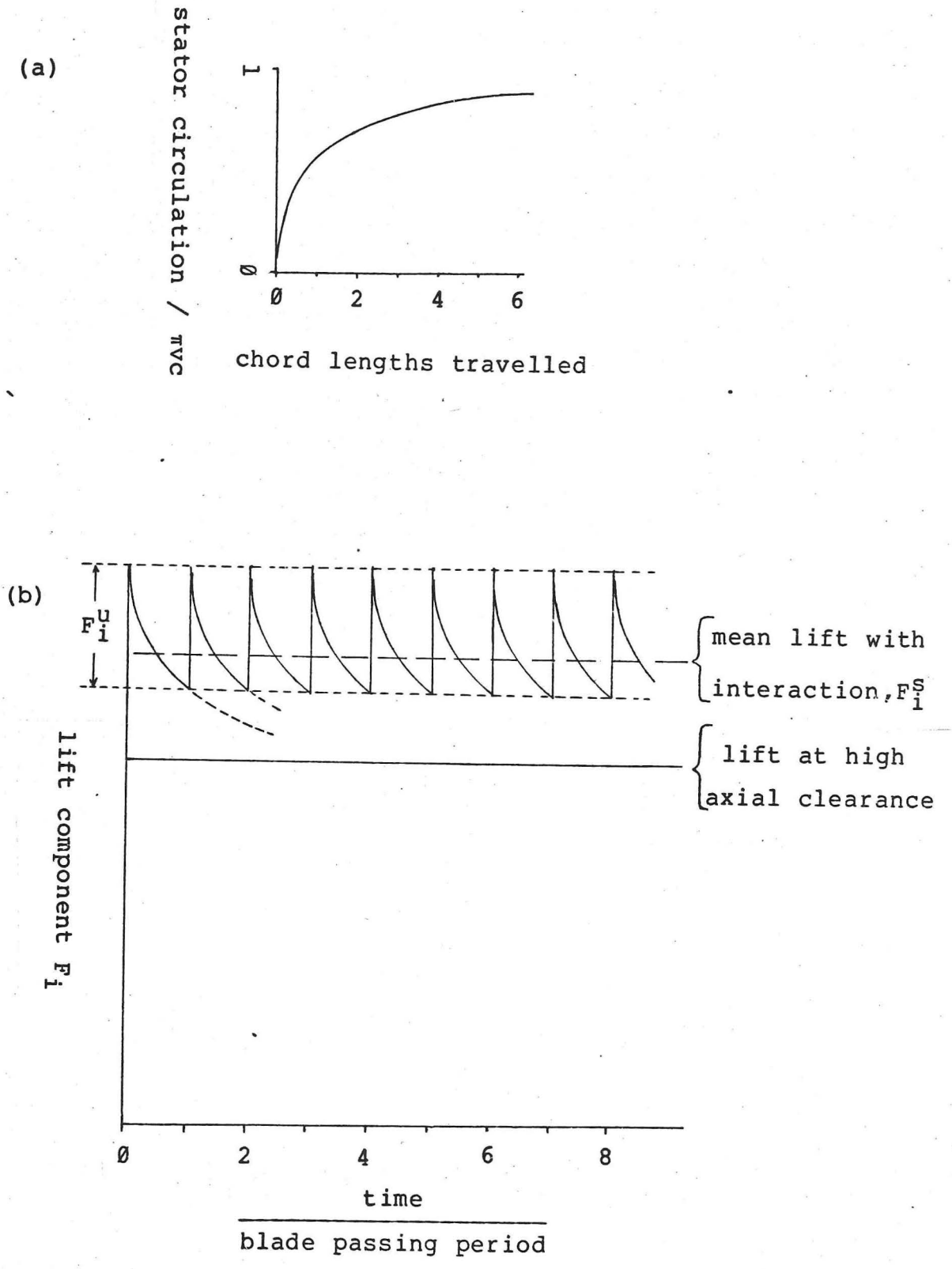

Figure 4.1. The unsteady lift on a pair of blades in a stage which uses the Weis-Fogh effect to boost the circulations. (a) The Wagner response function, for an aerofoil starting impulsively from rest. (b) The lift on one of the blades, assuming that the interaction raises the circulation which then follows the response (a) until the next interaction.

assume that the Kutta condition applies then we can make an estimate from the results of Wagner (1925). If the rotor and free stream velocities are approximately equal, and the blade spacing is equal to the chord, then the rotor will have travelled $\sqrt{2}$ times its chord relative to the stream between interactions. Ignoring the influence of the other blades after the interaction, Wagner calculates that the circulation will be 60 percent of the way to the asymptotic value. Thus the unsteady force will be 60 percent of the increase in the pressure rise due to using the Weis-Fogh principle. The unsteady force is therefore unlikely to be much larger than those found in existing machines. The harmonic content is rather different, however.

Kemp and Sears (1953) calculated the relative strengths of the first two harmonics of the blade passing frequency for a conventional stage, and found that the fundamental was the most significant. In our case we have seen that the force follows approximately a sawtooth pattern, and we can find the strengths of the harmonics by Fourier analysis. We represent the force by the usual Fourier series, based here on the blade passing frequency.

$$F_i = F_i^s + \sum_{n=1}^{\infty} A_i^n \sin(n\omega t) \tag{4.2}$$

where F_i^s is the mean (steady) force, ω is the blade passing frequency, and the A_i^n are constant coefficients to be determined. If we take the amplitude of the sawtooth to be F_i^u, then the A_i^n are given by

$$A_i^n = \frac{F_i^u}{n\pi} (-1)^n \tag{4.3}$$

The harmonics therefore decay like n^{-1}, and the contributions to the time derivative do not decay at all. The sound field is composed of equal quantities of all the harmonics, at least up to those

frequencies where the assumption of compactness breaks down. This contrasts with the situation in a conventional stage with large axial gaps, where the fundamental dominates. There are, however, other situations where a very similar sound field is found. A supersonic rotor produces radiating shock waves which to a stationary observer present sudden increases in the pressure, which must return to its original level between shocks. This will result in an approximate sawtooth waveform. Hawkings and Lowson (1974) give an analysis of this sound field, and calculate pressure waveforms which show unsteady pressures of around two percent of atmospheric pressure. If our stage had a pressure ratio of 1.5, and the unsteady force was ten percent of the mean level, then we would be producing unsteady pressures of five percent of an atmosphere. We would therefore conclude that the likely sound field will contain a fundamental at the blade passing frequency of comparible magnitude to that found in conventional machinery, and high harmonics which are somewhat louder. The similarity to the supersonic rotor sound field makes the buzz-saw noise (see Ffowcs Williams, 1970) based on the shaft rotation frequency a possibility also.

It is worth noting that if the interactions happen more frequently on the vortex shedding timescale, then the lift in figure 4.1 will have less time to decay. The amplitude of the unsteady force will be reduced to less than 60 percent of the increase in load due to using the Weis-Fogh principle, and the sound will be reduced accordingly.

This accounts for the sawtooth form of the unsteady lift, but in addition there is a pressure impulse when the gap between the blades is closed. The blades certainly cannot be considered compact for the calculation of the sound field caused by this effect, and we must find a different approach. Ffowcs Williams and Lovely (1977) have suggested a method for evaluating the sound field of impulsively

accelerated bodies, and it is this that we shall use here.

In our potential flow model the impulsive pressure at contact existed throughout space, and was connected with the sudden change in fluid velocity at all points close to the aerofoils. Real fluids are compressible, and the information that the blades have touched is transmitted at the speed of sound. Only the fluid immediately next to the gap is affected at the time of contact, the rest must wait until the sound reaches it. In this high frequency limit there is no time for dipole effects to cancel, and the signal is transmitted as a wave front from the blade surfaces. Ffowcs Williams and Lovely argue that under these conditions ray theory will be valid for the time around contact. The sound field is therefore composed of beams from each of the flat aerofoil surfaces, and the strength of each beam is determined by the change in pressure at the surface at impact. For the distant free-field observer on the blade normal the whole surface is at the same retarded time, so the sound wave is just related to the change in the blade loading at contact. In terms of the previously defined terms, the average pressure jump on the surface is

$$\Delta p = F_n^u / 2\alpha c^2 \ , \tag{4.4}$$

where the suffix n denotes the normal to the surface, c is the blade chord, and α the blade aspect ratio. This pressure jump will be the amplitude of the transmitted pulse, and we assume that the spacial width of the pulse is of the same order as the blade chord. The energy in the transmitted beam from each blade surface is then

$$E = \int \Delta p^2 / \rho c_s^2 \, dV = \tfrac{1}{4} F_n^{u\,2} / \rho \alpha c c_s^2 . \tag{4.5}$$

In practice the beam will not stay collimated to a large distance. Its energy will be shared in all directions as a result of scattering within the engine, and the mean sound intensity observed at a distance R will be

$$\frac{\omega}{2\pi} \frac{(F_n^{u\,2}/\rho\alpha c c_s^2)}{4\pi R^2} , \tag{4.6}$$

where ω is the blade passing frequency. Note that the sound frequencies for which ray theory is valid are much higher than ω. This can be compared with the energy from the low frequency components, which from equation (4.3) will give a mean intensity on the dipole axis of

$$\frac{(\omega^2/\pi^2)\ F_i^{u\,2}}{\rho c_s (4\pi c_s R)^2} , \tag{4.7}$$

which is $\alpha\omega c/2\pi^2 c_s$ times the sound intensity from the pressure impulse. Thus at low blade passing frequencies ($\omega c << c_s$) the higher harmonics of the sound field will be dominant. At higher blade passing frequencies the dominant contribution is from the unsteady forces, and the overall sound field would, we expect, be somewhat louder than and rather different in quality from a conventional stage. An increased number of blades on a ring would reduce the magnitude of the unsteady loads and also therefore the sound. We have no reason to expect that the noise will be so loud that the interaction is unuseable, but we admit that our estimate of its magnitude is a very crude one, and can give little more than a qualitative impression of the problem. We have found it extremely difficult to produce a more convincing estimate !

4.3 Cross-flow fans.

The axial flow fan maintains a steady circulation on each blade, and therefore does not share the requirement of Encarsia formosa for regular circulation changes. The axial flow fan was chosen for the initial calculations because it provides the simplest model to analyse. The tangential, or cross-flow, fan does require the circulation on each blade to change. It consists of blades whose spans are arranged to lie on the generators of a cylinder, and the flow crosses through the blades to the centre of the cylinder on one part of the circumference, and then outwards from the centre across another part. The air passes through the same blading twice, and if the blades are to do work on each occasion they must change the sign of their circulations twice per revolution. The main applications to date have been in domestic machinery such as hair driers and electric fan heaters, where efficiency is not of prime importance. The attractions of this type of fan include its high volume flow compared with centrifugal fans of the same size, and high pressure rise compared with simple axial fans.

Much interest has been shown recently in the possibility of using cross-flow fans for the control of aircraft boundary layers, where their geometry makes them ideally suitable. Unfortunately their efficiences are still too low to make this application clearly advantageous.

Current work on cross-flow fans tends to adopt an empirical approach, and although the flow through the fan has been modelled to understand better the role of the trapped vortex (see figure 4.2), little work has been done on the working conditions of individual blades. The circulation on a blade must change twice per revolution, and the blade must therefore shed vorticity. It can be seen that the trapped vortex can be accounted for as an accumulation of this shed

vorticity in a region where the stream velocity is low. The opposite vorticity is shed where the stream velocity is high, and it is therefore convected away, except in some machines which have casings designed to recirculate the flow in that region.

The interaction that we have been studying can be used to generate rapid changes in circulation, and a possible casing for a cross-flow fan which makes use of this is shown in figure 4.3. A centrebody (A) inside the rotor is necessary for one of the changes, but an interaction with the outer casing (B) is sufficient for the other. The trapped vorticity should be distributed around the centrebody, onto which vorticity is repeatedly being transferred from each blade that passes.

Again we find a geometry for a machine which is not unlike previous designs. The centrebody was a feature of a cross-flow fan designed by Mortier (1892) at the end of the last century.

The cross-flow fan offers a great opportunity for exploitation of the Weis-Fogh effect. The reason why we have not used it as our principal example of an application is the complexity of the flow through the rotor, and the relative lack of understanding of the blade operating conditions compared with the axial fan. In the light of the insects ability to change its circulations so rapidly to great advantage, we think that an examination of the flow through a cross-flow fan from this new point of view may lead to ways of improving the efficiency to the extent that the fan will find new areas of application, such as the above mentioned control of boundary layers.

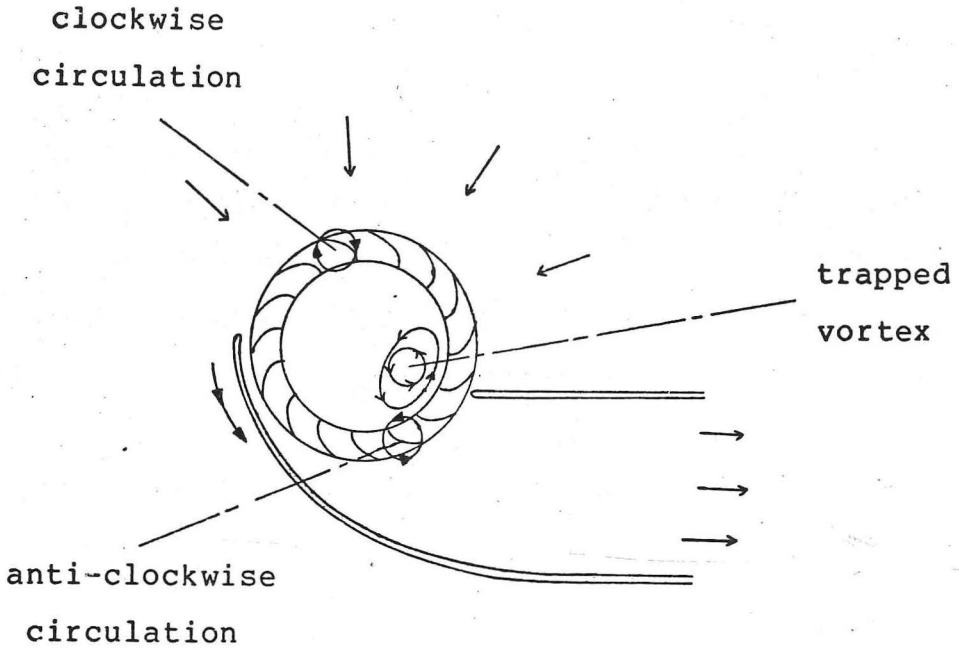

Figure 4.2. The main features of a cross-flow fan.

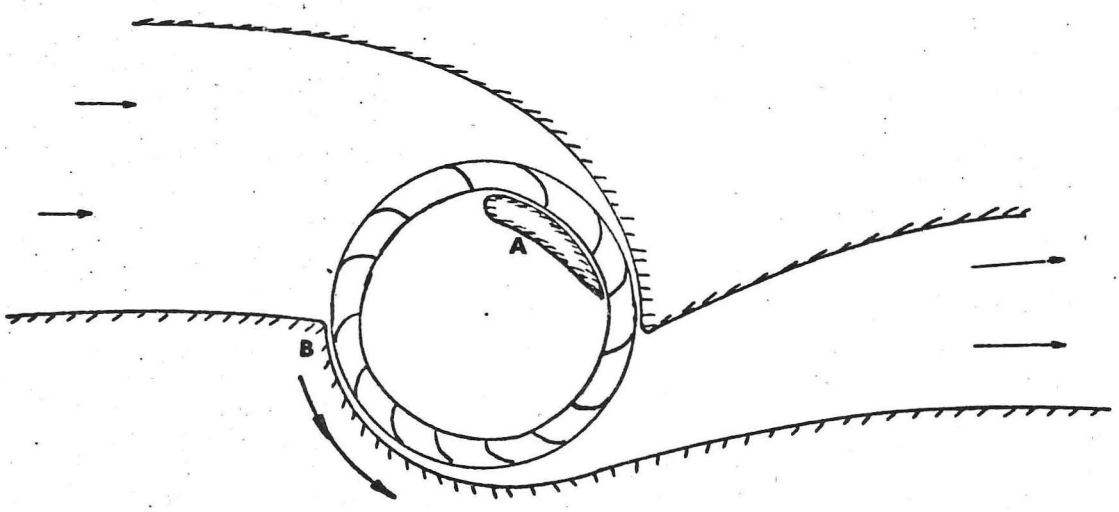

Figure 4.3. A design for a cross-flow fan which incorporates the Weis-Fogh effect to change the blade circulations.

5. CONCLUSIONS.

5.1 Discussion.

Recent studies of animal hovering motions have revealed a method of lift generation not previously considered by aerodynamicists. The insects that use the method achieve a lift coefficient double that achieved by animals that use a conventional vortex-shedding process. We have attempted to demonstrate that the principle of the new (to aerodynamicists, but not insects !) process may have engineering applications. Furthermore, being radically different in principle from that used in conventional aerodynamics, it might well offer some performance advantage.

We have suggested a design for an axial flow compressor using the new process, and shown how a simple model of this design may be analysed mathematically. The results show that the effect is strong enough to be of interest to designers of machines.

Experiments have been performed to establish that the circulations predicted by the theory were obtainable in practice, and to examine the influence of vortex shedding. At low rotor speeds compared with the stream speed some of the vorticity was shed into the stream rather than transferred onto the rotor, but we showed that this had little effect on the forces on the blades if the vorticity passed near the rotor. The potential flow model gave useful results so long as the rotor speed was not much less than the free stream speed.

The effect of varying levels of interaction in axial flow stages has been investigated experimentally. The results show a measurable improvement in performance as the interaction is increased, and we suggest that the improvement may well be due to the effect illustrated

by the theoretical model.

Weis-Fogh (1973) and Lighthill (1973) have explained the novel mechanism used by the insect to enhance its aerodynamic performance, and much interest has been shown by aerodynamicists in their work. We suggest that this interest should now be extended to a serious consideration of the application of the mechanism to the solution of engineering problems.

5.2 Suggestions for further work.

The work presented here has been done with the aim of demonstrating the applicability of the Weis-Fogh principle to turbomachinery. As such it indicates some of the possible areas of application, but provides no detailed design rules. Our findings suggest that at least for the applications which we have suggested there will be design changes if the effect is to be exploited to the full, but a complete redesign of the machine is not necessary. Further work is required, and we suggest the following areas as being worthy of immediate attention.

(i) A thorough search of the performance characteristics of past and present axial compressors, particularly those with low axial spacing, to see if there is evidence of the interaction taking place. If there is, how does it affect the performance ?

(ii) The investigation of a fully instrumented axial compressor stage, combining the transient pressure measurements of our isolated interaction rig with the variable axial separation of our stage rig. The apparatus should be designed so that the rotor-stator clearance can be reduced to below 1 percent of the chord along the entire span, and there should be enough pressure tappings to enable transient pressure profiles to be found. This would be a most valuable experiment.

(iii) The calculation technique we developed in section 2.6 to describe our results should be extended, probably by using a more sophisticated calculation method such as that used by Giesing (1968). If the displacement of the wake normal to the stream and full details of the blade shape were included (as they would be if Giesing's program were used) then the uncertainty would be reduced to the modelling of the trailing edge condition close to contact. If the method were

extended further to include cascade geometries, then together with the experiment (ii) above it would constitute a powerful aid to blade design.

(iv) Cross-flow fans should be investigated with a view to understanding the way blade interactions with the casing, and the resulting circulation changes, control the performance characteristics.

6. APPENDICES

6.1 The transducer amplifier.

The existing amplifier for the pressure transducer used here was DC coupled with adjustment for DC output and gain. The transducer was fairly noisy, as described in section 2.4, and the low frequency components of this noise were large compared with the typical signal levels arising in the experiments. Since we did not require a response down to DC, it was decided to construct a new amplifier with a high-pass filter set at about 0.1 Hertz. To reduce the noise further a low-pass filter with a turn over at about 1 kHz was also incorporated. Any frequency component above 500 Hz would be aliased to a different frequency anyway by the discrete sampling of the data.

The gain required to normalise the data to a level optimal for input to the analogue-to-digital converter was high, around two thousand, so a two stage amplifier was used. The ADC required inputs spanning 0 to 5 volts, therefore the LM324 operational amplifier was chosen, which produces outputs in this range and has the further advantage of running from a single rail +5 volt power supply instead of the usual +15, 0, and -15 volts. Each package contains four amplifiers, and each amplifier has easily sufficient open loop gain and frequency response for our needs. Various circuits were tried on a prototyping board, and the one shown in figure 6.1 was found to have the best performance.

Figure 6.1 shows the complete amplifier circuit, as well as the circuit producing the regulated 10 volt power supply for the angular position transducer. These circuits were mounted together in a freestanding box and powered jointly from a remote DC supply at 16 volts. Originally an internal mains electricity supply was used, but this (predictably) produced too much 50 Hz interference on the

outputs.

The power for the amplifiers was dropped from the 16 volt input to 5 volts through a monolithic voltage regulator, and this was further dropped through a resistor-zener diode combination to provide the 4 volt supply to the pressure transducer. The transducer output was DC decoupled from the amplifier input with a 10 microfarad tantalum capacitor, and the DC level of the input was adjusted with a voltage divider. The signal was then amplified through the first active high-pass filter, designed so that the output voltage DC component would follow the adjusted level of the input. There follows a passive low-pass filter, a second active high-pass filter similar to the first, and the output is then suitable for direct connection to the analogue-to-digital converter.

The circuit worked well as shown, the only problem being that the large capacitors used in the active filters to give low enough frequency response take a long time to charge to their working level. The amplifier took about twenty minutes after switch on before it started to operate. This is not really a major problem though, since it is usually as well to leave the electronics longer than this before taking readings to allow the temperature to stabilise.

The output from the angular position transducer was larger than the ADC input range, so a fixed resistor divider was all that was necessary there.

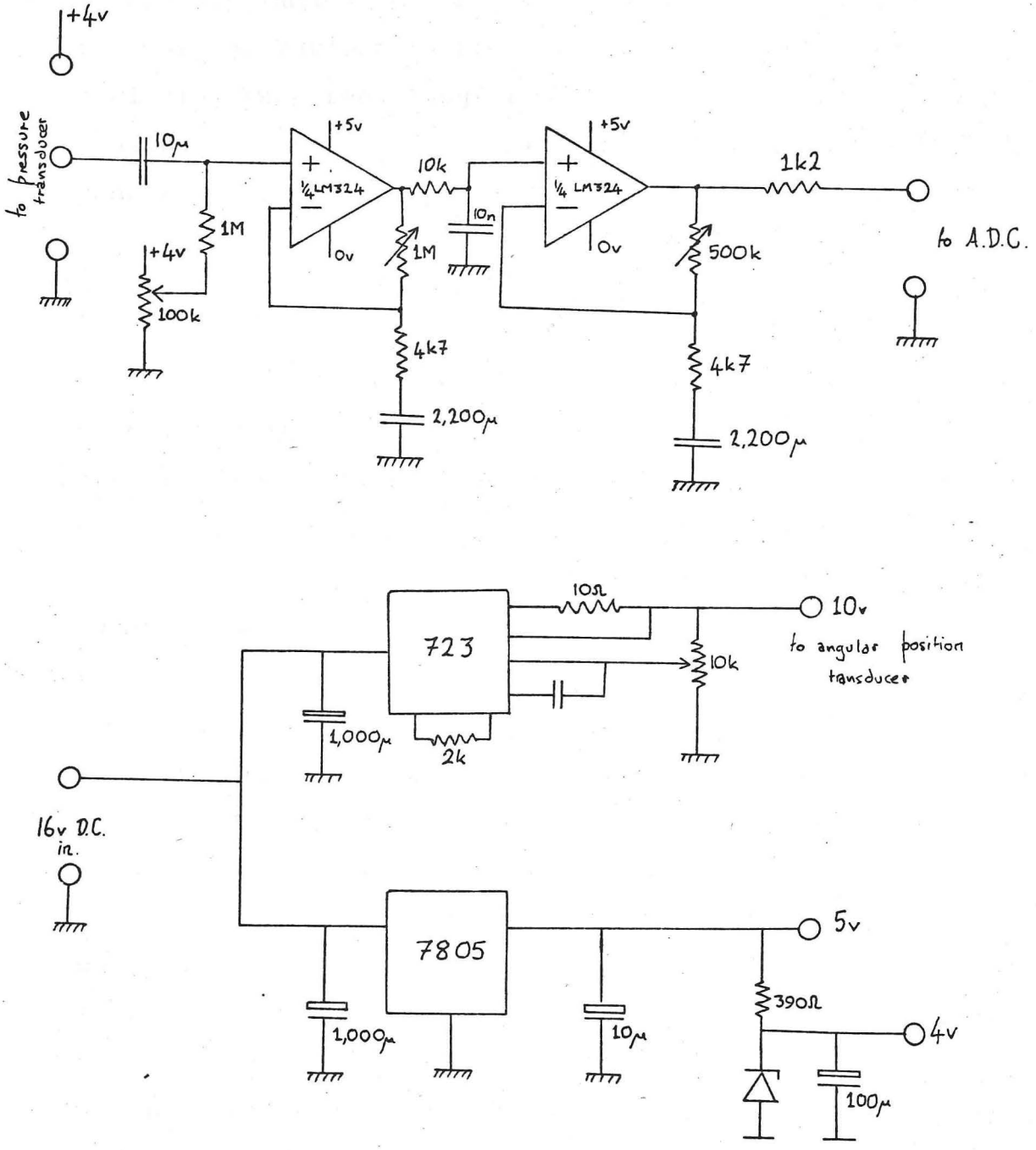

Figure 6.1. The circuit of the pressure transducer amplifier, also showing the power regulator for the angular position transducer.

6.2 The data logging system.

The experiment described in section 2.4 required that large amounts of information be recorded in a short length of time. 16384 transducer output levels were retained in 8 seconds for future processing. Various methods were considered for storing the data, including tape recording or using a mini-computer. The author had available a small microprocessor based system which had been constructed previously for other purposes, and since it was immediately available it was decided to use this. The same system was used for the initial preparation of the text of this dissertation.

The system layout is shown in figure 6.2, and a photograph may be found at the back of the dissertation (plate 2). The heart of the system is a 6502 8-bit processor, mounted on a standard eurocard with an interface to a bus mounted at the back of the system. Other modules are mounted alongside the processor card, including 40 kilobytes of dynamic memory, a driver card to produce characters on a standard video monitor, a floppy disc interface, and the I/O module. This last module houses the analogue-to-digital system and 40 general purpose digital I/O lines used here for driving the printer and communicating with the mini-computer. The floppy disk software was in permanent memory in the system, making the full range of programs held on disc immediately available after switch on. The two 5.25 inch disk drives were mounted in a large module on the second level in the same rack as the system electronics.

The signals from the transducers were in analogue form, and had to be digitised before the processor could handle them. This was done by a monolithic 16 channel ADC chip, which converted to a resolution of 8 bits. This corresponds to an accuracy of about .5 percent, allowing for ADC non-linearity. Since the transducer signal to noise ratio was only around 10dB at the pressures involved in the

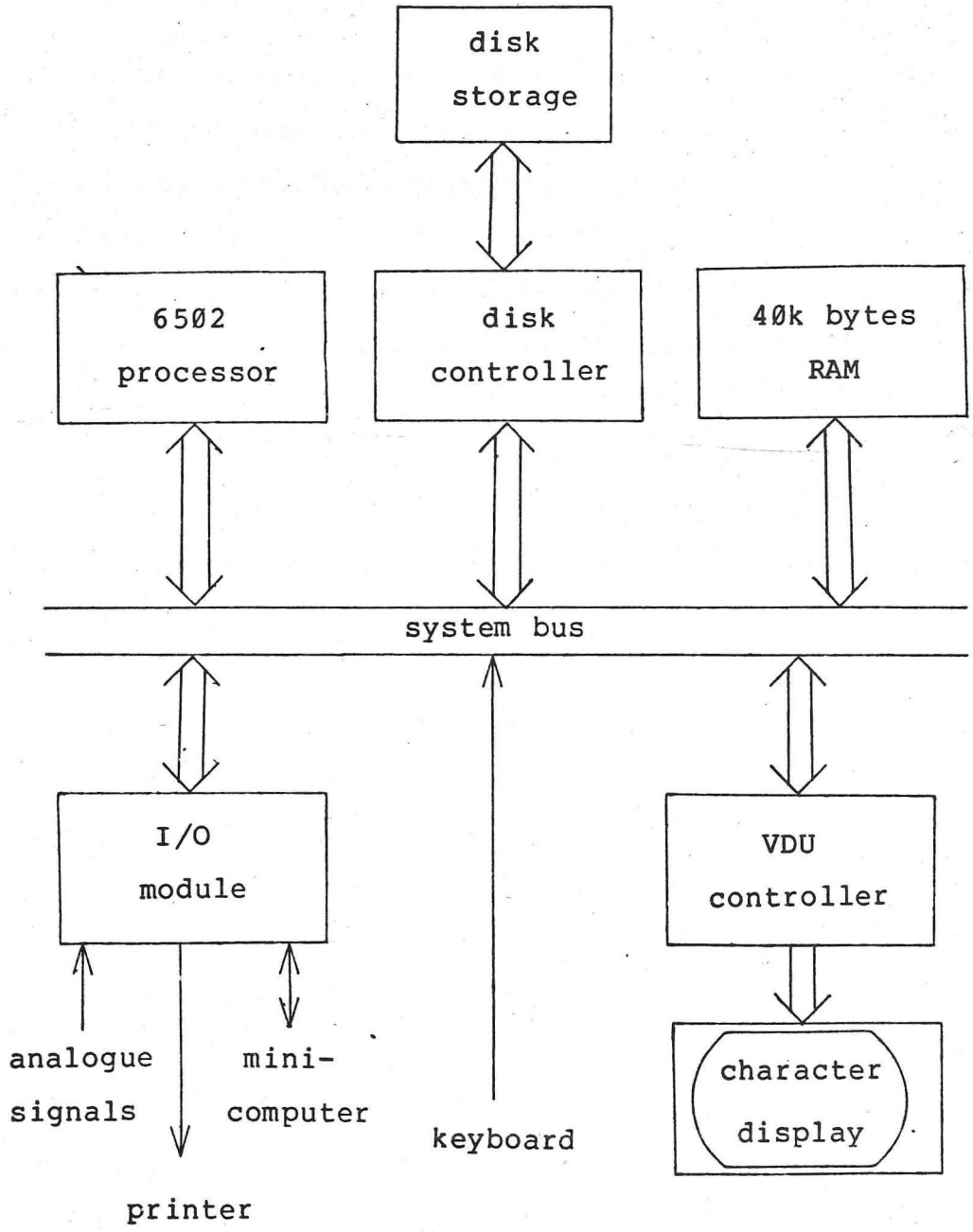

Figure 6.2. The general layout of the data logging system.

experiment, this accuracy was easily sufficient so long as the transducer was preamplified to give full scale on the highest readings required.

The digitised transducer readings were stored in the system memory during the course of the experiment, and then transferred onto mini-floppy disk. The complete system was moved after all the readings had been taken to transfer the data onto an Engineering Department mini-computer for analysis and plotting. The transfer was performed by connecting appropriate output lines on the microprocessor system to the fast paper tape reader input lines on the mini-computer. The mini-computer then loaded the data using standard software while a small assembler routine in the micro-computer made it appear exactly like the paper tape reader it replaced. The transfer of each block of 16 kilobytes took only a few seconds.

The microprocessor system had a high level language (Basic) which made rapid initial processing of the data possible while the system was still connected to the experimental apparatus, to check that all was working well. Defects in the transducer preamplifier were discovered and corrected as a result of this analysis, before too much time had been wasted. It was felt that this demonstrated a significant advantage of using an 'intelligent' data logging system over simply tape recording the transducer signals for processing later.

6.3 Stage details

These are details of the two stages used in the axial pump tests, cross-sections of which were shown in figures 3.6 (the special stage designed to emphasise the interacion effects) and 3.7 (the conventional stage).

The special stage:

rotor	chord	20 mm
	profile	10C4 on circular arc
	camber	30 degrees
	stagger	50 degrees
stator	chord	20 mm
	profile	special, see figure 3.6
	camber	70 degrees
	stagger	40 degrees

The conventional stage:

rotor	chord	20 mm
	profile	10C4 on circular arc
	camber	30 degrees
	stagger	45 degrees
stator	chord	20 mm
	profile	10C4 on circular arc
	camber	30 degrees
	stagger	30 degrees

All blade sets:

material	polycarbonate
hub diameter	66 mm
tip diameter	88mm
tip clearance	0.1 mm nominal

Test conditions:

rotor-stator clearances	0.1 to 5 mm
flow rates	5 to 13 kg/s
rotor speed	2500 rpm

7. REFERENCES.

Abramowitz, M. & Stegun, I.A. 1964 Handbook of Mathematical Functions. Washington, National Bureau of Standards.

Aschenbrenner, A. 1966 Investigation into the Effect of the Space between Rotor and Stator on the Operational Behaviour of the Blading of a Single Stage Pump. Konstruktion im Maschinen-Apparate und Geratebau.

Batchelor, G.K. 1967 An Introduction to Fluid Dynamics. Cambridge University Press.

Coester, R. 1959 Theoretical and Experimental Study of Cross-Flow Fans. Diss., Zurich.

Curle, N. 1955 Proc. Roy. Soc., 231A, 1187, 505-514.

Ffowcs Williams, J.E. 1970 Sources of Sounds in Fluid Flows. Proceedings of the International Symposium on the Fluid Mechanics and Design of Turbomachines. Pennsylvania State University. NASA SP-304.

Ffowcs Williams, J.E. & Lovely, D.J. 1977 J. Sound and Vib. 50, 333-343.

Giesing, J.P. 1968 J. Basic Eng., 387-394.

Goldstein, M.E. 1976 Aeroacoustics. McGraw-Hill.

Hawkings, D.L. & Lowson, M.V. 1974 J. Sound and Vib. 36, 1-20.

Horlock, J.H. 1958 Axial Flow Compressors. Butterworth Publications Limited.

Jeffreys, H. & Jeffreys, B.S. 1956 Methods of Mathematical Physics. Cambridge University Press.

Jenny, R. 1976 Variable Geometry Axial Compressors. VKI Lecture Series 91, Industrial Compressors.

Kemp, N.H. & Sears, W.R. 1953 Aero. Sci. 20, 585-597.

Lighthill, M.J. 1952 Proc. Roy. Soc., 211A, 1107, 564-587.

Lighthill, M.J. 1973 J. Fluid Mech. 60, 1-17.

Miller, D.C. 1971 The Effect of Axial Gaps on Compressor Performance. Rolls-Royce Ltd. int. publ. ref. no. G.N.14229.

Mortier, P. 1892 DRP 146,464

Smith, L.H.Jr. 1970 Casing Boundary Layers in Multistage Axial Flow Compressors. Flow Research on Blading, ed. L.S. Dzung. Elsevier.

von Kármán, Th. & Sears, W.R. 1938 J. Aero. Sci., 5, 379-390.

Wagner, H. 1925 Dynamischer Auftrieb von Trag-flugen. Zeitschr. f. Agnew. Math. u. Mech., Bd. 5, page 17.

Weinig, F. 1935 Die Stromung um die Schaufeln von Turbomachinen. Leipzig: Joh Ambr. Barth.

Weis-Fogh, T. 1973 J. Exp. Biol. 59, 169-230.

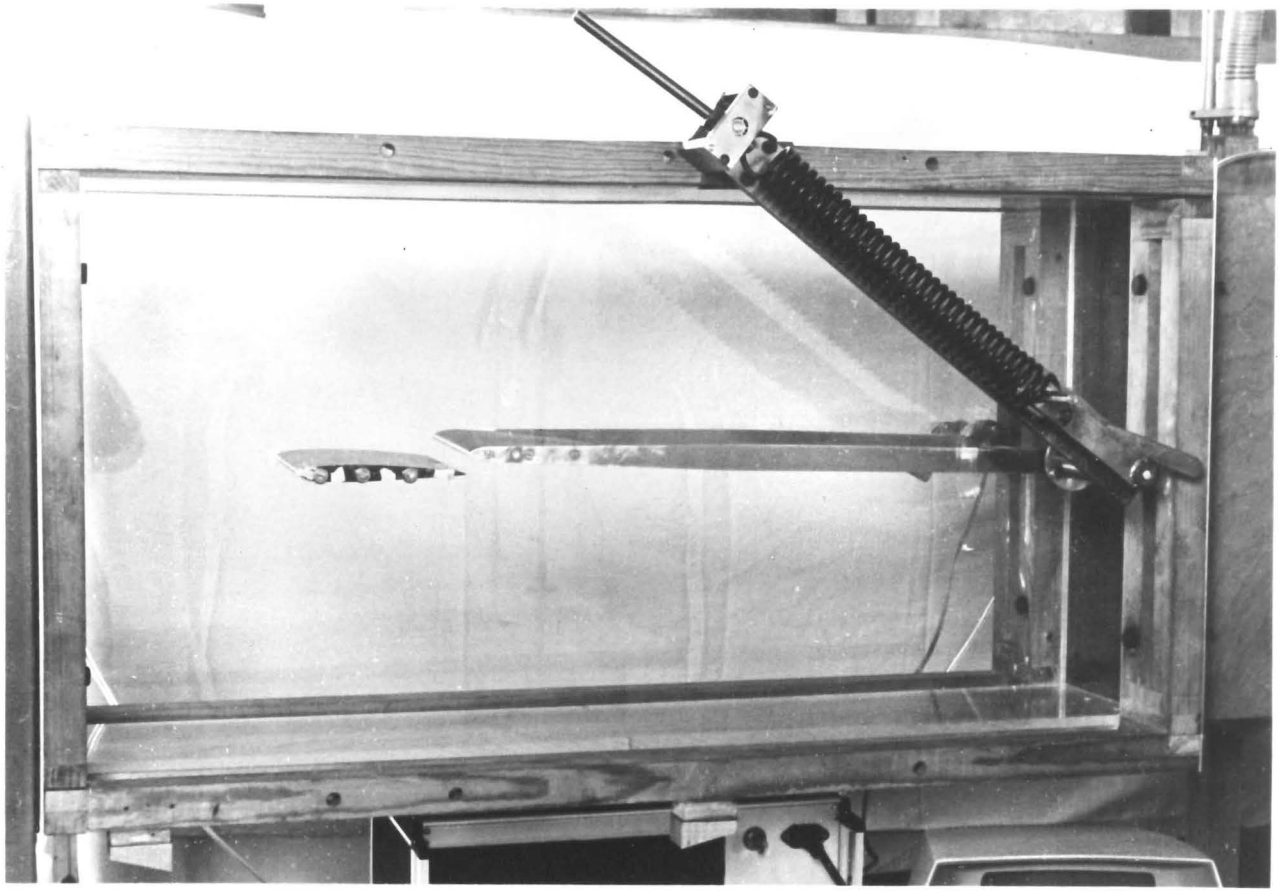

Plate 1. The apparatus used to investigate the isolated interaction.

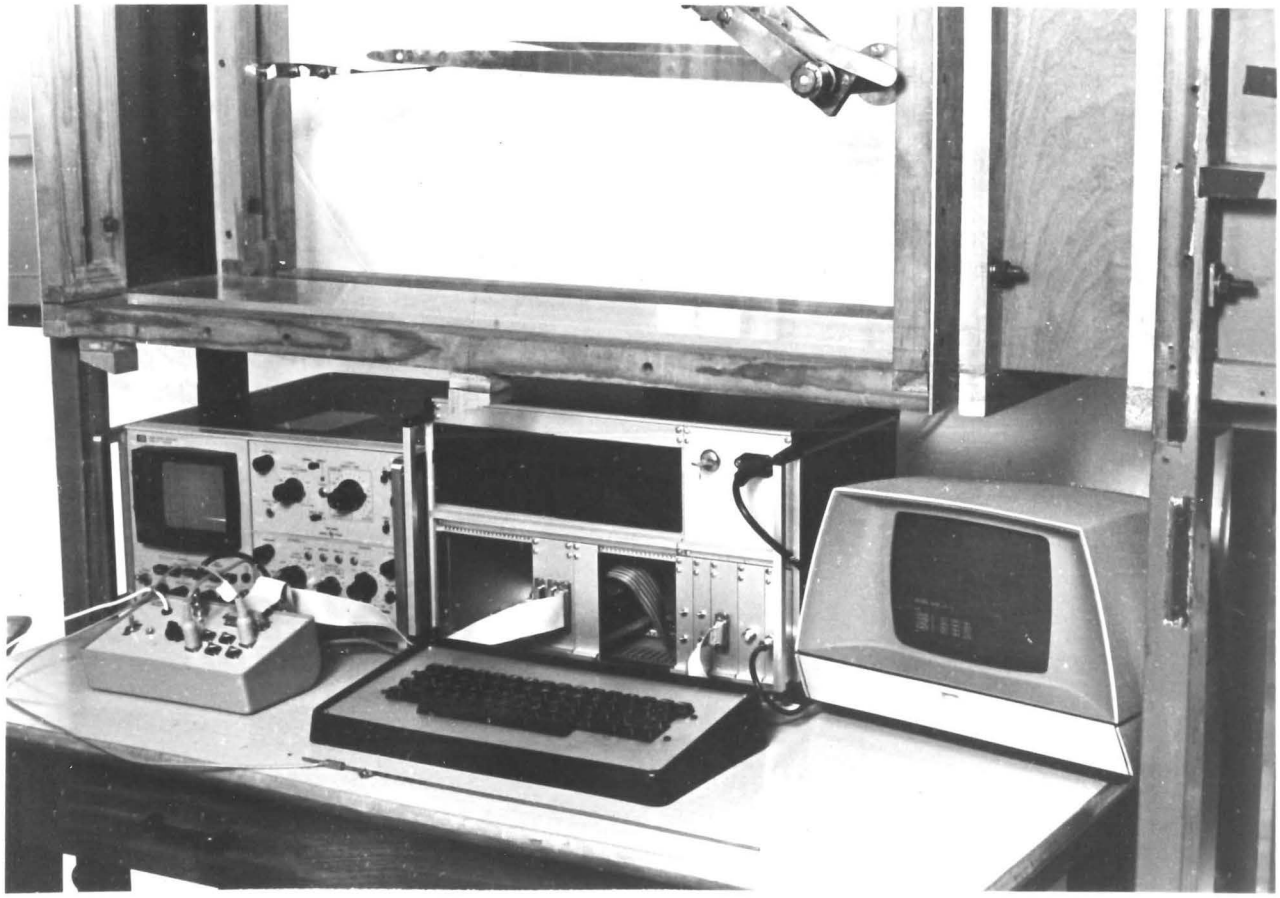

Plate 2. The data logging equipment, with the pressure transducer probe and amplifier.

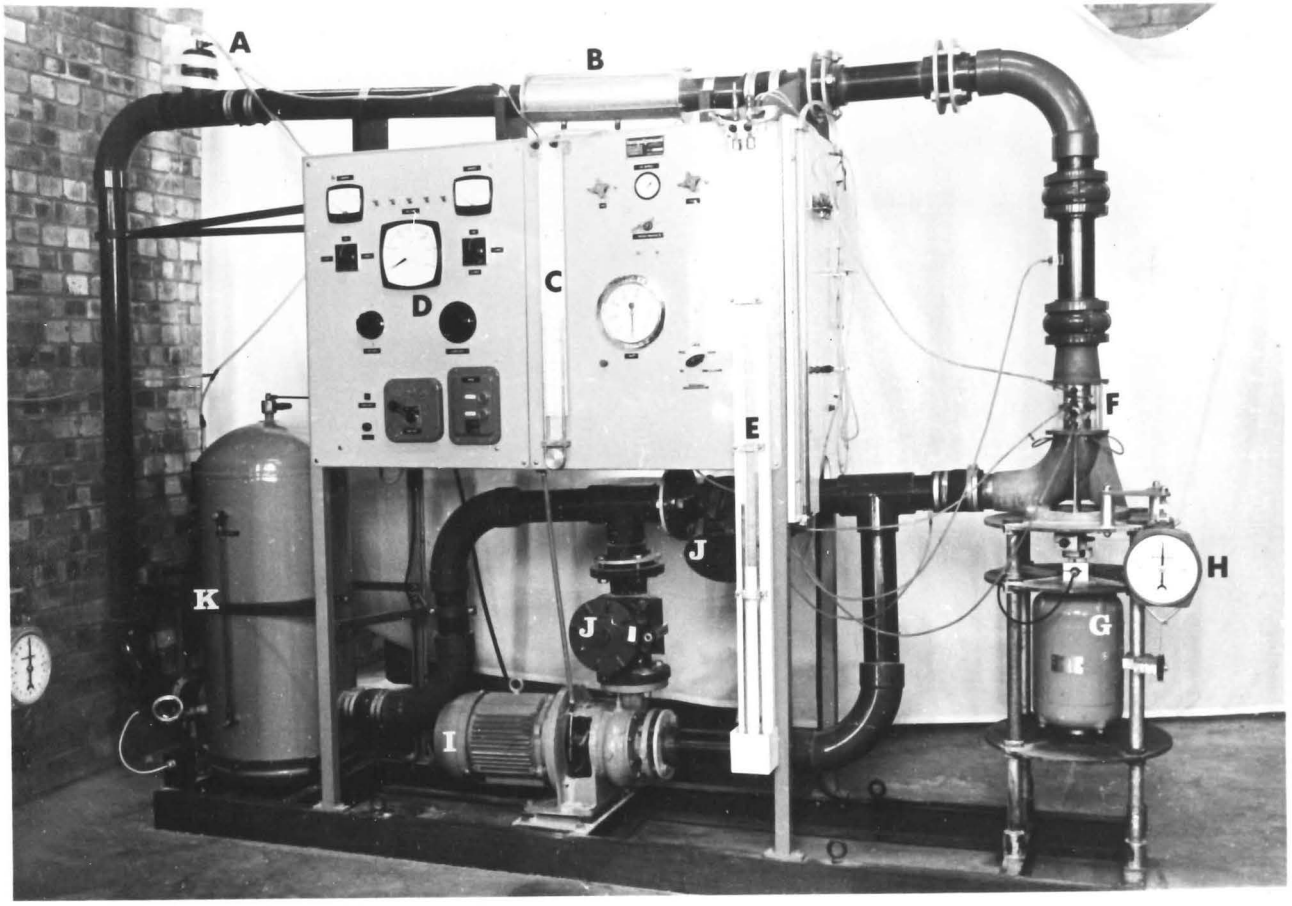

Key:

A - Vent

B - Venturi tube

C - Flow rate manometer

D - Rotor speed controls

E - Pressure rise manometer

F - Working section

G - Rotor drive motor

H - Torque indicator

I - Auxiliary pump motor

J - Flow control valves

K - Drainage tank

Plate 3. The apparatus used for the axial compressor stage tests.